

This is the peer reviewed version of the following article:

Enhancement of Benzothiazoles as Pteridine Reductase-1 Inhibitors for the Treatment of Trypanosomatidic Infections / Linciano, Pasquale; Pozzi, Cecilia; Iacono, Lucia Dello; di Pisa, Flavio; Landi, Giacomo; Bonucci, Alessio; Gul, Sheraz; Kuzikov, Maria; Ellinger, Bernhard; Witt, Gesa; Santarem, Nuno; Baptista, Catarina; Franco, Caio; Moraes, Carolina B; Müller, Wolfgang; Wittig, Ulrike; Luciani, Rosaria; Sesenna, Antony; Quotadamo, Antonio; Ferrari, Stefania; Pöhner, Ina; Cordeiro-da-Silva, Anabela; Mangani, Stefano; Costantino, Luca; Costi, Maria Paola. - In: JOURNAL OF MEDICINAL CHEMISTRY. - ISSN 0022-2623. - 62:8(2019), pp. 3989-4012. [10.1021/acs.jmedchem.8b02021]

Terms of use:

The terms and conditions for the reuse of this version of the manuscript are specified in the publishing policy. For all terms of use and more information see the publisher's website.

24/01/2025 04:28

(Article begins on next page)

24/01/2025 04:28

Enhancement of benzothiazoles as Pteridine Reductase-1 (PTR1) inhibitors for the treatment of Trypanosomatidic infections.

Pasquale Linciano, Cecilia Pozzi, Lucia Dello Iacono, Flavio di Pisa, Giacomo Landi, Alessio Bonucci, Sheraz Gul, Maria Kuzikov, Bernhard Ellinger, Gesa Witt, Nuno Santarem, Catarina Baptista, Caio Franco, Carolina Borsoi Moraes, Wolfgang Müller, Ulrike Wittig, Rosaria Luciani, Antony Sesenna, Antonio Quotadamo, Stefania Ferrari, Ina Pöhner, Anabela Cordeiro-da-Silva, Stefano Mangani, Luca Costantino, and Maria Paola Costi

J. Med. Chem., **Just Accepted Manuscript** • Publication Date (Web): 25 Mar 2019

Downloaded from <http://pubs.acs.org> on March 25, 2019

Just Accepted

“Just Accepted” manuscripts have been peer-reviewed and accepted for publication. They are posted online prior to technical editing, formatting for publication and author proofing. The American Chemical Society provides “Just Accepted” as a service to the research community to expedite the dissemination of scientific material as soon as possible after acceptance. “Just Accepted” manuscripts appear in full in PDF format accompanied by an HTML abstract. “Just Accepted” manuscripts have been fully peer reviewed, but should not be considered the official version of record. They are citable by the Digital Object Identifier (DOI®). “Just Accepted” is an optional service offered to authors. Therefore, the “Just Accepted” Web site may not include all articles that will be published in the journal. After a manuscript is technically edited and formatted, it will be removed from the “Just Accepted” Web site and published as an ASAP article. Note that technical editing may introduce minor changes to the manuscript text and/or graphics which could affect content, and all legal disclaimers and ethical guidelines that apply to the journal pertain. ACS cannot be held responsible for errors or consequences arising from the use of information contained in these “Just Accepted” manuscripts.



1
2
3
4
5
6
7
8
9
10
11
12
13
14
15
16
17
18
19
20
21
22
23
24
25
26
27
28
29
30
31
32
33
34
35
36
37
38
39
40
41
42
43
44
45
46
47
48
49
50
51
52
53
54
55
56
57
58
59
60

	Costi, Maria Paola; Universita degli Studi di Modena e Reggio Emilia, Dipartimento di Scienze della Vita

SCHOLARONE™
Manuscripts

Enhancement of benzothiazoles as Pteridine Reductase-1 (PTR1) inhibitors for the treatment of Trypanosomatidic infections.

Pasquale Linciano^{1*}, Cecilia Pozzi², Lucia dello Iacono², Flavio di Pisa², Giacomo Landi², Alessio Bonucci², Sheraz Gul³, Maria Kuzikov³, Bernhard Ellinger³, Gesa Witt³, Nuno Santarem⁴; Catarina Baptista⁴, Caio Franco⁵, Carolina B. Moraes⁵, Wolfgang Müller⁶, Ulrike Wittig⁶, Rosaria Luciani¹, Antony Sesenna¹, Antonio Quotadamo¹, Stefania Ferrari¹, Ina Pöhner⁷, Anabela Cordeiro-da-Silva⁴, Stefano Mangani^{2*}; Luca Costantino^{1*}, Maria Paola Costi^{1*}.

¹University of Modena and Reggio Emilia, Via Campi 103, 41125 Modena, Italy

²University of Siena, Dipartimento di Biotecnologie, Chimica e Farmacia, Via Aldo Moro 2, 53100 Siena, Italy

³Fraunhofer Institute for Molecular Biology and Applied Ecology Screening Port, 22525 Hamburg, Germany

⁴Institute for Molecular and Cell Biology, 4150-180 Porto, Portugal and Instituto de Investigação e Inovação em Saúde, Universidade do Porto and Institute for Molecular and Cell Biology, 4150-180 Porto, Portugal

⁵Laboratório Nacional de Biociências (LNBio), Centro Nacional de Pesquisa em Energia e Materiais (CNPEM), 13083-100 Campinas – SP, Brazil; Present Address: Department of Microbiology, Institute of Biomedical Sciences, University of Sao Paulo, 05508-900 Sao Paulo – SP, Brazil.

⁶Scientific Databases and Visualization Group, Heidelberg Institute for Theoretical Studies (HITS), D-69118 Heidelberg, Germany.

⁷Molecular and Cellular Modeling Group, Heidelberg Institute for Theoretical Studies (HITS), D-69118 Heidelberg, Germany.

Abstract

2-amino-benzo[d]thiazole was identified as new scaffold for the development of improved PTR1 inhibitors and anti-Trypanosomatidic agents. Molecular docking and crystallography guided the design and synthesis of 42 new benzothiazoles. The compounds were assessed for *T. brucei* and *L.*

1
2
3 *major* PTR1 inhibition and *in-vitro* activity against *T. brucei* and amastigote *L. infantum*. We
4
5 identified several 2-amino-benzo[d]thiazoles with improved enzymatic activity (*Tb*PTR1 IC_{50} =
6
7 0.35 μ M; *Lm*PTR1 IC_{50} = 1.9 μ M) and low μ M anti-parasitic activity against *T. brucei*. The ten
8
9 most active compounds against *Tb*PTR1, were able to potentiate the antiparasitic activity of
10
11 methotrexate when evaluated in combination against *T. brucei*, with a Potentiating Index between
12
13 1.2 and 2.7. The compound library was profiled for early ADME-Toxicity and 2-amino-*N*-
14
15 benzylbenzo[d]thiazole-6-carboxamide (**4c**) was finally identified as a novel potent, safe and
16
17 selective anti-trypanocidal agent (EC_{50} = 7.0 μ M). Formulation of **4c** with hydroxypropyl- β -
18
19 cyclodextrin yielded good oral bioavailability, encouraging progression to *in-vivo* studies.
20
21
22
23
24
25
26
27
28
29
30
31
32
33
34
35
36
37
38
39
40
41
42
43
44
45
46
47
48
49
50
51
52
53
54
55
56
57
58
59
60

INTRODUCTION

Kinetoplastidae are a group of flagellated protozoan parasites transmitted by insect vectors and responsible for severe human pathologies. Human African Trypanosomiasis (HAT; also known as African sleeping sickness), is caused by *Trypanosoma brucei* (*T. brucei*), the Chagas disease is caused by *Trypanosoma cruzi* (*T. cruzi*) and three different manifestations of leishmaniasis (visceral, cutaneous and mucocutaneous) are caused by infection with different species of *Leishmania*.¹ In particular, HAT can arise in an acute or chronic form. Cardiac and kidney diseases, among other serious complications, can lead to death if untreated. The second stage arises when the parasite migrates across the blood-brain barrier, resulting in neurological symptoms that ultimately can lead to coma and death.²

Although treatment options for these infections exist, their use is limited by several factors, including toxicity, poor efficacy, difficult administration and cost. Furthermore, increasing levels of drug resistance emphasize the need for new, improved and affordable drugs.^{3,4} Recently, after thirty years of research in this field, fexinidazole, a 5-nitroimidazole, has been finally approved as the first oral drug for the treatment of HAT.^{5,6}

In order to accelerate the discovery of new treatments for Trypanosomatidic infections, one approach already used for the treatment of bacterial infections and some parasitic diseases (e.g. malaria) entails the use of drugs targeting folate enzymes (e.g. thymidylate synthase, TS or dihydrofolate reductase, DHFR).^{7,8} As a result, the reduction of the cellular pool of deoxythymidine monophosphate, which is essential for DNA replication, causes cell death.⁸ Trypanosomatids are auxotrophic for folates and pterins; therefore, inhibiting the enzymes involved in the folate salvage pathways should provide effective treatment.⁹ However, the use of DHFR inhibitors (e.g. methotrexate (MTX) or pyrimethamine) for the treatment of these parasitic diseases is unsuccessful, partly due to pteridine reductase 1 (PTR1) activity.¹⁰ PTR1 is a short-chain dehydrogenase/reductase (SDR) that can reduce both conjugated and unconjugated pterins. Indeed,

1
2
3 expression of PTR1 is promoted when parasitic DHFR is inhibited, ensuring survival of the
4 parasite.^{11–13} The entanglement between parasitic PTR1 and DHFR activity is corroborated by the
5 limited anti-parasitic efficacy of full PTR1 inhibitors developed to date,^{14–19} and by the necessity to
6 co-administer a DHFR inhibitor to observe a trypanocidal activity.^{15,17,20} Recently, *T. brucei* PTR1
7 (*Tb*PTR1) inhibitors based on structural elaboration of 2-amino-1,3,4-thiadiazoles were proposed.¹⁷
8 The new compounds showed only micromolar activity against *Tb*PTR1 and potentiated the activity
9 of MTX when used in combination²⁴.

10
11
12 A double aromatic/heteroaromatic ring system was deemed necessary to implement the design of
13 the thiadiazole core. A two-ring system is expected to provide improved PTR1 inhibitors with
14 increased affinity for the protein, thus competing more strongly with the substrate pterin moiety.
15 Since 2010, a number of X-ray crystal structures have been made solved in which two
16 aromatic/heteroaromatic ring systems were bound to PTR1 as protein inhibitors mapping the active
17 site.^{17,21–24} From our preliminary studies on compound repositioning, riluzole and other 2-amino-
18 benzothiazole derivatives exhibited low micromolar affinity against PTR1.¹⁵ The aim of the present
19 work was to enlarge the benzothiazole library through a structure-based approach, to characterize
20 the biological activity against PTR1 and Trypanosomatidic parasites and evaluate the early ADME-
21 Toxicity profile to select at least one compound for progression to pharmacokinetic evaluation in
22 animal assays.

23
24
25 X-ray crystal structures with 2-amino-benzothiazole that could reveal the precise core active-site
26 interactions were not available. Therefore, we first obtained the X-ray crystal structure of (6-
27 (methylsulfonyl)benzo[d]thiazol-2-amine) with *Tb*PTR1 and, based on this structure, we designed
28 and synthesized a library of 42 compounds. The selection and prioritization of compounds for *in*-
29 *vivo* evaluation was performed following the criteria considered for the Target Inhibitor Profile
30 (TIP)^{25,26} resulting in one compound selected for pharmacokinetic studies.

RESULTS AND DISCUSSION

*Tb*PTR1– NADP(H)–**3a** crystal structure

The chemical starting point of the present study relied on the benzothiazole **1b** and **3a** that originated from previous virtual screening studies.¹⁵ As a result of their moderate inhibitor activity against *T. brucei* ($IC_{50} = 34.2 \mu\text{M}$ and $15.1 \mu\text{M}$ for **3a** and **1b**, respectively) and high ligand efficiency ($LE = 0.32$ for both **3a** and **1b**), the two fragments, together with the 2-amino-benzothiazole core scaffold, were considered to be important sub-structures at the outset of this work.

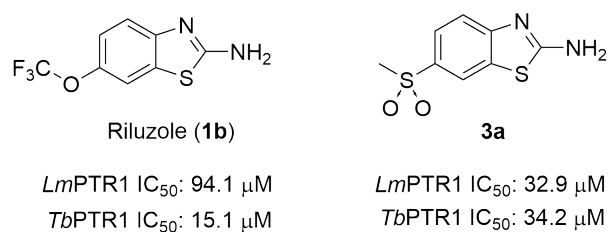


Figure 1. Chemical structures and enzymatic inhibitor activities against *T. brucei* and *Leishmania major* (*L. major*) PTR1 of the benzothiazoles fragments **1b** and **3a**.

Previous docking studies, performed on **1b** and **3a** against *L. major* PTR1 (*Lm*PTR1) showed binding at the active site with the benzothiazole core sandwiched between the cofactor nicotinamide and phenylalanine, forming an array of hydrogen bonds with catalytic residues and the cofactor phosphate and ribose.¹⁵ To provide crucial information that could assist the design of improved inhibitors, crystallographic studies were attempted. **1b** and **3a** were used for crystallization trials with *Tb*PTR1 and the structure of the ternary complex *Tb*PTR1–NADPH–**3a** was successfully obtained.

The structure of *Tb*PTR1 in complex with the cofactor NADP(H) and compound **3a** (IC₅₀ of 34.2 μM, PDB ID 6GCL) was determined to 1.95 Å resolution (Figure 2). The crystal asymmetric unit includes the whole functional *Tb*PTR1 tetramer whose structure is highly conserved with those previously described in the literature^{17,24,27} (subunits were completely traced apart from two surface-exposed loops, including residues 104-112 and 143-15, that are usually poorly visible in *Tb*PTR1 structures). The 2-amino-benzothiazole core of **3a** occupies the catalytic cavity, as previously predicted by molecular modelling,¹⁵ in which it exploits its extended aromatic system to generate the peculiar π -sandwich interaction within Phe97 and the cofactor nicotinamide. A network of H-bonds entailed by the amine moiety, donating two hydrogen bonds to the cofactor β -phosphate, stabilizes the scaffold. In addition, hydroxyl of Ser95 and benzothiazole nitrogen both receives an H-bond from the hydroxyl of the cofactor ribose. The sulfonic group of **3a** is located in the active site pocket lined by the side chains of Cys168, Val206, Leu209, Pro210, Met213, and Trp221.

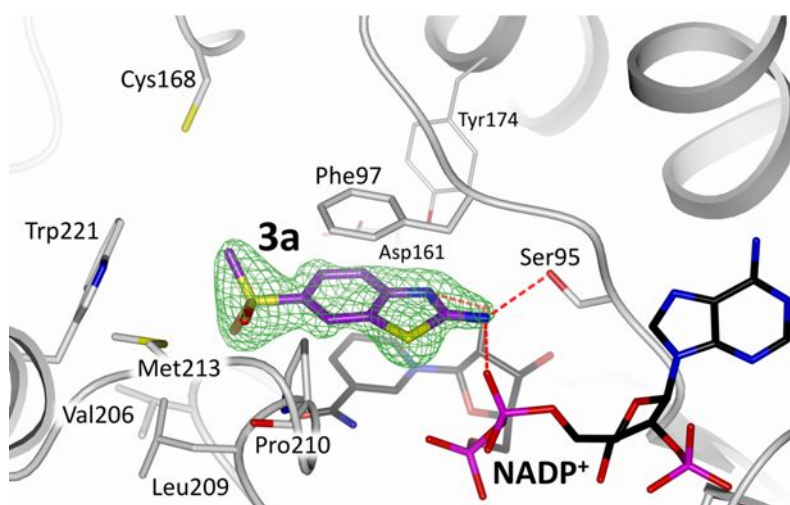


Figure 2. Active site view of *Tb*PTR1 (white cartoon, active site residues in sticks with white carbons) in complex with the cofactor NADP(H) (in sticks, black carbons) and **3a** (in sticks, purple carbons). The inhibitor is surrounded by the omit map (green wire) contoured at the 2.5 σ level. H-bonds are represented as red dashed lines. Atom color code: nitrogen (blue), oxygen (red) and sulfur (yellow). (PDB ID: 6GCL)

Benzothiazoles design

In accordance with the binding mode of the 2-amino-benzothiazole fragment observed in the X-ray structure of *Tb*PTR1-NADP(H)-**3a** and the architecture of the parasitic *Tb*PTR1, new PTR1 inhibitors based on the benzothiazole scaffold were designed and synthesized. The catalytic pocket of *Tb*PTR1 is located in the deepest part of the active site and it is delimited by Phe97, Ser95, Arg14, Asp161, Leu209, Pro210, Tyr174 and the nicotinamide moiety of NADPH. The entrance of the pocket is a hydrophobic tunnel (hydrophobic pocket 1, Figure 3) formed by Val206, Trp221 and Met213 where the *p*-amino benzoic acid (*p*ABA) ring of a folic acid substrate is accommodated (see PDB: 3BMC²⁸). Next to hydrophobic pocket 1, a second hydrophobic pocket is present (Figure 3), delimited by Cys168, Val206, Phe97 and closed on the top by Phe171.

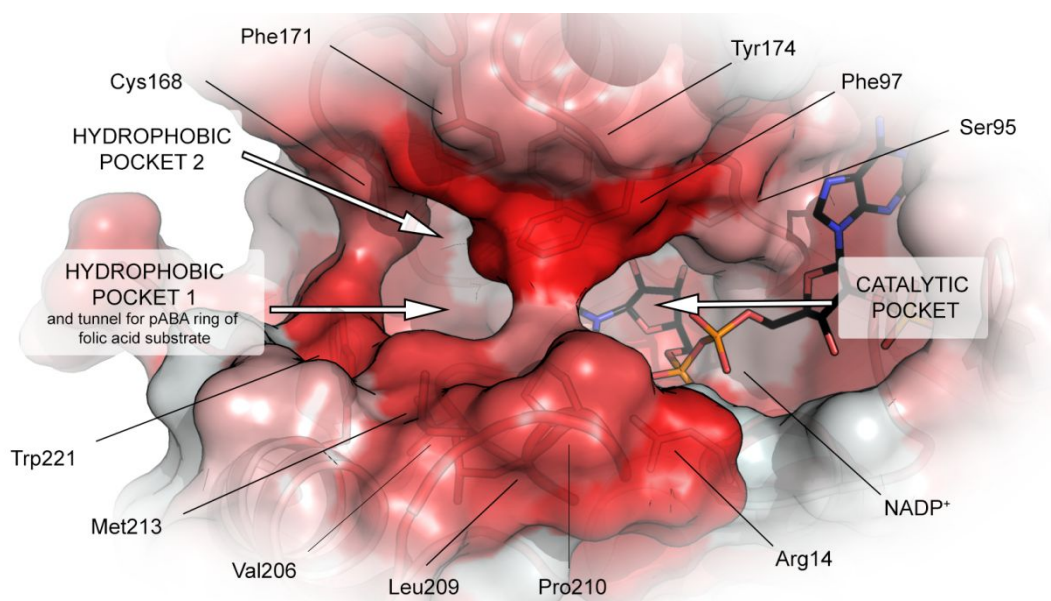
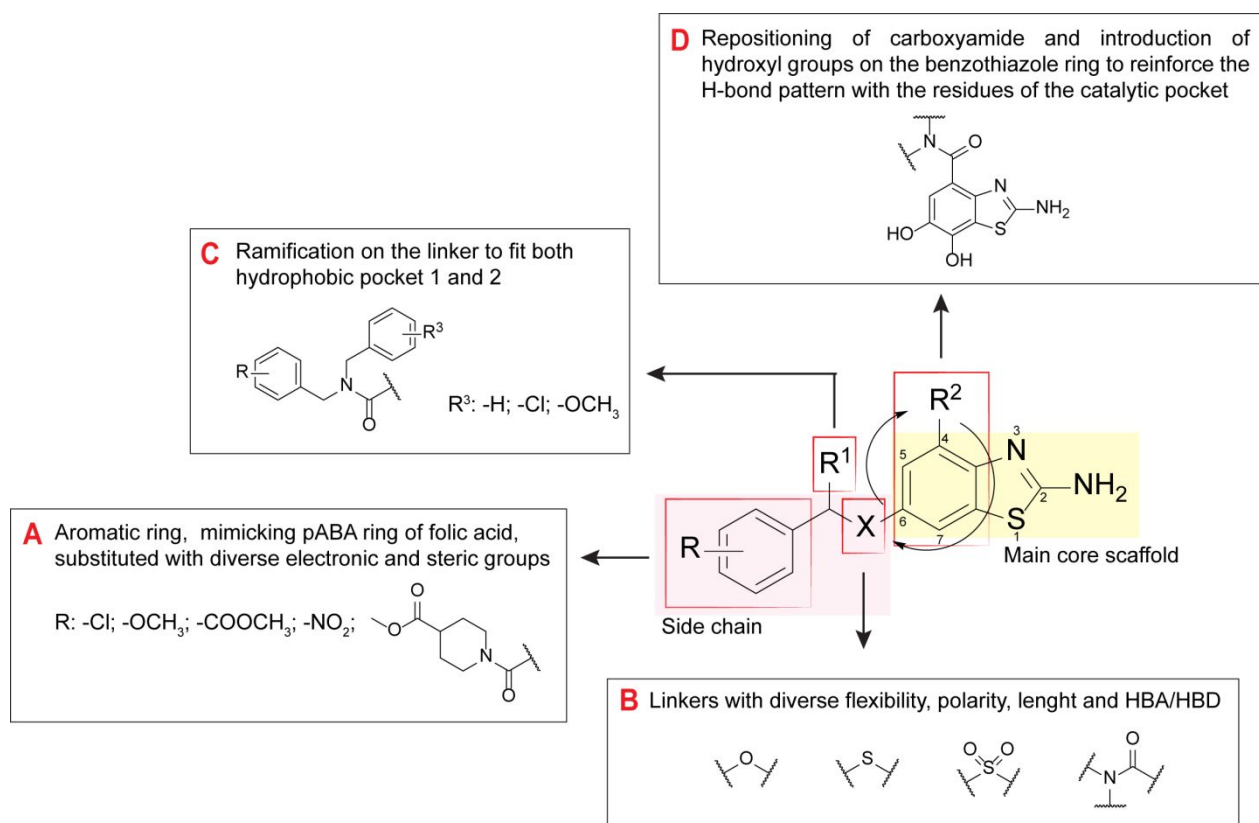


Figure 3. *Tb*PTR1 active site. The catalytic, primary and secondary hydrophobic pockets are highlighted. The surface of the protein is colored based on the hydrophobicity of the amino acid residues (from red: hydrophobicity to white: hydrophilicity). The relevant residues delimiting the pocket and NADP(H) are displayed as sticks. (PDB ID: 6GCL)

1
2
3
4
5
6 An internal virtual library of around 500 synthetically accessible benzothiazole derivatives was
7
8 rationally designed in a structure-based approach. The crystal structure of **3a** was taken as a
9
10 template for the design; the 2-amino-benzothiazole core scaffold anchors the molecule within the
11
12 catalytic pocket of the *TbPTR1* active site and during the design it was retained unaltered and
13
14 decorated as reported in Figure 4. The compounds were designed based on the following
15
16 considerations. Aliphatic or aromatic side chains were appended in position 6 of the benzothiazole
17
18 ring to probe the hydrophobic pocket 1 or the secondary hydrophobic cleft (Figure 4A). The side-
19
20 chain on C-6 of the aromatic substituent was linked to the main core scaffold by means of four
21
22 different linkers, varying in flexibility, polarity, lipophilicity and length (e.g. ether, sulfide, sulfone
23
24 and amide) as shown in Figure 4B. Moreover, more sterically hindered amidic derivatives were also
25
26 explored to simultaneously fill both hydrophobic pockets (Figure 4C). Finally, hydroxyl groups
27
28 were introduced at carbon 6 and carbon 7 on the benzothiazole core scaffold to explore the H-bond
29
30 interactions with the residues of the active site (Figure 4D). The diverse substituents were properly
31
32 combined to generate a library that was screened by molecular docking with Autodock 4.2 on the
33
34 3JQ7 crystal structure (see Supporting Information).^{28,29}
35
36
37
38
39
40
41
42
43
44
45
46
47
48
49
50
51
52
53
54
55
56
57
58
59
60



30 **Figure 4.** Main structural components of the 500 compounds virtual library based on the 2-
31 amino-benzothiazoles core.

32
33
34
35
36
37
38
39
40 The docking model was first validated by re-docking the DX2 inhibitor²¹ into the parent crystal
41 structure with the resulting RMSD being within 0.83Å. Thereafter, the virtual benzothiazole based
42 library was docked and docking poses were filtered first according to the predicted scores ($\Delta G_{\text{binding}}$
43 ranging from -6 to -9 kcal/mol). The ligand-protein complexes were then visually inspected and
44 compounds able to reproduce the binding pattern of the 2-amino-benzothiazole core scaffold
45 observed in the *TbPTR1*- NADP(H)-**3a** crystal structure were selected for synthesis (series 1-4,
46 Table 1-4). Figure 5 shows the most reliable predicted binding mode of the designed benzothiazoles
47 addressed by the synthesis.
48
49
50
51
52
53
54
55
56
57
58
59
60

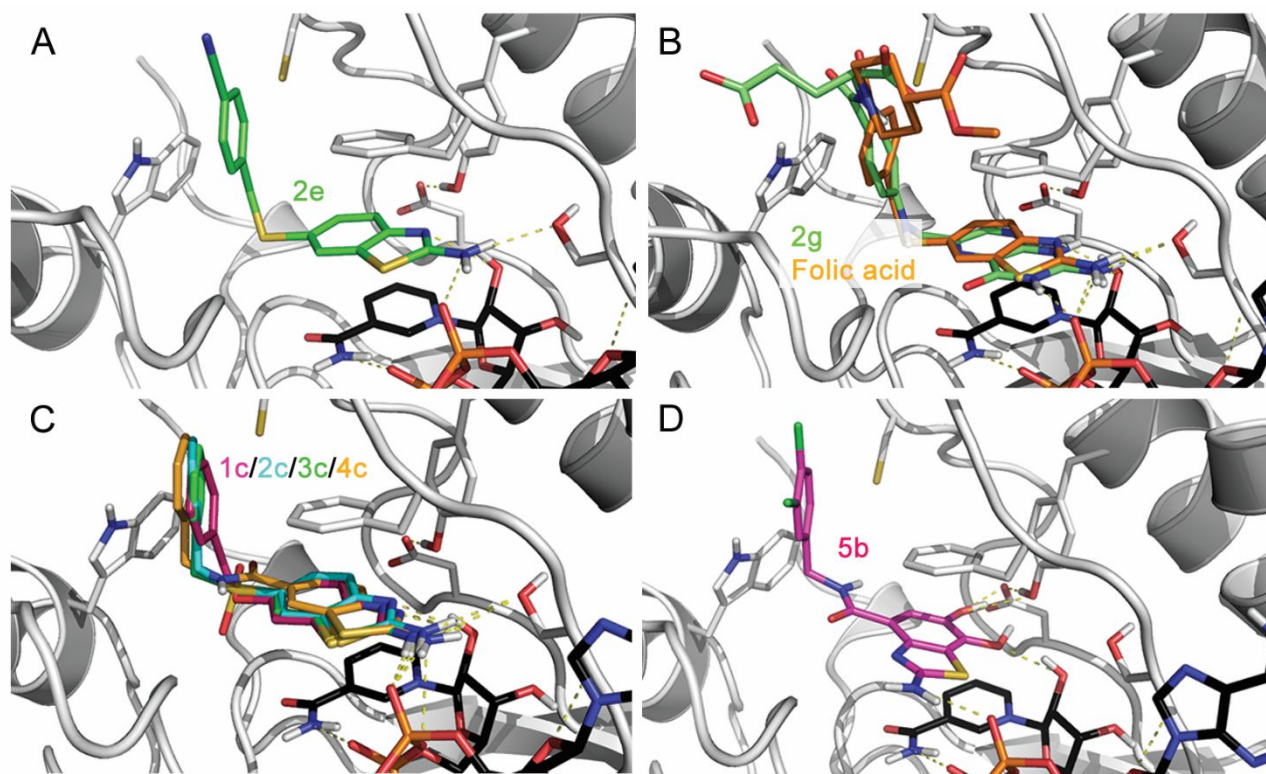
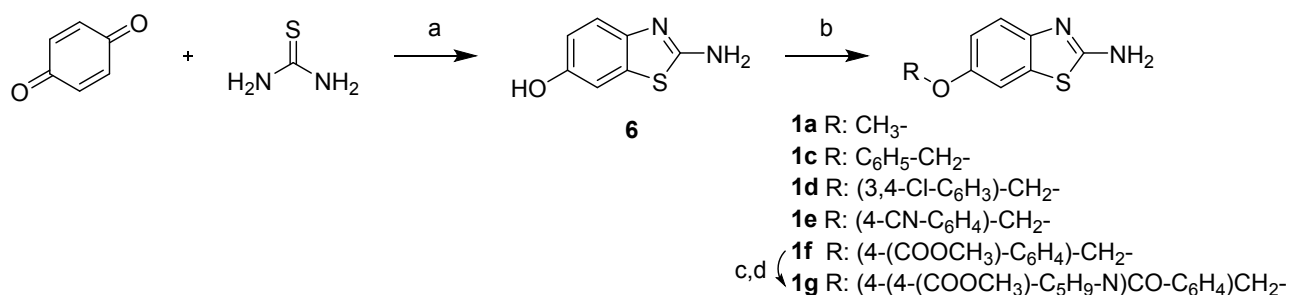


Figure 5. Predicted binding mode by docking calculation against *TbPTR1* of some representative designed benzothiazoles. A) Predicted pose of **2e** (green carbon) reproducing the binding mode of 2-amino-benzothiazole in the catalytic pocket and showing the placement of the aromatic side chain in the hydrophobic pocket 1. B) Superimposition of the ternary complex $\text{NADP}^+ - \text{TbPTR1} - \text{Folate}$ (PDB ID: 3BMC, folic acid in green carbons) and the predicted binding mode of **4g** (in orange carbons). C) Superposition of the predicted binding mode of four homologous benzothiazoles differing only for the linker (**1c**, **2c**, **3c** and **4c** respectively in magenta, cerulean, green and yellow carbons). D) Predicted binding mode of hydroxylated benzothiazole **5b** (in magenta carbons). Model atoms except for carbons are color coded with protein carbons (white), oxygen (red), nitrogen (blue), sulfur (yellow) and phosphorous (orange). The protein backbone is shown as white cartoon.

42 molecules with the best docking scores and poses were synthesized (Table 1-5). The four homologous series, in accordance with the linker type, were divided in etheric (**1a, c-g**, Table 1), sulfide (**2a-h**, Table 2), sulfone (**3a, c-g**, Table 3) and amide (**4c-h**, Table 4) benzothiazoles. Derivatives **1h**, **3b** and **4a-b** could not be synthesized. Assuming no more than one violation to the rule of 5, (molecular weight, number of H-bond donor and acceptor, number of rotatable bonds, $\log P_{o/w}$ and polar surface area), all the designed compounds were in accordance with Lipinski's rule (Table SI-1). The compounds passed the check for pan-assay interference compounds (PAINS) evaluated with the *in silico* tool FAFdrugs4.^{30,31}

Chemistry

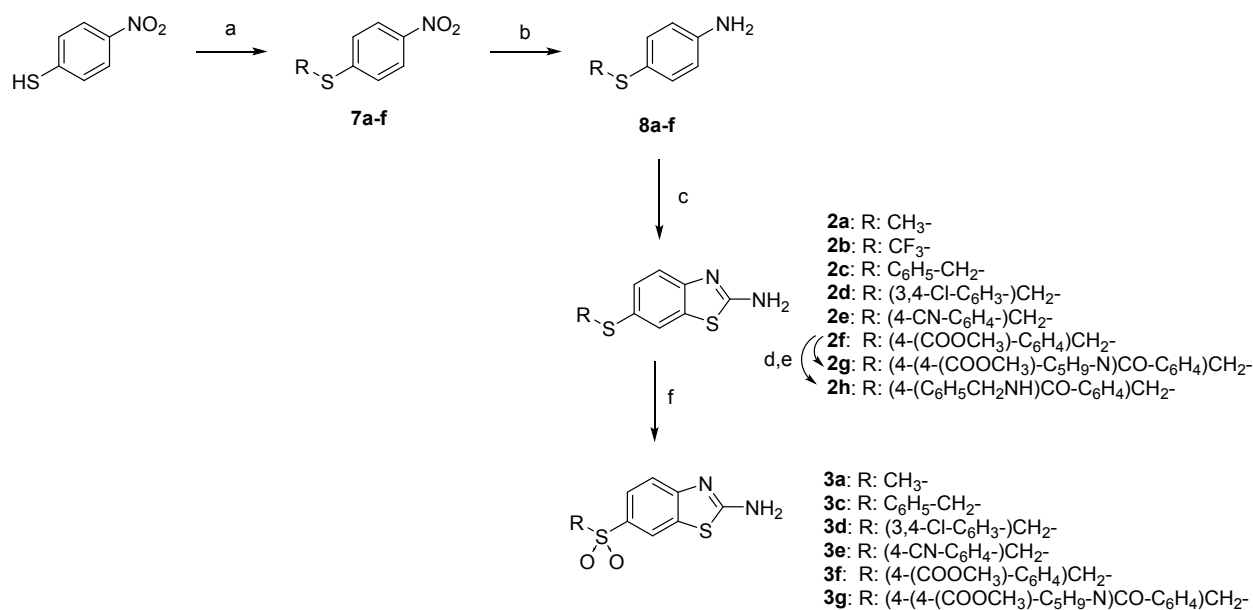
Etheric benzothiazoles **1a, c-g** were prepared as reported in **Scheme 1**. 6-hydroxy-2-aminobenzothiazole (**6**) was synthesized first through condensation between benzoquinone and thiourea in refluxing ethanol in presence of concentrated hydrochloric acid as catalyst. **6** was further reacted in standard S_N2 condition with iodomethane (to prepare **1a**) or with the appropriate benzyl-bromide to obtain **1c-f**. **1g** was synthesized by hydrolyzing **1f** with 1N NaOH in THF:MeOH 3:1 at room temperature for 24 hours. The carboxylic acid thus obtained was further reacted with methyl isonipecotate via standard coupling condition with EDC, HOBt in DMF at room temperature for 24 hours to give **1g**.



Scheme 1. Reagents and conditions: (a) HCl conc. (0.1 eq.), EtOH, refl., 6 h. (b) K₂CO₃ (2.5 eq.), DMF, r.t., 12 h. (c) 1N NaOH aq. (1.5 eq.), THF:MeOH 3:1, r.t., 24 h. (d) methyl isonipecotate (1

eq.), EDC (1 eq.), HOBT (1 eq.), DMF, 0°C to r.t, 24 h.

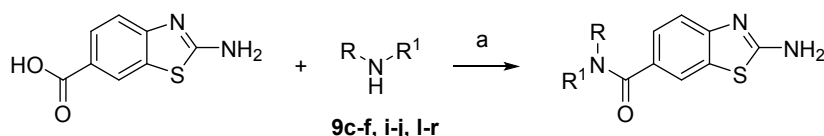
Synthesis of 6-(sulfone)-2-aminobenzothiazoles **3a, c-g** was performed as reported in **Scheme 2**, passing by the synthesis of the relative sulfides **2a-h**. 4-nitrothiophenol was reacted first with the appropriate benzyl bromide and K_2CO_3 as base in DMF to afford 4-nitro-*S*-benzylbenzenes **7a-f** that were subsequently reduced to the respective anilines **8a-f** with zinc and ammonium chloride in refluxing methanol. Anilines **8a-f** were then cyclized to benzothiazoles **2a-f** with potassium thiocyanate in glacial acetic acid using elemental bromine as oxidizing agent. For the synthesis of sulfides **2g-h**, **2f** was hydrolyzed first to carboxylic acid and consequentially reacted in standard coupling condition with methyl-isonipecotate (to give **2g**) or benzylamine (to give **2h**). Sulfides **2a-g** thus obtained were further oxidized to the respective sulfones **3a, c-g** with *m*-CPBA in DCM at room temperature for 24 hours. It was not possible to synthesize sulfones **3b** and **3h** due to decomposition of the precursors **2b** and **2h** in presence of oxidizing agents.



Scheme 2. Reagents and conditions: (a) K_2CO_3 (2.5 eq.), DMF, r.t., 24 h. (b) Zn (2 eq.), NH_4Cl

(2.5 eq.), MeOH, refl. 2 h. (c) Br₂ (2 eq.), KSCN (4 eq.), glacial acetic acid, T < 10 °C, 1-6 h. (d) 1N NaOH aq. (1.5 eq.), THF:MeOH 3:1, r.t., 24 h. (e) methyl isonipecotate (1 eq.) or benzylamine (1 eq.), EDC (1 eq.), HOBt (1 eq.), DMF, 0°C to r.t., 24 h. (f) *m*-CPBA (2 eq.), DCM, 0°C → r.t., 24 h.

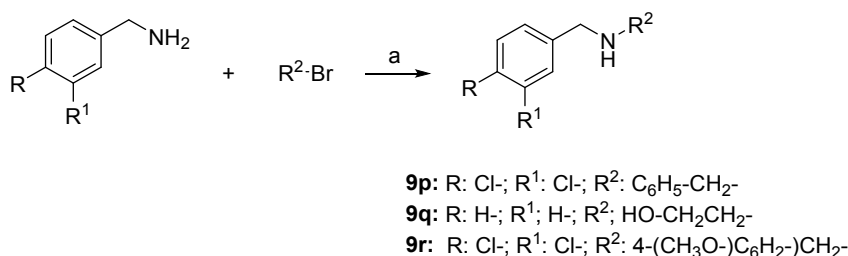
Synthesis of 6-amide-benzothiazoles **4c-r** was performed as depicted in **Scheme 3**. Commercially available 2-amino-6-carboxybenzothiazole was reacted with the appropriate amine **9c-f**, **i-j**, **l-r** through standard coupling conditions with EDC and HOBt as condensing agents, in DMF at room temperature for 24 hours. Amines **9c-f**, **i-j**, **l-o** were commercially available and directly used.



- 4c**: R: C₆H₅-CH₂-; R¹: H-
4d: R: (3,4-Cl-C₆H₃-)CH₂-; R¹: H-
4e: R: (4-CN-C₆H₄-)CH₂-; R¹: H-
4f: R: (4-(4-(COOCH₃)-C₆H₄-)CH₂-); R¹: H-
4g: R: (4-(4-(COOCH₃)-C₅H₉-N)-CO-C₆H₄)CH₂-; R¹: H-
4h: R: (4-(C₆H₅CH₂NH)CO-C₆H₄)CH₂-; R¹: H-
4i: R: (3,4,5-(CH₃O)-C₆H₂-)CH₂-; R¹: H-
4j: R: (2-NO₂-C₆H₄-)CH₂-; R¹: H-
4k: R: (2-NH₂-C₆H₄-)CH₂-; R¹: H-
4l: R: *bis*-(C₆H₅-)CH-; R¹: H-
4m: R: 4-(4-(COOCH₃)-C₅H₉-N-); R¹: H-
4n: R: 2-(2'-thiophenyl)-CH₂CH₂-; R¹: H-
4o: R: 2-(3'-indolyl)-CH₂CH₂-; R¹: H-
4p: R: (3,4-Cl-C₆H₃-)CH₂-; R¹: C₆H₅-CH₂-
4q: R: C₆H₅-CH₂-; R₁: HO-CH₂CH₂-
4r: R: (3,4-Cl-C₆H₃-)CH₂-; R¹: 3,4-(CH₃O)-C₆H₂-)CH₂-;

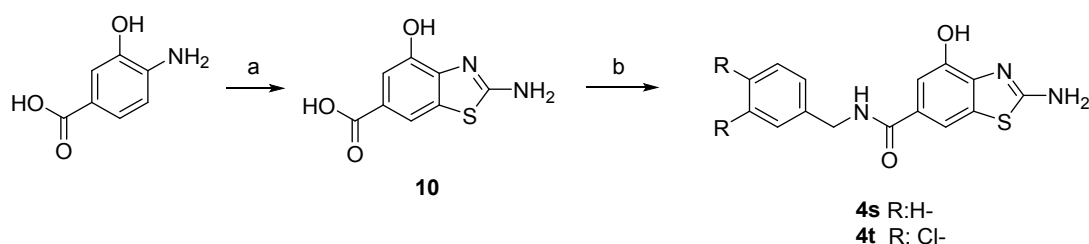
Scheme 3. Reagents and conditions: (a) EDC (1 eq.), HOBt (1 eq.), DMF, 0°C to r.t., 24 h; (b) 1N NaOH aq. (1.5 eq.), THF:MeOH 3:1, r.t., 24 h. (c) methyl isonipecotate (1 eq.) or benzylamine (1 eq.), EDC (1 eq.), HOBt (1 eq.), DMF, 0°C to r.t., 24 h; (d) Zn (2 eq.), NH₄Cl (2.5 eq.), MeOH, refl. 6 h.

Contrary, amines **9p-r** were synthesized first through S_N2 reaction between the appropriate benzylamines and alkylbromides (**Scheme 4**).



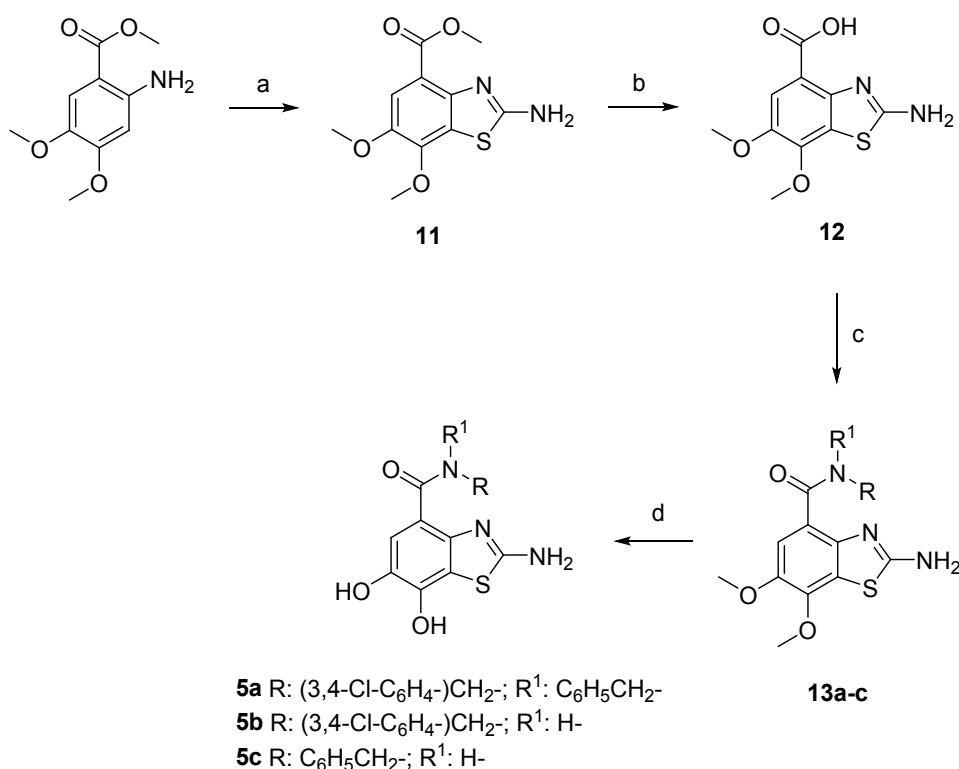
Scheme 4. Reagents and conditions: (a) benzylamine (2.5 eq.), alkylbromide (1.0 eq.), K₂CO₃ (2.5 eq.), DMF, r.t., 1-6 h.

6-amido-4-hydroxy-benzothiazoles **4s-t** were prepared as depicted in Scheme 5. 2-amino-6-hydroxy-benzothiazol-6-carboxylic acid **10** was synthesized first by cyclization of the respective aniline with potassium thiocyanate and bromine, in glacial acetic acid as previously described. **10** was further condensed with benzylamine (to give **4s**) or 3,4-dichlorobenzylamine (to give **4t**) in standard coupling conditions (**Scheme 5**).



Scheme 5. Reagents and conditions: (a) Br₂ (2 eq.), KSCN (4 eq.), glacial acetic acid, T < 10 °C, 1-6 h. (b) benzyl amines (1 eq.), EDC (1 eq.), HOBt (1 eq.), DMF, 0°C to r.t., 24 h.

Finally, for the synthesis of the catecholic 4-amido-benzothiazoles **5a-c**, the benzothiazole core was synthesized first starting from commercially available methyl 2-amino-4,5-dimethoxybenzoate by reaction with potassium thiocyanate and bromine, in glacial acetic acid as previously describe. The intermediate **11** was hydrolyzed to carboxylic acid **12** with aqueous NaOH and further condensed with the appropriate benzyl amine by coupling reaction. The methoxy groups of intermediates **13a-c** were deprotected with BBr_3 in DCM under nitrogen atmosphere to give the final products **5a-c** (Scheme 6).



Scheme 6. Reagents and conditions: (a) Br_2 (2 eq.), KSCN (4 eq.), glacial acetic acid, $T < 10^\circ\text{C}$, 1-6 h. (b) 1N NaOH aq. (1.5 eq.), THF:MeOH 3:1, r.t., 24 h. (c) benzyl amines (1 eq.), EDC (1 eq.), HOBt (1 eq.), DMF, 0°C to r.t., 24 h. (d) BBr_3 1M in DCM (6 eq.), dry DCM, N_2 , 0°C to r.t., overnight.

1
2
3 **Relationships between the structural properties, the enzymatic activity and the binding mode**
4 **to *Tb*PTR1.**
5
6

7
8 All 42 new benzothiazoles **1a-g**, **2a-h**, **3a,c-g**, **4c-t** and **5a-c** were evaluated for their inhibitory
9 activity against *T. brucei* and *L. major* PTR1, initially at 50 μM and those compounds yielding > 60
10 % inhibition were profiled in dose-response experiments to determine their potency. The results are
11 reported in Tables 1-5 and pyrimethamine was routinely utilised as a positive control compound
12 (*Tb*PTR1 IC_{50} 0.09 μM and *Lm*PTR1 IC_{50} 13.6 μM). Almost all the synthesized compounds showed
13 a measurable IC_{50} (< 100 μM) in the range of 0.3 – 57.6 μM against *Tb*PTR1 and 1.9 – 94 μM
14 against *Lm*PTR1. Eight compounds against *Tb*PTR1 (**1a**, **2a**, **3d-f**, **4i,s-t**) and 17 compounds against
15 *Lm*PTR1 (**1a**, **c-d**, **2a**, **3c-f**, **4g**, **i**, **m-r**, **t**) yielded IC_{50} > 100 μM and therefore were considered
16 inactive. Overall, the compounds resulted from 2 to 100-fold more active against *Tb*PTR1 than
17 *Lm*PTR1. Only compounds **3a**, **4j** and **5a-c** showed comparable activity against both PTR1
18 enzymes, whereas the only inversion in tendency was observed for **4s** showing *Lm*PTR1 IC_{50} = 2.48
19 μM but no inhibitory activity against *Tb*PTR1. The entire structure activity relationship is resumed
20 in Figure 6. In addition, the LE against *Tb*PTR1 was calculated for all the synthesized compounds.
21 LE, instead of IC_{50} , removes the bias due to the increased size of the ligands, highlighting the
22 structural modifications favourable or deleterious for the inhibitor. Focusing on *Tb*PTR1, the
23 elongation of the 2-amino-benzothiazole main scaffold in a folic acid substrate-like shape resulted
24 in a worthwhile strategy. The introduction of an aromatic ring as a side chain, able to mimic the
25 *p*ABA ring of folic acid, led to low/sub micromolar *Tb*PTR1 inhibitors. Docking calculations
26 predicted the side aromatic ring to be mainly placed in hydrophobic pocket 1, forming face-to-face
27 and edge-to-face π - π interactions with Trp221 or Phe97, respectively. On the contrary, compounds
28 **1-3a** or **4m**, possessing a methyl group or a non-aromatic ring, respectively as the side chain, were
29 completely inactive. The only exceptions were compounds **1b** and **2b** possessing a CF_3 group as
30 the side chain (*Tb*PTR1 IC_{50} = 15.1 and 0.50 μM for **1b** and **2b**, respectively). In particular, the
31
32
33
34
35
36
37
38
39
40
41
42
43
44
45
46
47
48
49
50
51
52
53
54
55
56
57
58
59
60

1
2
3 replacement of the oxygen atom of the starting benzothiazole **1b** with a sulphur atom in compound
4
5 **2b** resulted in a 30-times improvement of the inhibitor activity against *Tb*PTR1. The efficacy of this
6
7 chemical modification is reflected in the meaningful improvement in LE for **2b** (LE = 0.42)
8
9 compared to **1b** (LE = 0.32). The role of the linker was subsequently analysed. Sulfide derivatives
10
11 (*Tb*PTR1 IC₅₀ = 0.35 – 1.9 μM), followed by etheric derivatives (*Tb*PTR1 IC₅₀ = 0.67 – 15.1 μM)
12
13 resulted in the most active compounds of the library, compared to the homologous sulfone and
14
15 amide derivatives. The efficacy and the importance of the linker is reflected in the overall range of
16
17 LE of each subseries of compounds. Comparing benzothiazoles differing only for the linker
18
19 between the main core scaffold and the side chain, the higher LE was always observed for sulphide
20
21 (LE = 0.20 – 0.42) and etheric derivatives (LE = 0.18 to 0.32), followed by sulfones (LE = 0.14 –
22
23 0.25) and amides (LE = 0.15 – 0.26). The introduction of small polar substituents on the aromatic
24
25 ring (e.g. nitrile, nitro, amino and methyl ester) was always tolerated (*Tb*PTR1 IC₅₀ **1e** = 0.67 μM;
26
27 **1f** = 1.7 μM; **2e** = 0.35 μM; **2f** = 0.90 μM; **3e** = 3.00 μM) resulting in a LE ranging between 0.25
28
29 (for **3e**) and 0.31 (for **1e**). On the contrary, bulky side chains (e.g. phenyl ring in **4l**, indole in **4o** or
30
31 trimethoxy in **4i**) led to a drop both in activity and LE (< 0.19).
32
33
34
35
36
37

38 In our previous work¹⁶ we stated that the substitution of folate glutamate with the cyclic analogous
39
40 methyl isonipecotate was well tolerated for inhibitory activity against PTR1s. This structural
41
42 modification was therefore introduced on 2-amino-benzothiazole scaffolds to closely match the
43
44 structures of folic acid, resulting in compounds **1-4g** and **2,4h**. The improvement in activity for
45
46 these derivatives was only modest, as suggested in addition by a LE < 0.20, probably due to the
47
48 exposition of the folic acid side chain to the solvent (*Tb*PTR1 IC₅₀ **1g** = 3.3 μM; **2g** = 0.93 μM; **3g** =
49
50 24.3 μM; **4g** = 21.8 μM).
51
52
53
54

55 The introduction of a hydroxyl group in position 4 on the benzothiazole ring (**4s-t**) resulted in a
56
57 significant reduction in inhibitory activity against *Tb*PTR1. From docking calculation, the hydroxyl
58
59 group appears to force the benzothiazole ring to assume an unusual pose within the active site. The
60

scaffold is flipped by 180° with the intra-ring sulphur pointing toward Tyr174, and the benzothiazole displaced from the standard stacking geometry between Phe97 and NADP(H).

All the tested compounds were twice to 100-times less active against *Lm*PTR1 than *Tb*PTR1 reflecting the efficacy of the design which was mainly performed on the architecture of the *Tb*PTR1 enzyme. Even though an overall comparable SAR among the two enzymes can be observed, these differences are presumable due to the structural diversity of the distal region of the binding site of the two enzymes. Contrary to *Tb*PTR1, *Lm*PTR1 possesses a more polar and solvent-exposed active site entrance surface.²⁴ Thus, the elongation of the 2-amino-benzothiazole main scaffold in a folic acid substrate-like shape, pointed the side chain toward a polar area, preventing the capability of the side benzyl ring to form π - π stacking or additional hydrophobic contacts (as in *Tb*PTR1), probably explaining the observed lower activity against *Lm*PTR1 compared to *Tb*PTR1.

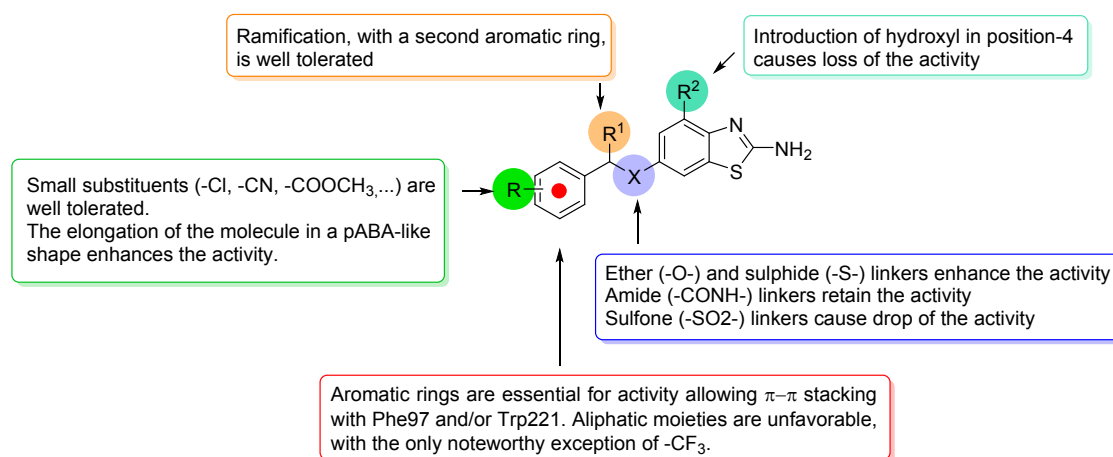


Figure 6. Schematic highlights of the structure-activity relationship of the synthesized compounds against *Tb*PTR1 and *Lm*PTR1. All the inhibitors resulted more active against *Tb*PTR1 than *Lm*PTR1. The above reported structure-activity considerations are consistent for both enzymes.

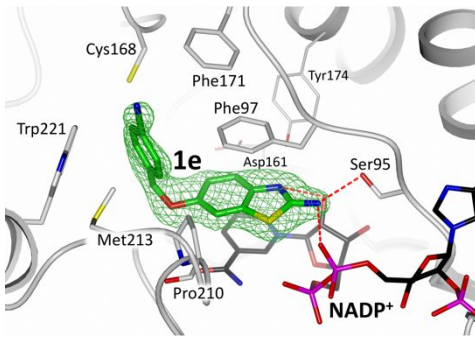
A notable exception is represented by three compounds of series 5 (**5a-c**), showing comparable inhibitory activity against both enzymes. From docking calculations, these sub-classes of

1
2
3 benzothiazoles could assume a different binding mode (Figure 5D) compared to the poses of series
4
5 1-4, allowing them to adapt to both *Tb*PTR1 and *Lm*PTR1 binding sites.
6
7

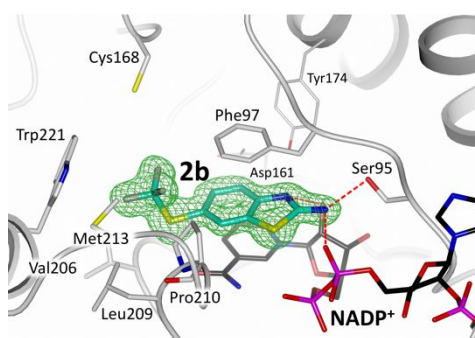
8 **Comparison between crystallographic ternary complexes of the inhibitors with *Tb*PTR1 and -**
9 **NADP(H) with the docked binding modes.**
10

11
12
13 Compounds showing IC₅₀ values lower than 1 μM and a low toxicity and seven compounds
14
15 belonging to series 4 bearing a high structural diversity were subjected to structural studies. The
16
17 structure of *Tb*PTR1 was solved in complex with the cofactor NADP(H) and nine benzothiazole
18
19 derivatives (**1e**, **2b**, **2d**, **2g**, **2h**, **4c**, **4d**, **4g** and **4i**) showing IC₅₀ values ranging from 0.5 μM
20
21 (compounds **2b** and **2h**) to 21.8 μM (compound **4g**). In all structures, described in Table 6, the
22
23 shared benzothiazole core of the inhibitors adopts a highly conserved binding mode, retaining also
24
25 the same interaction patterns described for the forefather **3a**.
26
27
28
29
30
31
32
33
34
35
36
37
38
39
40
41
42
43
44
45
46
47
48
49
50
51
52
53
54
55
56
57
58
59
60

Table 6. Crystal structures of *TbPTR1* in complex with NADP(H) and the benzothiazole compounds. A brief description of the main interactions entailed by the inhibitors in the catalytic pocket is reported (the shared benzothiazole moiety forms conserved interactions in the cavity, as already described for the forefather **3a**). The picture column reports an active site view of *TbPTR1* (white cartoon and carbon atoms) in complex with the cofactor NADP(H) (in sticks, black carbons) and **1e** (in sticks, green carbons), **2b** (in sticks, cyan carbons), **2d** (in sticks, light blue carbons), **2g** (in sticks, brown carbons), **2h** (in sticks, lilac carbons), and **4c** (in sticks, orange carbons), **4d** (in sticks, dark green carbons), **4g** (in sticks, dark red carbons), and **4l** (in sticks, pink carbons). Inhibitors are surrounded by their omit map (green wire) contoured at the 2.5 σ level. Water molecules are represented as red spheres and H-bonds as red dashed lines. Atom color code: nitrogen (blue), oxygen (red), sulfur (yellow), phosphorous (magenta), chlorine (dark grey) and fluorine (grey).

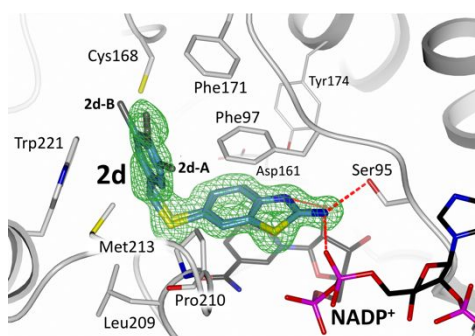
Complex	Picture	Description
<i>TbPTR1</i> – NADP(H) – 1e		<ul style="list-style-type: none"> • PDB: 6GCK • Resolution: 2.14 Å • 4-cianophenyl moiety of 1e (IC₅₀ of 0.67 μM) is stabilized in pocket 1 by van der Waals interactions with Phe97, Leu209, Pro210, Met213, and Trp221 (interactions shared within the tetramer). • 1e populates four subunits of the tetramer (100 % occupancy).

***Tb*PTR1 –
NADP(H) – 2b**



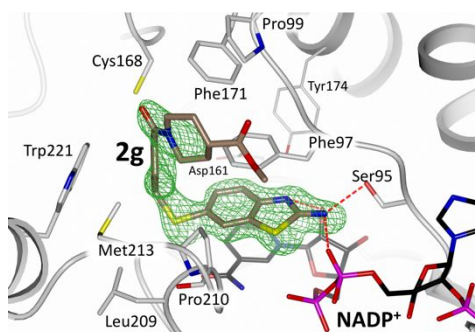
- PDB: **6GCQ**
- Resolution: 1.58 Å
- Trifluoromethyl moiety of **2b** (IC_{50} of 0.5 μ M) is accommodated in the active site pocket 1 (halogens directed towards Phe97, Pro210, and Trp221 in all enzyme subunits).
- **2b** populates four subunits of the tetramer (70-100% occupancy).

***Tb*PTR1 –
NADP(H) – 2d**



- PDB: **6GCP**
- Resolution: 1.52 Å
- The 3,4-dichlorophenyl moiety of **2d** (IC_{50} of 0.9 μ M), stabilized in pocket 1 by van der Waals interactions with Phe97, Leu209, Pro210, Met213, and Trp221, is observed in two alternate orientations (named 2d-A and 2d-B, mutually rotated by 180°).
- In chain B, only one conformation (having the *m*-chlorine facing Pro210) is visible.
- **2d** populates four subunits of the tetramer (90% occupancy).

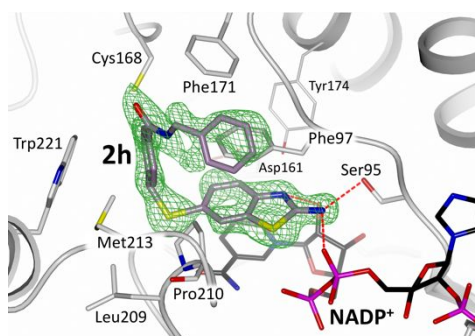
***Tb*PTR1 –
NADP(H) – 2g**



- PDB: **6GDO**
- Resolution: 1.78 Å
- The molecule of **2g** (IC_{50} of 0.93 μ M) is completely rebuilt only in chain D, whereas in chain C, only the cofactor is visible (60 % occupancy).
- Phenyl ring of **2g** is stabilized in pocket 1 by van der Waals interactions with Phe97, Leu209, Pro210, Met213, and Trp221.
- Piperidine moiety of **2g** forms hydrophobic interactions with Phe171 and Pro99.
- **2g** populates three subunits of the

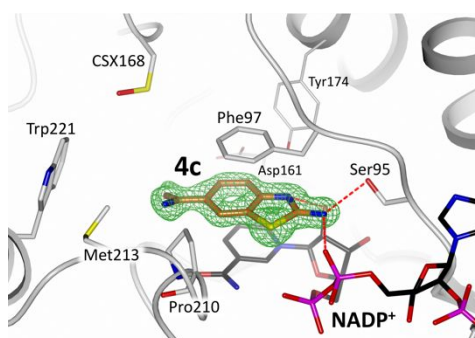
tetramer (80% occupancy).

***Tb*PTR1 –
NADP(H) – 2h**



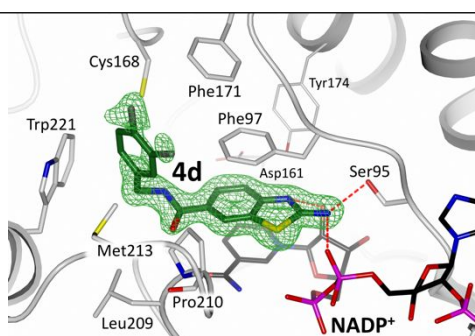
- PDB: **6GEX**
- Resolution: 1.78 Å
- The molecule of **2h** (IC_{50} of 0.5 μ M) is completely rebuilt only in chain D (highly flexible terminal phenyl ring) whereas in chain C, only the cofactor is detected (60 % occupancy).
- Phenyl ring of **2g** is stabilized in pocket 1 by van der Waals interactions with Phe97, Leu209, Pro210, Met213, and Trp221.
- **2h** populates three subunits of the tetramer (80% occupancy).

***Tb*PTR1 –
NADP(H) – 4c**



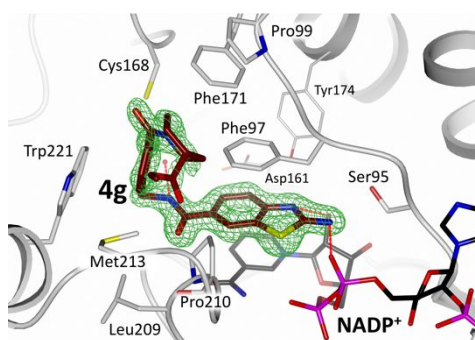
- PDB: **6GD4**
- Resolution: 1.42 Å
- The phenyl moiety on the variable tail of **4c** (IC_{50} of 10.0 μ M) is highly flexible (excluded from our model, only molecular core and amide linker of the inhibitor are traced).
- Cys168 is modified as S-oxy-cysteine (CSX168) in the four subunits of the tetramer.
- **4c** populates four subunits of the tetramer (50-80% occupancy).

***Tb*PTR1 –
NADP(H) – 4d**



- PDB: **6GEY**
- Resolution: 1.56 Å
- The 3,4-dichlorophenyl of **4d** (IC_{50} of 5.4 μ M) is stabilized in the hydrophobic pocket 1 by van der Waals interactions with Phe97, Leu209, Pro210, Met213, and Trp221.

***Tb*PTR1 –
NADP(H) – 4g**



- Different orientations of the 3,4-dichlorophenyl moiety are observed within the tetramer (Figure SI-1).

- **4d** populates four subunits of the tetramer (60-90% occupancy).

- PDB: **6GD0**

- Resolution: 1.74 Å

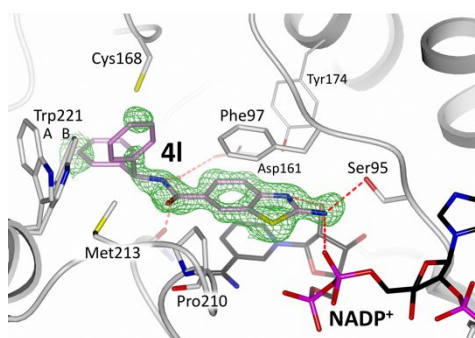
- The molecule of **4g** (IC_{50} of 21.8 μ M) is completely rebuilt only in chain A.

- The phenyl moiety of **4g** is stabilized in pocket 1 by van der Waals interactions with Phe97, Val206, Leu209, Pro210, Met213, and Trp221.

- The amide nitrogen of **4g** forms a network of water mediated interactions within the active site.

- **4g** populates three subunits of the tetramer (90% occupancy).

***Tb*PTR1 –
NADP(H) – 4l**



- PDB: **6GPD**

- Resolution: 1.52 Å

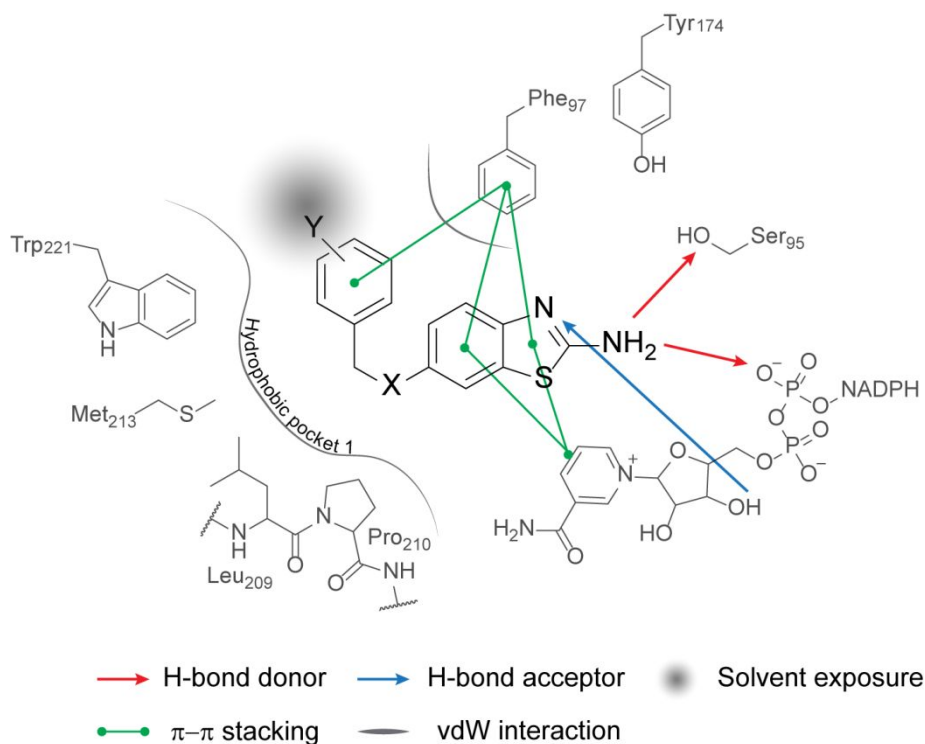
- Two alternate states are observed in the catalytic cavity: ligand-bound (aperture of Trp221, A-conf) and ligand-free (closure of Trp221, B-conf) states (estimated to 50 %).

- Phenyl moieties of **4l** (IC_{50} of 18.5 μ M) occupy the hydrophobic pockets 1 (van der Waals interaction with Trp221 and Met213) and 2 (Figure 3).

- The amide nitrogen of **4l** forms water mediated interactions with Asp161 and Gly205 (backbone oxygen).

- **4l** populates three subunits of the tetramer (50% occupancy).

1
2
3 The analysis of the ten ternary X-ray complexes (Figure 2 and Table 6) revealed a conserved
4 binding mode and some common interactions of the ten inhibitors within *Tb*PTR1. In all ten
5 binding mode and some common interactions of the ten inhibitors within *Tb*PTR1. In all ten
6 binding mode and some common interactions of the ten inhibitors within *Tb*PTR1. In all ten
7 binding mode and some common interactions of the ten inhibitors within *Tb*PTR1. In all ten
8 complexes, the benzothiazole core is always located within the catalytic pocket of *Tb*PTR1,
9 complexes, the benzothiazole core is always located within the catalytic pocket of *Tb*PTR1,
10 interacting with the four key amino acids (Ser95, Phe97, Asp161 and Trp221) and NADP(H), as
11 interacting with the four key amino acids (Ser95, Phe97, Asp161 and Trp221) and NADP(H), as
12 previously described (Figure 7). The main contribution to binding originates from the π -stacking
13 previously described (Figure 7). The main contribution to binding originates from the π -stacking
14 between the nicotinamide moiety of NADP(H) and Phe97 and H-bonds with phosphate or ribose
15 between the nicotinamide moiety of NADP(H) and Phe97 and H-bonds with phosphate or ribose
16 hydroxyls of the cofactor. An additional conserved H-bond interaction is always observed between
17 hydroxyls of the cofactor. An additional conserved H-bond interaction is always observed between
18 the amino group in position 2 on the benzothiazole ring and the hydroxyl group of Ser95.
19 the amino group in position 2 on the benzothiazole ring and the hydroxyl group of Ser95.
20 Additional weak electrostatic interaction with Asp161 was observed for sulfone (for **3a**) or amide
21 Additional weak electrostatic interaction with Asp161 was observed for sulfone (for **3a**) or amide
22 (for **4d,g,l**) benzothiazoles. Moreover, for all the inhibitors possessing an aromatic ring as the side
23 (for **4d,g,l**) benzothiazoles. Moreover, for all the inhibitors possessing an aromatic ring as the side
24 chain, mimicking the *p*ABA moiety of the folate substrate (**1e**, **2d,g,h**, **4g,l**), the side-chain is
25 chain, mimicking the *p*ABA moiety of the folate substrate (**1e**, **2d,g,h**, **4g,l**), the side-chain is
26 always located within the hydrophobic pocket 1 stabilized by van-der-Waals (vdW) interactions
27 always located within the hydrophobic pocket 1 stabilized by van-der-Waals (vdW) interactions
28 with Leu209, Pro210, Met213, and Trp221, and mainly by face-to-edge π - π stacking with Phe97
29 with Leu209, Pro210, Met213, and Trp221, and mainly by face-to-edge π - π stacking with Phe97
30 (Figure 7).
31 (Figure 7).
32 (Figure 7).
33 (Figure 7).
34 (Figure 7).
35 (Figure 7).
36 (Figure 7).
37 (Figure 7).
38 (Figure 7).
39 (Figure 7).
40 (Figure 7).
41 (Figure 7).
42 (Figure 7).
43 (Figure 7).
44 (Figure 7).
45 (Figure 7).
46 (Figure 7).
47 (Figure 7).
48 (Figure 7).
49 (Figure 7).
50 (Figure 7).
51 (Figure 7).
52 (Figure 7).
53 (Figure 7).
54 (Figure 7).
55 (Figure 7).
56 (Figure 7).
57 (Figure 7).
58 (Figure 7).
59 (Figure 7).
60 (Figure 7).



1
2
3 **Figure 7.** Common binding interactions of benzothiazoles with the main amino acids delimiting
4 the *TbPTR1* active site and NADPH based on the crystallographic ternary complex of compounds
5
6
7
8 **1e, 2b,d,g-h, 3a, 4c-d,g,l.**
9

10
11
12
13 The binding mode of the ten benzothiazoles crystalized was compared by superimposition with the
14 respective docking poses (Figure 8B-K). In both X-ray and docked poses, the main 2-amino-
15 benzothiazole core always shows the same binding mode and orientation within the *TbPTR1*
16 catalytic pocket. In addition, the orientation and placement of the side chain are well reproduced for
17 the inhibitors with small ‘tails’ attached to the main benzothiazole scaffold (such as for compounds
18 **1e, 2b,d, 3a, 4c,d,l**). On the contrary, for compounds **4g** (Figure 8D), **2g** (Figure 8J) and **2h** (Figure
19 8K) the distal part of the longer side chain is not well reproduced, since it points outside the
20 confined *TbPTR1* pocket and can assume multiple conformations. An overall good correlation
21 between the *TbPTR1* pIC₅₀ of all inhibitors and the respective Autodock Docking Score was
22 observed (Figure 8A, Table SI-4), revealing the capability of the docking protocol and the design
23 and selection strategy adopted to foresee valid potential *TbPTR1* inhibitors.
24
25
26
27
28
29
30
31
32
33
34
35
36
37
38
39
40
41
42
43
44
45
46
47
48
49
50
51
52
53
54
55
56
57
58
59
60

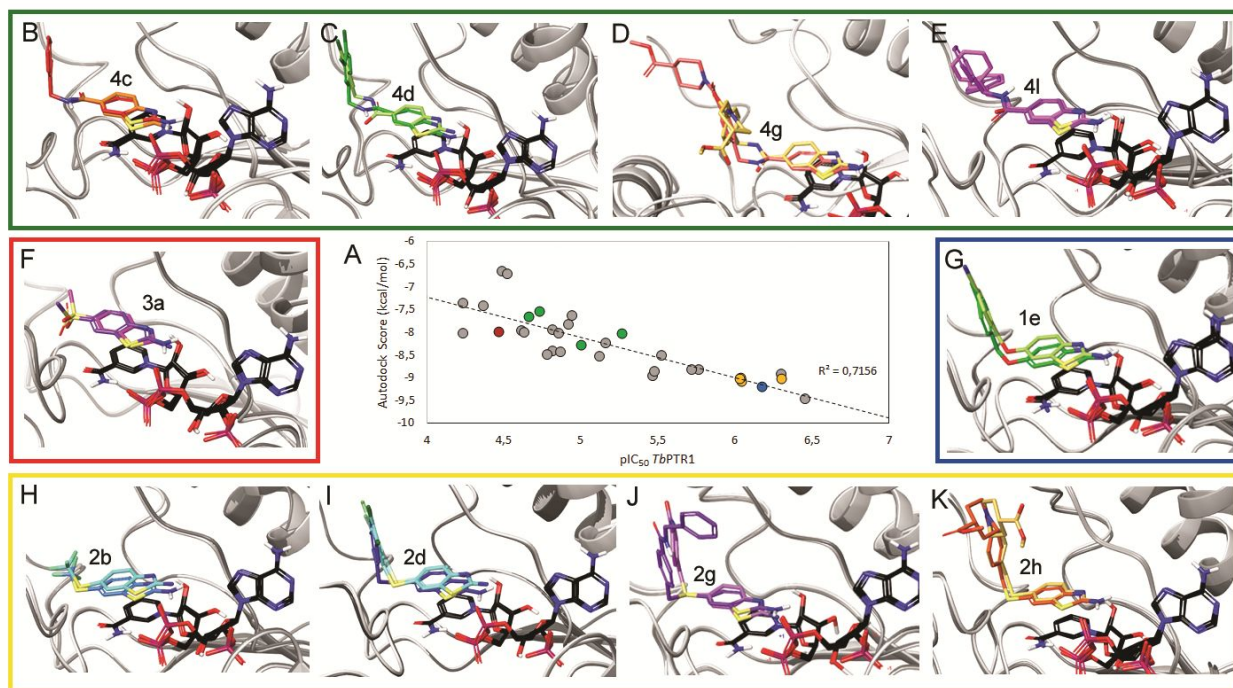


Figure 8. (A) Correlation between the enzymatic inhibitor activity against *TbPTR1* (expressed as pIC_{50}) and the Autodock Score. Colored dots correspond to the inhibitors for which the X-ray complex is available. The color of the dots is in accordance with the chemical series: ether (blue), sulfide (yellow), sulfone (red), amide (green). (B-K) Superimposition between the binding mode observed by X-ray crystallography and the respective pose predicted by docking calculation for inhibitors **4c** (B, carbon in light orange for X-ray pose and in red for docked pose), **4d** (C, carbon in light green for X-ray pose and in dark green for docked pose), **4g** (D, carbon in yellow for X-ray pose and in orange for docked pose), **4l** (E, carbon in purple for X-ray pose and in violet for docked pose), **3a** (F, carbon in purple for X-ray pose and in violet for docked pose), **1e** (G, carbon in light green for X-ray pose and in dark green for docked pose), **2b** (H, carbon in cerulean for X-ray pose and in blue for docked pose), **2d** (I, carbon in cerulean for X-ray pose and in blue for docked pose), **2g** (J, carbon in purple for X-ray pose and in violet for docked pose), **2h** (K, carbon in yellow for X-ray pose and in orange for docked pose). The X-ray poses are colored in lighter tone and the docked pose in a darker tone. Color code: nitrogen (blue), oxygen (red), sulfur (yellow), phosphorous (magenta), chlorine (dark green), fluorine (green).

Anti-parasitic activity as single agents and in combination

All synthesized benzothiazoles were evaluated first for *in-vitro* anti-parasitic activity against cultured bloodstream forms of *T. brucei*. To evaluate a potential broad-spectrum anti-trypansomatidic activity all the compounds were in addition screened against the amastigote form of *Leishmania infantum* (*L. infantum*) and trypomastigote form of *T. cruzi*, which reproduce a more physiological and disease-relevant model. Human leukemic monocyte cell line THP-1 was infected with *L. infantum* while osteosarcoma human U2OS cell-line was infected with trypomastigote forms of the Y strain of *T. cruzi*. Compounds were screened at 10 μ M against *T. brucei* and intracellular amastigote *L. infantum*, and at 50 μ M against intracellular amastigote *T. cruzi* during a HTS phenotypic screening campaign that included thousands of compounds. The anti-parasitic activity was expressed as % of parasitic cell growth inhibition at the defined compound concentration. For compounds associated with > 60 % cell growth inhibition (against *T. brucei* and *L. infantum*) and > 85 % cell growth inhibition (against *T. cruzi*), dose-response studies were performed to determine the EC₅₀ values (Table 1-5). The *T. brucei* assay relied on indirect determination of parasite population viability by quantification of total DNA present in the well using the Sybr Green I DNA fluorescent dye.³² Pentamidine was used as the reference compound exhibiting an EC₅₀ of 3.8 nM which is comparable with the value reported in literature.³³ Amphotericin B and miltefosine were utilized as positive controls in the *L. infantum* assay yielding EC₅₀ 1.14 μ M and 1.29 μ M respectively, while benznidazole was used as reference compound in the *T. cruzi* assay, exhibiting an EC₅₀ of 2.4 μ M, which is comparable with the value reported in literature.³⁴ Almost all tested benzothiazoles yielded weak anti-*T. brucei* activity ranging below 20 % cell growth inhibition at 10 μ M (Table 1-5). Only three compounds (**4c**, **4r** and **4t**) showed a % cell growth inhibition > 60 % at 10 μ M resulting in an EC₅₀ of 7.0 μ M (**4c**), 9.7 μ M (**4r**) and 5.9 μ M (**4t**) respectively. In contrast, no compounds showed an appreciable anti-parasitic activity

1
2
3 against the two intracellular forms of *L. infantum* and *T. cruzi* (% cell growth inhibition < 21 % at
4
5 10 μM , Table 1-5).
6
7

8
9 As stated before, the effective inhibition of parasite growth can be observed if both PTR1 and
10 DHFR enzymes are inhibited.¹⁷ On this basis, we studied the effect of the PTR1 inhibitors in
11 combination with MTX, a known DHFR inhibitor, against *T. brucei* to observe the potentiation
12 effect that the PTR1 inhibitors have on MTX parasite growth inhibition. With this aim, we selected
13 some inhibitors showing the highest inhibition effect against *Tb*PTR1, namely, compounds **1d-e**,
14 **2b,d-h**, **3e** and **4c**. The selected compounds were combined at 10 μM with MTX at 4 μM
15 (corresponding to the EC_{30} against *T. brucei*).²⁴ Only compound **4c** was tested at 1 μM , because it
16 showed an anti-parasitic activity >80% at 10 μM which is an inhibition potency too high to allow
17 any potentiation effects in combination to be observed. The anti-parasitic activity was expressed as
18 % cell growth inhibition and is reported in Figure 9 and Table 7. The potency in combination
19 studies was estimated through determination of a Potentiating Index (PI) given by **eq. 1**.
20
21
22
23
24
25
26
27
28
29
30
31
32
33

$$PI = \frac{\% \text{ inhibition of the combination}}{(\% \text{ inhibition of compound} + \% \text{ inhibition at } 4 \mu\text{M MTX})} \quad \text{eq. 1}$$

34
35
36
37
38
39
40

41 A PI higher than 1 reflects the capacity of the compounds to increase the anti-parasitic activity of
42 MTX beyond what would be expected by the simple addition of the individual effects (Figure 9 and
43 Table 7). A PI effect was observed for all compounds except for **2d** and **2b**. Compounds **1e** and **2f**
44 were most potent compounds showing $\text{PI} > 2$.
45
46
47
48
49
50
51
52
53
54
55
56
57
58
59
60

Table 7. *T. brucei* antiparasitic activity of compounds **1d-e**, **2b,d-h**, **3e**, **4c** tested as single agents (at 10 μ M) and potentiation of MTX activity in combination.

Compound	% <i>T. brucei</i> growth inhibition		PI
	Single agent (at 10 μ M)	+ 4 μ M MTX	
MTX	19 \pm 6	Not detectable	-
1d	55 \pm 1	89 \pm 8	1.2 \pm 0.1
1e	21 \pm 5	80 \pm 2	2.0 \pm 0.0
2b	11 \pm 0	33 \pm 7	1.1 \pm 0.1
2d	41 \pm 4	65 \pm 4	1.1 \pm 0.0
2e	29 \pm 5	63 \pm 1	1.3 \pm 0.3
2f	7 \pm 11	69 \pm 7	2.7 \pm 0.4
2g	53 \pm 3	93 \pm 1	1.3 \pm 0.0
2h	33 \pm 12	80 \pm 0	1.6 \pm 0.2
3e	13 \pm 4	48 \pm 8	1.5 \pm 0.2
4c^a	Not detectable	30 \pm 5	1.6 \pm 0.1

a. tested at 1 μ M

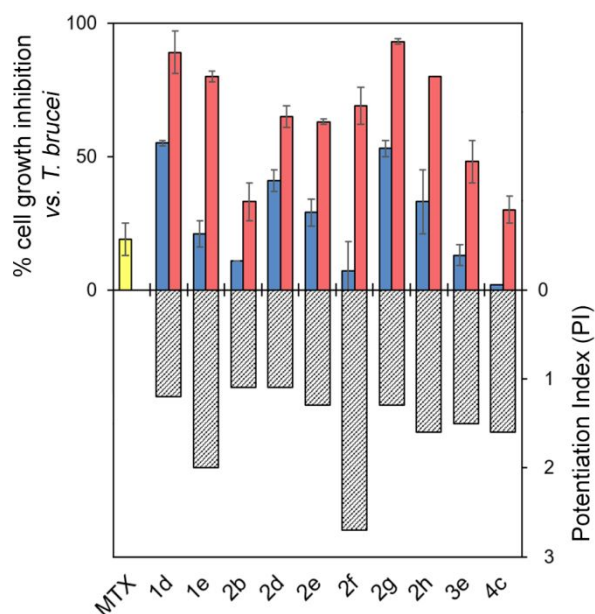


Figure 9. Anti-parasitic activity against *T. brucei* of compounds **1d-e**, **2b,d-h**, **3e** tested as single agent at 10 μ M (in cerulean) and in combination with 4 μ M of MTX (in vermillion). Compound **4c** was tested at 1 μ M as a single agent. The anti-parasitic activity of MTX as single agent at 4 μ M is reported as a blue bar. As a quantitative measure of potentiation, a PI of the combination was determined (lined bar).

Early ADME-Toxicity studies

Early toxicity studies were performed for all compounds synthesized with the aim to identify liabilities and to select the safest compounds among the most active compounds, for progression towards further studies. The panel of early toxicity assays included (1) cardiac toxicity by measuring the inhibitory effect on human cardiac potassium channel (*h*ERG), (2) inhibition of five major drug metabolizing cytochrome P450 enzymes (CYP 1A2, 2C9, 2C19, 2D6, 3A4), (3) cytotoxicity against three human cell-line, namely A549 (human lung adenocarcinoma epithelial cells), THP-1 (macrophages-like cells), U2OS (osteosarcoma cells) and (4) mitochondrial toxicity in 786-O (renal carcinoma) cell-line. Compounds were initially screened at 10 μ M against *h*ERG, CYPs, mitochondria and A549 cell-lines and at 50 μ M against U2SO cells and for active compounds, the respective IC₅₀ values and GI₅₀ against cell lines were experimentally determined. Cytotoxicity against THP-1 macrophages was expressed as No Observed Adverse Effect Level (NOAEL), measuring the maximum dose administered without observing toxic effects. The early ADME-toxicity studies were performed for all the synthesized compounds **1a-g**, **2a-h**, **3a,c-g**, **4c-t**, **5a-c** and reference drugs pentamidine. The data were organized using a traffic light representation for rapid and intuitive visualization of the complex data set (Figure 10).

To reduce the liabilities of the compounds an IC₅₀ or GI₅₀ > 10 μ M was set as the cut-off for an acceptable liability profile²⁴, following the features a compound that should behave as a good inhibitor *in vitro*, should have for progression to animal studies according to the TIP. An ideal compound should have all parameters colored in green in Figure 9. Almost all the evaluated benzothiazoles showed a safe early toxicity profile against *h*ERG, CYP isoforms and cell-lines. Only a few compounds showed toxicity (IC₅₀ < 10 μ M) against *h*ERG (i.e. **1a**, **1c**, **2a**, **4g**, **4n** and **5a**) and mitochondria (i.e. **1a**, **2a**, **2e**, **4d**, **4g** and **4j**). No cytotoxicity was observed against U2OS and THP-1 and only three compounds resulted cytotoxic against A549 with GI₅₀ < 10 μ M (**1a**, **2b** and **2h**). In contrast, benzothiazoles appeared to interfere with the activity of CYP isoforms with

1
2
3 particular impact on CYP2D6 and CYP3A4. However, the absolute IC₅₀ and GI₅₀ should be
4
5 compared with the EC₅₀ against the target parasite for the determination of a Selectivity Index (SI),
6
7 calculated as a ratio of the IC₅₀ or GI₅₀ against the liability target and the anti-parasitic EC₅₀. This
8
9 was used for the qualitative evaluation of the dose of compound necessary to achieve the desired
10
11 pharmacological effect and minimal toxicity. Accordingly to our TIP, a SI > 10-fold between the
12
13 anti-parasitic activity and the liability targets and/or cytotoxicity was preferred in order to consider
14
15 the compounds safe for *in vivo* evaluation. Thus, **4c**, **4r** and **4t** which exerted anti-parasitic activity
16
17 against *T. brucei* as single agents (**4c** TbEC₅₀ 7.0 ± 0.5 μM; **4r** TbEC₅₀ 9.7 ± 2.5 μM; **4t** TbEC₅₀ 5.9
18
19 ± 0.2 μM) enabled calculation of their SI values, which are reported in Figure 11. For compounds
20
21 associated with IC₅₀, GI₅₀ and NOAEL > 100 μM, the respective SI is underestimated. From these
22
23 studies, **4c** showed a suitable selectivity (SI > 10) with respect to its anti-*T. brucei* activity, and an
24
25 acceptable early toxicity profile that fits the expected TIP criterion⁴⁰ for progression of promising
26
27 hits to *in vivo* pharmacokinetic studies.
28
29
30
31
32
33
34
35
36
37
38
39
40
41
42
43
44
45
46
47
48
49
50
51
52
53
54
55
56
57
58
59
60

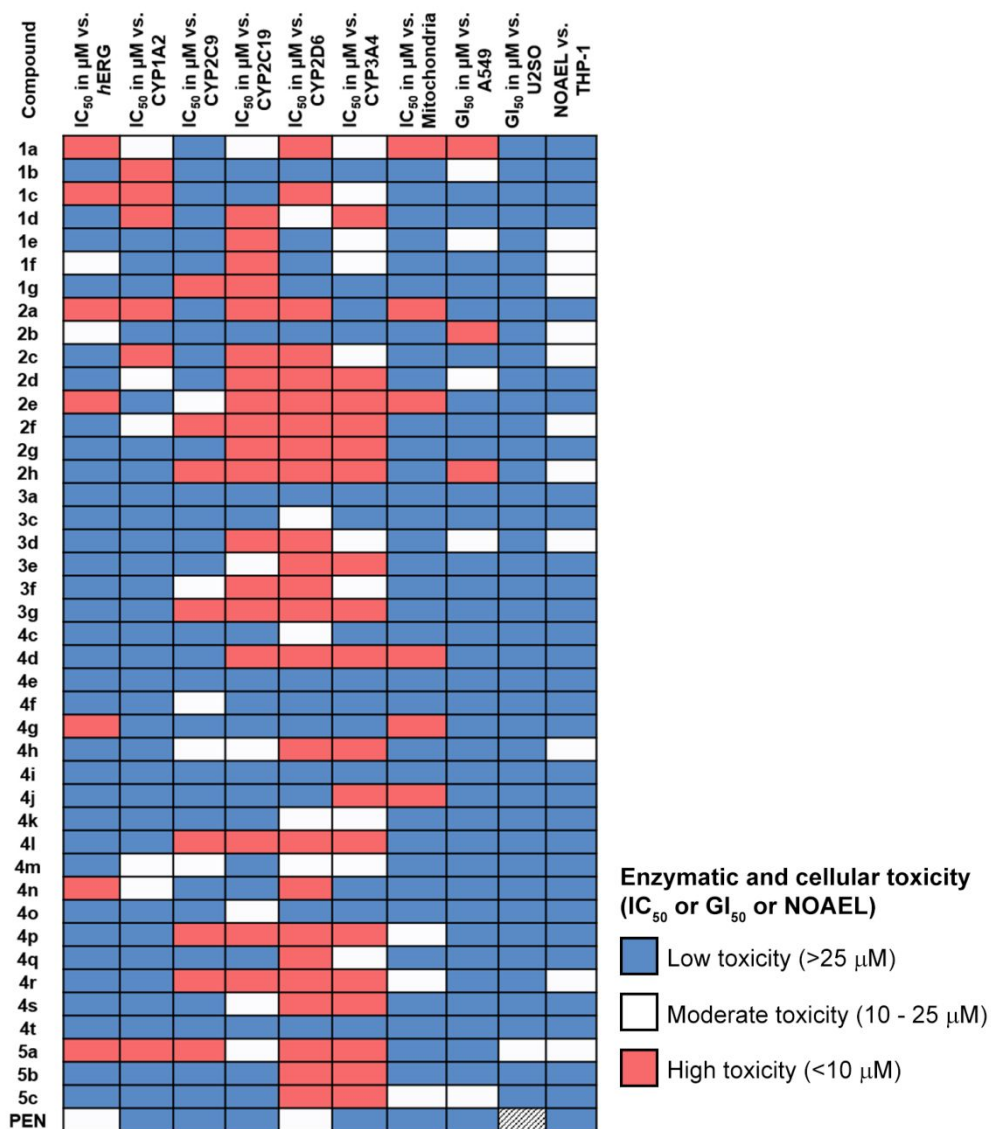


Figure 10. Early toxicity profile of benzothiazoles evaluated in the present studio and the reference drug pentamidine. The data were expressed in term of micromolar IC₅₀ against *h*ERG, CYP isoforms and mitochondrial toxicity, micromolar GI₅₀ against A549 and U2OS cell lines and NOAEL (maximum dose (μM) administered without observing toxic effects). The cells are colored adopting a trafficligh system in vermillion for high toxic potential (IC₅₀ or GI₅₀ or NOAEL < 10 μM), in white for moderate toxicity (IC₅₀ or GI₅₀ or NOAEL ranging from 10 – 25 μM) and in cerulean for low/no toxicity (IC₅₀ or GI₅₀ or NOAEL > 10 μM). To reduce the liabilities of the compounds (acceptable liability profile) an IC₅₀ or GI₅₀ or NOAEL > 10 μM (cerulean/white color) was set as a cut-off.

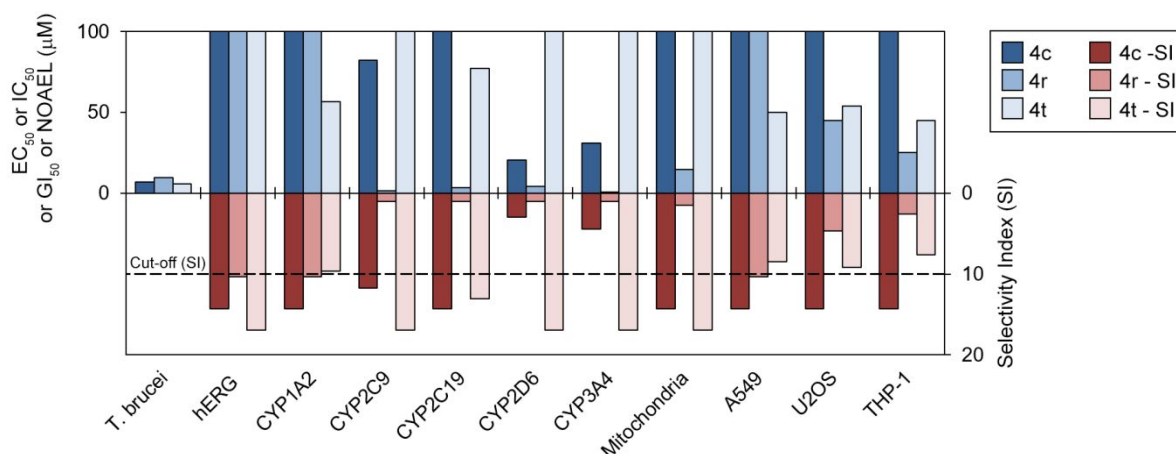


Figure 11. Early toxicity profile (IC_{50} against *h*ERG, CYPs and mitochondria, GI_{50} against A549 and U2OS and NOAEL against THP-1) of compounds **4c** (dark blue), **4r** (blue) and **4t** (cerulean) and relative selectivity index (SI, in dark red, vermillion and pink, respectively) with respect to *T. brucei* anti-parasitic activity (EC_{50}).

Pharmacokinetic evaluation of **4c**

Before proceeding to *in vivo* studies, the solubility of **4c** was evaluated first by UV-Vis spectroscopy as describe by Bard et al.³⁵ The thermodynamic solubility was measured in four different media (*i.e.* pure water, phosphate buffered saline (PBS), PBS + 10 % DMSO and PBS + 50 % DMSO) in accordance with the administration procedure. Maximum solubility in water and PBS was 13.12 $\mu\text{g/mL}$ and 10.94 $\mu\text{g/mL}$ respectively, and > 100 $\mu\text{g/mL}$ in both PBS with 10 % or 50 % of DMSO, resulting a moderately-highly soluble compound for *in vivo* evaluation.³⁶ The preliminary pharmacokinetic profile of **4c** was evaluated in healthy BALB/c mice using a SNAP-PK approach and the free form of **4c** was administered IV at the dose of 1 mg/kg and *per os* at the dose of 20 mg/kg (Table 8). Compound **4c** showed a short half-life ($t_{1/2} = 3.45$ h) after IV administration and it was not detected in blood after 2 hours. In addition, neither after IV nor *per os*

administration the compound reached a plasmatic concentration comparable or higher to its anti-*T. brucei* activity ($EC_{50} = 7.0 \mu\text{M}$). With the aim of improving the plasma concentrations, **4c** was solubilized with hydroxypropyl- β -cyclodextrin (HP- β -CD) and administered *per os* at the dose of 20 mg/kg. Formulated with HP- β -CD, compound **4c** reached a maximum plasmatic concentration (C_{max}) of 13 μM (3545 ng/mL), 1.9 times higher than the respective *T. brucei* EC_{50} . The formulation **4c** + CD showed, in addition, an improved half-life ($t_{1/2} = 34.8 \text{ h}$) keeping the plasmatic concentration higher than the anti-parasitic EC_{50} for the first hour after administration (Table 8).

Table 8. Pharmacokinetic parameters of **4c** administered IV and *per os*

4c	Dose	C_{max} (ng/mL)	AUC^a (ng/mL·h)	t_{1/2} (h)	Clearance (mL/min/kg)
IV	1 mg/kg	1630	1057	3.45	946
<i>per os</i>	20 mg/kg	826	4686	43.5	68
<i>per os</i> + CD	20 mg/kg	3545	7932	34.8	41

a. Area under the curve

The pharmacokinetic profile could be modulated and improved by the formulation with HP- β -CD (Table 8). **4c** was then progressed *in vivo* against *T. brucei* infected BALB/c mice. The observed pharmacokinetic improvement in healthy mice was insufficient to enable the significant reduction of the infection or increase the survival of the animals with respect to the untreated control (data not shown). The potential effect of the compound will be further explored going back to chemical modification and different delivery systems.

CONCLUSION

The aim of the present work was to enhance the benzothiazole library through a structure-based approach, to characterize the biological activity against PTR1 and Trypanosomatidic parasites and evaluate the ADME-Toxicity profile to select at least one compound for progression to pharmacokinetic evaluation in animal assays.

1
2
3 We were able to expand the library around the previously identified riluzole and a few other
4 benzothiazole derivatives. The initial X-ray crystal structure of *Tb*PTR1 with the compound of
5 reference, 2-amino-benzothiazole, guided the structure-based design of the new library. We
6 designed and synthesized 42 new 2-amino-benzothiazoles that were investigated for their on-target
7 activity (both *T. brucei* and *L. major* PTR1), anti-parasitic effect, and early toxicity *in vitro*. These
8 experiments allowed the compounds' biological profile to be largely explored, not only a specific
9 description of the targets' inhibition such as two PTR1 enzymes and the corresponding parasitic
10 DHFR other than the corresponding human enzymes, but also the effect against different other
11 enzymes and cells involved in compounds toxicity. Among them, at least six CYP enzymes
12 inhibition, the *h*ERG channel binding, the mitochondrial inhibition effects and different human cells
13 including the human macrophages THP-1. The huge amount of data obtained represents an added
14 value to the compound characterization in a very peculiar way; in fact, while the biological effect
15 on the parasitic enzymes and cells are specifically directed to assess the potential anti-parasitic
16 activity, the ADME-Toxicity data represents an independent dataset that can help in the
17 understanding the crucial structural fragment responsible for the compounds toxicity, other than
18 provide data that are definitely associated with the compounds as their chemical-physical
19 properties, their structural features and will be available for further research even in other medicinal
20 chemistry fields.
21
22
23
24
25
26
27
28
29
30
31
32
33
34
35
36
37
38
39
40
41
42
43
44

45 Ten new x-ray crystal structures of PTR1/compound complexes were solved, and the
46 crystallographic binding mode observed reproduced the poses predicted by the docking studies,
47 validating and confirming the robustness of the *in-silico* approach adopted. It was possible to
48 explain how the compounds structural features modulate the compounds interactions with the
49 targets.
50
51
52
53
54
55

56
57 Progression of compounds into *in vivo* evaluation was based on a compound's property profile its
58 efficacy and safety compared to the features that the expected ideal compound should have.³⁷ We
59
60

therefore defined the profile of the selected compounds and the criterion for go/no go in the drug discovery process as reported in Figure 12. The criteria included chemical (*i.e.* purity, undesirable chemical function, synthetic cost and solubility) and molecular biology properties (*i.e.* knowledge of the target, crystal structures, activity against the target enzyme and SAR), anti-parasitic activity against the three parasites being objects of this study, early enzymatic, cytotoxicity and *in vivo* pharmacokinetic parameters (Figure 12, Table SI-5).⁴⁰ Pentamidine, the first line drug for the treatment of HAT was used as a reference compound and its chemical, biochemical, anti-parasitic, toxicity and pharmacokinetic profile has been reported³⁸ and serves as a guide to benchmark the TIP and identify compounds for progression. Among all the 42 new benzothiazoles evaluated in the present work, **4c** was the most promising compound and fitted the progression criteria summarized in Table SI-5, for each property shown in Figure 12, as it inhibited the target enzymes, had anti-parasitic activity and an acceptable early toxicity profile (enzymatic liability and cytotoxicity). Compound **4c** and pentamidine profiles are reported in Figure 12.

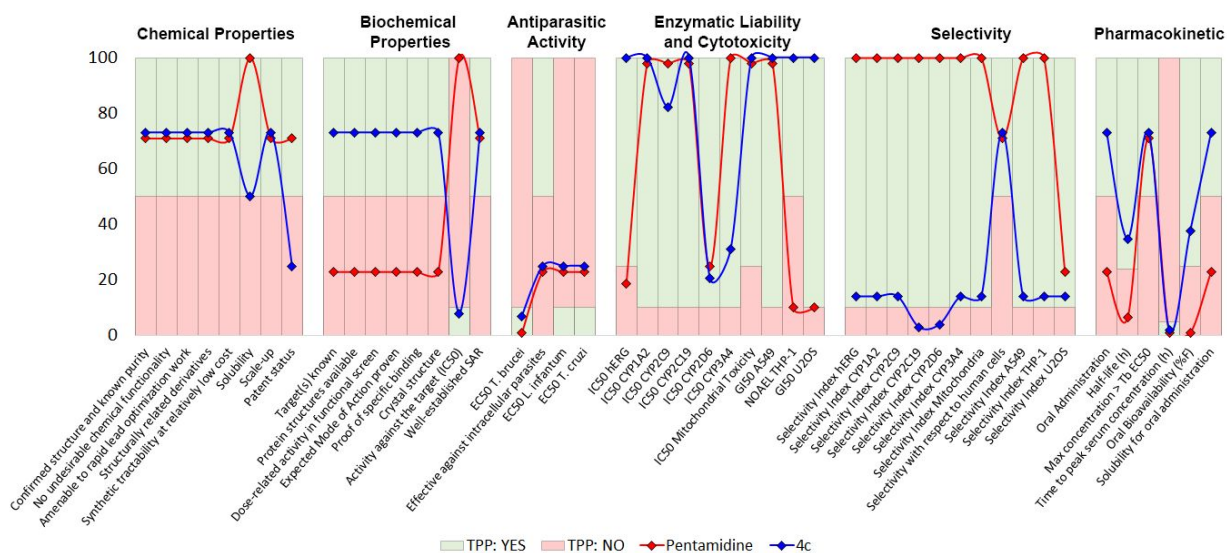


Figure 12. TIP of benzothiazole **4c** (blue line) compared with the reference drug pentamidine (red line). For parameters requiring a yes/no answer, the cut-off was set at 50% of the y-axes. For

1
2
3 parameters requiring a numeric value, the marker line between proper and improper behaviour
4
5 was set to the corresponding cut-off value described in the main text. Pale green colour covers the
6
7 area for which the compound parameters agree with the desired values, whereas pale red colour
8
9 covers the area with an improper profile. Red dots represent data relative to pentamidine, blue
10
11 dots are related to **4c**.
12
13
14
15
16

17
18 Despite the apparent higher toxicity of pentamidine compared to **4c** (some dots related to toxicity
19
20 are in the red field, Figure 12), the drugs higher potency favors a higher specificity *in vitro*.
21
22 Significantly, **4c** presented oral availability, in contrast to pentamidine, a major hallmark in drug
23
24 development for these diseases.
25
26

27
28 Although **4c** was optimal for trypanotoxicity, inhibition of *TbPTR1 in vitro*, had a promising early
29
30 toxicity and pharmacokinetic profile for oral administration it was not curative in the *in vivo* model.
31
32

33
34 Despite the *in vivo* result, this class of compounds offer the potential for optimization into novel
35
36 oral drugs for the treatment of HAT. The detailed chemical and biological information obtained
37
38 from these studies provides a rational for the design of further series of compounds with improved
39
40 PTR1 enzyme inhibition and anti-parasitic activity. Future work will address the formulation of **4c**
41
42 in a more suitable stable delivery system that could enhance its *in vivo* anti-parasitic activity.
43
44
45
46
47

48 **EXPERIMENTAL SECTION**

49
50
51 **Synthetic procedures.** All commercially available chemicals and solvents were reagent grade and
52
53 were used without further purification unless otherwise specified. The following solvents and
54
55 reagents have been abbreviated: methanol (MeOH); acetonitrile (ACN); ethyl acetate (AcOEt);
56
57 formic acid (FA); 1-Ethyl-3-(3-dimethylaminopropyl)carbodiimide (EDC); Hydroxybenzotriazole
58
59 (HOBt). Reactions were monitored by thin-layer chromatography on silica gel plates (60F-254, E.
60

Merck) and visualized with UV light, cerium ammonium sulfate or alkaline KMnO_4 aqueous solution. NMR spectra were recorded on a Bruker 400 spectrometer with ^1H at 400.134 MHz and ^{13}C at 100.62 MHz. Proton chemical shifts were referenced to the solvent residual peaks. Chemical shifts are reported in parts per million (ppm, δ units). Coupling constants are reported in Hertz (Hz). Splitting patterns are designed as s, singlet; d, doublet; t, triplet; q quartet; dd, double doublet; m, multiplet; b, broad. Melting points were recorded on a Stuart, SMP3 (Barloworld Scientific Limited Stone, Staffordshire, UK) and are uncorrected. Analysis of compound purity was determined through liquid chromatography (LC) UV/Vis using a Jasco LC system equipped with a Jasco PU-2080 Plus pump, coupled with a Jasco PU-2075 Plus UV/Vis detector. LC separation was performed on an Agilent Poroshell 120 50 mm \times 3.0 mm analytical column, packed with EC-C18 2.7 μM as stationary phase (Agilent Technologies, Milan, Italy). 20 μL of a 100 $\mu\text{g}/\text{mL}$ solution of compound in 0.1% FA in water/ACN 9:1 was injected. A gradient was delivered at 0.2 mL/min using (A) 0.1% FA in water and (B) ACN. Samples were eluted with 5% B (0.00–1.00 min); 1–95% B (1.00–6.00 min); 95% B (6.00–10.00 min) and 5% B (10.00–20.00 min). The eluate was detected by UV at $\lambda = 220$ nm. All the compounds showed a level of purity above 95%.

General procedure for the synthesis of benzothiazoles **1a**, **c-f**

To a solution of **6** (1 eq.) in DMF (5 mL), K_2CO_3 (2.5 eq.) and iodomethane (1.1 eq., for **1a**) or the appropriate benzylbromide (1.2 eq., for **1b-f**) were added. The mixture was stirred at room temperature overnight. The solvent was evaporated under reduced pressure and the residue suspended in AcOEt and washed with K_2CO_3 saturated solution and brine. The organic phase was dried over Na_2SO_4 and concentrated. The crude was chromatographed on silica gel to afford the desired product.

6-methoxybenzo[d]thiazol-2-amine (**1a**)

White solid. 64% yield. ^1H NMR (400 MHz, $\text{DMSO}-d_6$) δ 3.74 (s, 3H), 6.81 (dd, $J = 2.7, 8.7$ Hz, 1H), 7.14 – 7.28 (m, 3H), 7.29 (d, $J = 2.6$ Hz, 1H). ^{13}C NMR (101 MHz, DMSO) δ 55.50, 105.49,

1
2
3 112.82, 118.02, 131.87, 146.80, 154.23, 164.66. m.p. [164.2-165.8°C]. $k' = 5.32$. HRMS m/z
4
5 [M+H]⁺ Calcd for C₈H₈N₂OS: 180.0357. Found: 180.0360.
6
7

8 **6-(benzyloxy)benzo[d]thiazol-2-amine (1c)**

9
10
11 White solid. 84% yield. ¹H NMR (400 MHz, DMSO-*d*₆) δ 5.06 (s, 2H), 6.87 (dd, $J = 2.6, 8.7$ Hz,
12
13 1H), 7.14 – 7.27 (m, 3H), 7.26 – 7.55 (m, 6H). ¹³C NMR (101 MHz, DMSO) δ 69.80, 106.73,
14
15 113.68, 118.01, 127.64, 127.71, 128.35, 131.81, 137.26, 147.02, 153.24, 164.78. m.p. [135°C with
16
17 dec.]. $k' = 7.23$. HRMS m/z [M+H]⁺ Calcd for C₁₄H₁₂N₂OS: 256.0670. Found: 256.0672.
18
19

20 **6-((3,4-dichlorobenzyl)oxy)benzo[d]thiazol-2-amine (1d)**

21
22
23 Pale yellow solid. 59 % yield. ¹H NMR (400 MHz, DMSO-*d*₆) δ 5.10 (s, 2H), 6.90 (dd, $J = 2.6, 8.7$
24
25 Hz, 1H), 7.24 (d, $J = 8.5$ Hz, 3H), 7.38 (d, $J = 2.6$ Hz, 1H), 7.44 (dd, $J = 2.0, 8.3$ Hz, 1H), 7.66 (d, J
26
27 = 8.2 Hz, 1H), 7.71 (d, $J = 1.9$ Hz, 1H). ¹³C NMR (101 MHz, DMSO) δ 68.26, 106.90, 113.67,
28
29 118.03, 127.74, 129.37, 130.21, 130.61, 131.02, 131.86, 138.57, 147.27, 152.80, 164.92. m.p. [174
30
31 °C with dec]. $k' = 8.30$. HRMS m/z [M+H]⁺ Calcd. for C₁₄H₁₀Cl₂N₂OS: 323.9891. Found:
32
33 323.9885.
34
35
36

37 **6-(((2-aminobenzo[d]thiazol-6-yl)oxy)methyl)benzonitrile (1e)**

38
39
40
41 Pale yellow solid. 69 % yield. ¹H NMR (400 MHz, DMSO-*d*₆) δ 5.20 (s, 2H), 6.91 (dd, $J = 2.7, 8.7$
42
43 Hz, 1H), 7.18 – 7.34 (m, 3H), 7.38 (d, $J = 2.7$ Hz, 1H), 7.66 (dd, $J = 8.2, 10.0$ Hz, 2H), 7.78 – 7.96
44
45 (m, 2H). ¹³C NMR (101 MHz, DMSO) δ 68.86, 106.85, 110.35, 113.65, 118.04, 118.73, 127.87,
46
47 128.01, 131.86, 132.35, 132.41, 143.16, 147.27, 152.81, 164.92. m.p. [196.2 – 197.0 °C]. $k' = 6.25$.
48
49 HRMS m/z [M+H]⁺ Calcd. for C₁₅H₁₁N₃OS: 281.0623. Found: 281.0625.
50
51
52

53 **methyl 4-(((2-aminobenzo[d]thiazol-6-yl)oxy)methyl)benzoate (1f)**

54
55
56 White solid. 85 % yield. ¹H NMR (400 MHz, DMSO-*d*₆) δ 3.86 (s, 3H), 5.18 (s, 2H), 6.91 (dd, $J =$
57
58 2.6, 8.7 Hz, 1H), 7.16 – 7.30 (m, 3H), 7.39 (d, $J = 2.6$ Hz, 1H), 7.59 (d, $J = 8.2$ Hz, 2H), 7.91 – 8.08
59
60

(m, 2H). ^{13}C NMR (101 MHz, DMSO) δ 52.09, 69.17, 106.83, 113.68, 118.03, 127.42, 128.86, 129.25, 131.85, 142.88, 147.21, 152.99, 164.88, 165.98. m.p. [195 °C with dec.]. $k' = 6.78$. HRMS m/z $[\text{M}+\text{H}]^+$ Calcd. for $\text{C}_{16}\text{H}_{14}\text{N}_2\text{O}_3\text{S}$: 314.0725. Found: 314.0725.

methyl 1-(4-(((2-aminobenzo[d]thiazol-6-yl)oxy)methyl)benzoyl)piperidine-4-carboxylate (1g)

1f (200 mg, 1 eq., 0.64 mmol) was solubilized in THF:MeOH 3:1 (8 mL) and 1N NaOH aqueous solution (960 μL , 1.5 eq., 0.96 mmol) was added. The mixture was stirred at room temperature for 24 hours and then concentrated. The crude was solubilized in water and washed with AcOEt. The aqueous phase was acidified with 1N HCl and the precipitate formed, collected through filtration, washed with water and dried. The carboxylic acid (172 mg, 1 eq., 0.57 mmol) thus obtained was solubilized in DMF (5 mL) at 0 °C and EDC·HCl (109 mg, 1 eq. 0.57 mmol), HOBt (76 mg, 1 eq., 0.57 mmol) and methyl isonipecotate (88 μL , 1 eq., 0.57 mmol) were subsequently added. The mixture was stirred at room temperature overnight and concentrated. The residue was suspended in AcOEt and washed with K_2CO_3 saturated solution and brine. The organic phase was dried over Na_2SO_4 and concentrated. The residue was crystalized from diethyl ether to give 145 mg of a white solid (61 % yield). ^1H NMR (400 MHz, $\text{DMSO}-d_6$) δ 1.51-1.54 (m, 2H), 1.75-1.98 (m, 2H), 2.67 (tt, $J = 4.0, 11.0$ Hz, 1H), 2.84 – 3.23 (m, 2H), 3.48-3.62 (m, 4H), 4.21-4.44 (m, 1H), 5.12 (s, 2H), 6.80 – 7.01 (m, 1H), 7.17 – 7.31 (m, 2H), 7.38-7.43 (m, 3H), 7.50-7.54 (m, 3H). ^{13}C NMR (101 MHz, DMSO) δ 27.61, 40.48 (from HSQC), 44.44 (from HSQC), 51.52, 69.39, 106.74, 113.63, 118.03, 126.82, 127.48, 131.86, 135.52, 138.59, 147.12, 153.16, 164.84, 168.78, 174.21. m.p. [127°C with dec.]. $k' = 7.42$. HRMS m/z $[\text{M}+\text{H}]^+$ Calcd. for $\text{C}_{22}\text{H}_{23}\text{N}_3\text{O}_4\text{S}$: 425.1409. Found: 425.4010.

General procedure for the synthesis of sulfide-benzothiazoles 2a-f

To a suspension of aminobenzene-sulphides **8a-f** (1 eq.) in glacial acetic acid (10 mL *per* mmol) cooled at 10 °C, KSCN (4 eq.) was added. A solution of elemental bromine (2 eq.) in glacial acetic acid (10 mL *per* mmol) was added drop wise over 1 hour keeping the mixture refrigerated at a

1
2
3 temperature below 10 °C. After the addition, the temperature was spontaneously risen, and the
4
5 mixture reacted at room temperature for 1 – 6 hours. The mixture was chilled down, quenched with
6
7 water and alkalized with 30% aqueous NH₄OH. The precipitated formed was extracted in AcOEt.
8
9 The organic phase was washed with brine, dried over anhydrous Na₂SO₄ and concentrated. The
10
11 crude was crystalized from diethyl ether to afford the desired product.
12
13

14 15 **6-(methylthio)benzo[d]thiazol-2-amine (2a)**

16
17
18 Pale yellow solid. 58 % yield. ¹H NMR (400 MHz, DMSO-*d*₆) δ 2.46 (s, 3H), 7.16 (dd, *J* = 2.0, 8.3
19
20 Hz, 1H), 7.26 (d, *J* = 8.3 Hz, 1H), 7.45 (s, 2H), 7.64 (d, *J* = 1.9 Hz, 1H). ¹³C NMR (101 MHz,
21
22 DMSO) δ 16.68, 117.92, 119.84, 125.51, 128.96, 132.06, 151.01, 166.22. m.p. [148.5 – 149.8°C].
23
24 *k*' = 5.72. HRMS *m/z* [M+H]⁺ Calcd. for C₈H₈N₂S₂: 196.0129. Found: 196.0130.
25
26
27

28 29 **6-((trifluoromethyl)thio)benzo[d]thiazol-2-amine (2b)**

30
31 Pale yellow solid. 32 % yield. ¹H NMR (400 MHz, DMSO-*d*₆) δ 7.41 (d, *J* = 8.4 Hz, 1H), 7.50 (dd,
32
33 *J* = 2.0, 8.3 Hz, 1H), 7.88 (s, 2H), 8.07 (d, *J* = 1.9 Hz, 1H). ¹³C NMR (101 MHz, DMSO) δ 112.75
34
35 (q, *J* = 3.0 Hz, 1C), 118.29, 129.28, 129.64 (q, *J* = 309 Hz, 1C), 132.29, 134.01, 155.39, 169.15.
36
37 m.p. [154.2 – 156.1°C]. *k*' = 6.21. HRMS *m/z* [M+H]⁺ Calcd. for C₈H₅F₃N₂S₂: 249.9846. Found:
38
39 249.9845.
40
41
42

43 44 **6-(benzylthio)benzo[d]thiazol-2-amine (2c)**

45
46 Pale brown solid. 59 % yield. ¹H NMR (400 MHz, DMSO-*d*₆) δ 4.15 (s, 2H), 7.13 – 7.36 (m, 7H),
47
48 7.52 (s, 2H), 7.68 (dd, *J* = 0.5, 1.9 Hz, 1H). ¹³C NMR (101 MHz, DMSO) δ 38.86 (overlapping
49
50 with DMSO peaks), 117.82, 123.15, 126.28, 126.87, 128.23, 128.53, 128.76, 131.72, 137.90,
51
52 151.92, 166.76. m.p. [142.3 – 143.1°C]. *k*' = 7.45. HRMS *m/z* [M+H]⁺ Calcd. for C₁₄H₁₂N₂S₂:
53
54 272.0442. Found: 272.0445.
55
56
57

58 59 **6-((3,4-dichlorobenzyl)thio)benzo[d]thiazol-2-amine (2d)**

1
2
3 White solid. 71 % yield. ^1H NMR (400 MHz, $\text{DMSO-}d_6$) δ 4.19 (s, 2H), 7.10 – 7.41 (m, 3H), 7.48 –
4 7.69 (m, 4H), 7.73 (d, $J = 1.9$ Hz, 1H). ^{13}C NMR (101 MHz, DMSO) δ 37.71, 117.85, 123.81,
5 125.12, 129.03, 129.09, 129.14, 129.33, 130.31, 130.64, 131.74, 139.58, 152.16, 166.99. m.p.
6 [134.6 – 136.2°C]. $k' = 8.50$. HRMS m/z $[\text{M}+\text{H}]^+$ Calcd. for $\text{C}_{14}\text{H}_{10}(\text{}^{35}\text{Cl})_2\text{N}_2\text{S}_2$: 339.9662. Found:
7 339.9660. Calcd. for $\text{C}_{14}\text{H}_{10}(\text{}^{35}\text{Cl})(\text{}^{37}\text{Cl})\text{N}_2\text{S}_2$: 341.9633. Found: 341.9633.
8
9

10 11 12 13 14 15 **4-(((2-aminobenzo[d]thiazol-6-yl)thio)methyl)benzotrile (2e)**

16
17
18 White solid. 65 % yield. ^1H NMR (400 MHz, $\text{DMSO-}d_6$) δ 4.22 (s, 2H), 7.15 (dd, $J = 1.9, 8.3$ Hz,
19 1H), 7.22 (d, $J = 8.3$ Hz, 1H), 7.36 – 7.48 (m, 2H), 7.55 (s, 2H), 7.66 (d, $J = 1.9$ Hz, 1H), 7.69 –
20 7.76 (m, 2H). ^{13}C NMR (101 MHz, DMSO) δ 38.02 (overlapping with DMSO peaks), 109.53,
21 117.87, 118.75, 123.81, 125.04, 129.10, 129.71, 131.76, 132.12, 144.28, 152.24, 167.00. M.p. [164-
22 7 – 166.0°C]. $k' = 6.67$. HRMS m/z $[\text{M}+\text{H}]^+$ Calcd. for $\text{C}_{15}\text{H}_{11}\text{N}_3\text{S}_2$: 297.0394. Found: 297.0395.
23
24
25
26
27
28
29

30 31 32 **methyl 4-(((2-aminobenzo[d]thiazol-6-yl)thio)methyl)benzoate (2f)**

33
34 White solid. 82 % yield. ^1H NMR (400 MHz, $\text{DMSO-}d_6$) δ 3.83 (s, 3H), 4.21 (s, 2H), 7.03 – 7.29
35 (m, 2H), 7.32 – 7.45 (m, 2H), 7.54 (s, 2H), 7.68 (d, $J = 1.8$ Hz, 1H), 7.80 – 7.89 (m, 2H). ^{13}C NMR
36 (101 MHz, DMSO) δ 38.77 (overlapping with DMSO peaks), 52.02, 117.84, 123.66, 125.43,
37 128.10, 128.99, 129.09 (overlapping of 2C signals), 131.73, 143.88, 152.17, 165.96, 166.91. m.p.
38 [152°C with dec.]. $k' = 7.20$. HRMS m/z $[\text{M}+\text{H}]^+$ Calcd. for $\text{C}_{16}\text{H}_{14}\text{N}_2\text{O}_2\text{S}_2$: 330.0497. Found:
39 330.0495.
40
41
42
43
44
45
46
47

48 49 50 51 **Synthesis of methyl 1-(4-(((2-aminobenzo[d]thiazol-6-yl)thio)methyl)benzoyl)piperidine-4- 52 carboxylate (2g)**

53 To a solution of **2f** (100 mg, 0.30 mmol, 1 eq.) in $\text{THF}:\text{MeOH}$ 3:1 (8 mL) aqueous 1N NaOH (0.45
54 mL, 0.45 mmol, 1.5 eq.) was added. The mixture was stirred at room temperature overnight. The
55 solvent was evaporated and the residue suspended in water and washed with AcOEt . The aqueous
56 phase was acidified with HCl 1N. The precipitate formed was collected, washed with water and
57
58
59
60

1
2
3 diethyl ether to give 85 mg of a white solid, used in the next step without further purification. 40 mg
4 of carboxylic acid (0.13 mmol, 1 eq.) were solubilized in DMF at 0 °C. EDC (1 eq., 0.13 mmol, 24
5 mg), HOBt (1 eq. 0.13 mmol, 16 mg) and methyl isonipecotate (1 eq., 0.13 mmol, 18 mg) were
6
7 sequentially added. The mixture was stirred at room temperature overnight and concentrated. The
8 residue was solubilized in AcOEt and washed with saturated solution of K₂CO₃, saturated solution
9 of NH₄Cl, brine, dried over anhydrous Na₂SO₄ and concentrated. The residue was crystalized from
10 diethyl ether to give 23 mg of a pale-yellow solid. 40 % yield. ¹H NMR (400 MHz, DMSO-*d*₆) δ
11 1.50 (m, 2H), 1.85 (m, 2H), 2.59 – 2.72 (m, 1H), 2.96 (m, 2H), 3.62 (s, 3H), 4.05 – 4.46 (m, 4H),
12 7.03 – 7.48 (m, 5H), 7.53 (d, *J* = 3.2 Hz, 2H), 7.68 (dd, *J* = 1.9, 17.6 Hz, 1H), 8.03 (d, *J* = 8.3 Hz,
13 1H). ¹³C NMR (101 MHz, DMSO) δ 28.29, 36.18, 40.48, 44.44, 51.30, 120.30, 121.58, 126.61,
14 126.83, 128.85, 133.74, 136.79, 137.14, 139.62, 152.70, 166.30, 170.27, 175.54. m.p. [153.2 –
15 154.1 °C]. *k'* = 7.84. HRMS *m/z* [M+H]⁺ Calcd. for C₂₂H₂₃N₃O₃S₂: 441.1181. Found: 441.1180.
16
17
18
19
20
21
22
23
24
25
26
27
28
29

30 31 **Synthesis of 4-(((2-aminobenzo[d]thiazol-6-yl)thio)methyl)-N-benzylbenzamide (2h)**

32
33
34 40 mg of the free carboxylic acid **2f** (0.13 mmol, 1 eq.) were solubilized in DMF at 0 °C. EDC (1
35 eq., 0.13 mmol, 24 mg), HOBt (1 eq. 0.13 mmol, 16 mg) and benzylamine (1 eq., 0.13 mmol, 14
36 mg) were sequentially added. The mixture was stirred at room temperature overnight and
37 concentrated. The residue was solubilized in AcOEt and washed with K₂CO₃ saturated solution,
38 NH₄Cl saturated solution, brine, dried over anhydrous Na₂SO₄ and concentrated. The residue was
39 crystalized from diethyl ether to give 34 mg of a pale yellow solid. 65 % yield. ¹H NMR (400 MHz,
40 DMSO-*d*₆) δ 4.20 (s, 2H), 4.46 (d, *J* = 5.9 Hz, 2H), 7.09 – 7.28 (m, 3H), 7.28 – 7.46 (m, 6H), 7.54
41 (s, 2H), 7.69 (d, *J* = 1.8 Hz, 1H), 7.74 – 7.91 (m, 2H), 8.98 (t, *J* = 6.0 Hz, 1H). ¹³C NMR (101 MHz,
42 DMSO) δ 38.51 (overlapping with DMSO peaks), 42.54, 117.85, 123.43, 125.78, 126.65, 127.15,
43 127.22, 128.21, 128.64, 128.78, 131.76, 132.86, 139.63, 141.48, 152.08, 165.85, 166.86. m.p.
44 [184.4 – 185.9 °C]. *k'* = 8.78. HRMS *m/z* [M+H]⁺ Calcd. for C₂₂H₁₉N₃OS₂: 405.0970. Found:
45 405.0970.
46
47
48
49
50
51
52
53
54
55
56
57
58
59
60

General procedure for the synthesis of sulfone-benzothiazoles 3c-g

To a solution of benzothiazoles **2c-g** (1 eq.) in DCM at 0 °C, *m*-CPBA (2.5 eq.) was added. The suspension was reacted at room temperature overnight. The reaction was diluted with DCM and washed with K₂CO₃ saturated solution. The organic phase was dried over anhydrous Na₂SO₄ and concentrated. The residue was crystallized from diethyl ether to give the desired product.

6-(benzylsulfonyl)benzo[d]thiazol-2-amine (3c)

Pale yellow solid. 87 % yield. ¹H NMR (400 MHz, DMSO-*d*₆) δ 4.60 (s, 2H), 7.14 (dd, *J* = 1.9, 7.7 Hz, 2H), 7.23 – 7.35 (m, 3H), 7.39 (d, *J* = 8.5 Hz, 1H), 7.47 (dd, *J* = 2.0, 8.5 Hz, 1H), 7.85 – 8.22 (m, 3H). ¹³C NMR (101 MHz, DMSO) δ 61.27, 116.97, 121.60, 125.82, 128.12, 128.19, 129.00, 129.71, 130.90, 131.21, 156.87, 170.25. m.p. [184.5 – 186.2°C]. *k*' = 5.65. HRMS *m/z* [M+H]⁺ Calcd. for C₁₄H₁₂N₂O₂S₂: 304.0340. Found: 304.0345.

6-((3,4-dichlorobenzyl)sulfonyl)benzo[d]thiazol-2-amine (3d)

Pale yellow solid. 74 % yield. ¹H NMR (400 MHz, DMSO-*d*₆) δ 4.74 (s, 2H), 7.16 (dd, *J* = 2.0, 8.3 Hz, 1H), 7.37 – 7.71 (m, 4H), 8.01 – 8.24 (m, 3H). ¹³C NMR (101 MHz, DMSO) δ 59.79, 117.05, 121.73, 125.87, 129.16, 130.27, 130.35, 130.67, 131.08, 131.13, 131.34, 132.72, 157.10, 170.43. m.p. [238°C with dec.]. *k*' = 6.81. HRMS *m/z* [M+H]⁺ Calcd for C₁₄H₁₀(³⁵Cl)₂N₂O₂S₂: 371.9561. Found: 371.9560. Calcd. for C₁₄H₁₀(³⁵Cl)(³⁷Cl)N₂O₂S₂: 373.9531. Found: 373.9530.

4-(((2-aminobenzo[d]thiazol-6-yl)sulfonyl)methyl)benzotrile (3e)

Pale yellow solid. 79 % yield. ¹H NMR (400 MHz, Chloroform-*d*) δ 4.67 (d, *J* = 1.5 Hz, 2H), 7.21-7.23 (m, 2H), 7.31 – 7.35 (m, 1H), 7.39-7.42 (m, 1H), 7.72-7.79 (m, 5H). ¹³C NMR (100 MHz, Chloroform-*d*) δ 62.92, 110.45, 119.13, 119.34, 122.05, 126.55, 129.51, 130.82, 131.03, 133.48, 138.56, 157.87, 170.00. m.p. [223°C with dec.]. *k*' = 4.86. HRMS *m/z* [M+H]⁺ Calcd. for C₁₅H₁₁N₃O₂S₂: 329.0293. Found: 329.0295.

methyl 4-(((2-aminobenzo[d]thiazol-6-yl)sulfonyl)methyl)benzoate (3f)

Pale yellow solid. 61 % yield. ^1H NMR (400 MHz, $\text{DMSO-}d_6$) δ 3.84 (s, 3H), 4.74 (s, 2H), 7.28-7.30 (m, 3H), 7.39 (d, $J = 8.4$ Hz, 1H), 7.46 (dd, $J = 2.0, 8.5$ Hz, 1H), 7.87 (d, $J = 8.3$ Hz, 2H), 8.05 (d, $J = 1.9$ Hz, 2H). ^{13}C NMR (101 MHz, DMSO) δ 52.15, 60.95, 116.99, 121.63, 125.84, 128.89, 129.32, 129.46, 131.26, 131.29, 134.46, 157.01, 165.88, 170.36. m.p. [251.3 – 252.8°C]. $k' = 5.06$. HRMS m/z $[\text{M}+\text{H}]^+$ Calcd. for $\text{C}_{16}\text{H}_{14}\text{N}_2\text{O}_4\text{S}_2$: 362.0395. Found: 362.0395.

methyl 1-(4-(((2-aminobenzo[d]thiazol-6-yl)sulfonyl)methyl)benzoyl)piperidine-4-carboxylate (3g)

White solid. 43 % yield. ^1H NMR (400 MHz, $\text{DMSO-}d_6$) δ 1.51 (m, 2H), 1.86 (m, 2H), 2.64 (m, 1H), 2.94 (m, 2H), 3.63 (s, 3H), 4.26 (m, 2H), 4.66 (s, 2H), 7.11 – 7.32 (m, 5H), 7.39 (d, $J = 8.6$ Hz, 1H), 7.43 – 7.55 (m, 1H), 7.93 – 8.16 (m, 3H). m.p. [232.1 – 235.1°C]. $k' = 5.93$. HRMS m/z $[\text{M}+\text{H}]^+$ Calcd. for $\text{C}_{22}\text{H}_{23}\text{N}_3\text{O}_5\text{S}_2$: 473.1079. Found: 473.1070.

General procedure for the synthesis of amide 4c-f, i-j, l-r.

2-amino-6-carboxy-benzothiazole (1 eq.) were solubilized in DMF at 0 °C. EDC (1 eq.), HOBt (1 eq.) and the appropriate amine **9c-f, i-j, l-r** (1 eq.) were consequentially added. The mixture was stirred at room temperature overnight and concentrated. The residue was solubilized in AcOEt and washed consecutively with K_2CO_3 saturated solution, NH_4Cl saturated solution, brine, dried over anhydrous Na_2SO_4 and concentrated. The crude was purified on silica gel to afford the desired product.

2-amino-N-benzylbenzo[d]thiazole-6-carboxamide (4c)

White solid. 65 % yield. ^1H NMR (400 MHz, $\text{DMSO-}d_6$) δ 4.48 (d, $J = 6.0$ Hz, 2H), 7.03 – 7.48 (m, 6H), 7.66 – 7.84 (m, 3H), 8.21 (d, $J = 1.8$ Hz, 1H), 8.90 (t, $J = 6.0$ Hz, 1H). ^{13}C NMR (101 MHz, DMSO) δ 42.60, 116.81, 120.30, 125.04, 126.61, 126.83, 127.16, 128.19, 130.81, 139.85, 155.22,

1
2
3 165.89, 168.43. m.p. [245.3 – 247.1°C]. $k' = 6.17$. HRMS m/z $[M+H]^+$ Calcd. for $C_{15}H_{13}N_3OS$:
4
5 283.0779. Found: 283.0780.
6
7

8 **2-amino-N-(3,4-dichlorobenzyl)benzo[d]thiazole-6-carboxamide (4d)**
9

10 White solid. 61 % yield. 1H NMR (400 MHz, DMSO- d_6) δ 4.44 (d, $J = 1.3$ Hz, 2H), 6.58 (s, 2H),
11
12 7.05 – 7.21 (m, 1H), 7.28 – 7.52 (m, 2H), 7.58 (d, $J = 1.4$ Hz, 2H), 8.05 (t, $J = 1.0$ Hz, 1H), 9.00 (s,
13
14 1H). ^{13}C -NMR (101 MHz, DMSO) δ : 43.96, 118.63, 121.08, 123.23, 127.53, 129.54, 129.60
15
16 (overlapping of 2C signals), 130.30, 130.80, 131.62, 140.13, 155.96, 167.07, 169.16. m.p. [243.5 –
17
18 245.2°C]. $k' = 7.16$. HRMS m/z $[M+H]^+$ Calcd. for $C_{15}H_{11}(^{35}Cl)_2N_3OS$: 351.0000. Found:
19
20 351.0000. Calcd. for $C_{15}H_{11}(^{35}Cl)(^{37}Cl)N_3OS$: 352.9970. Found: 352.9965.
21
22
23
24
25

26 **2-amino-N-(4-cyanobenzyl)benzo[d]thiazole-6-carboxamide (4e)**
27

28 White solid. 45 % yield. 1H -NMR (DMSO – d_6) δ : 4.50 (s, 2H), 6.66 (s, 2H), 7.53-7.55 (m, 2H),
29
30 7.67-7.77 (m, 4H), 8.37 (s, 1H), 9.08 (s, 1H). ^{13}C NMR (101 MHz, DMSO) δ 42.45, 109.40,
31
32 116.85, 118.89, 120.37, 125.06, 126.47, 127.97, 130.87, 132.20, 145.79, 155.37, 166.13, 168.54.
33
34 m.p. [253.6-254.7°C]. $k' = 5.39$. HRMS m/z $[M+H]^+$ Calcd. for $C_{16}H_{12}N_4OS$: 308.0732. Found:
35
36 308.0730.
37
38
39
40

41 **methyl 4-((2-aminobenzo[d]thiazole-6-carboxamido)methyl)benzoate (4f)**
42

43 White solid. 53 % yield. 1H NMR (400 MHz, DMSO- d_6) δ 3.85 (s, 3H), 4.55 (d, $J = 5.9$ Hz, 2H),
44
45 7.37 (d, $J = 8.4$ Hz, 1H), 7.42 – 7.51 (m, 2H), 7.71 – 7.86 (m, 3H), 7.86 – 8.01 (m, 2H), 8.22 (d, $J =$
46
47 1.9 Hz, 1H), 8.99 (t, $J = 6.0$ Hz, 1H). ^{13}C NMR (101 MHz, DMSO) δ 42.44, 52.00, 116.84, 120.36,
48
49 125.07, 126.58, 127.30, 128.02, 129.18, 130.86, 145.56, 155.33, 166.03, 166.08, 168.50. m.p.
50
51 [246.0 – 247.1°C]. $k' = 6.00$. HRMS m/z $[M+H]^+$ Calcd. for $C_{17}H_{15}N_3O_3S$: 341.0834. Found:
52
53 341.0834.
54
55
56
57

58 **2-amino-N-(3,4,5-trimethoxybenzyl)benzo[d]thiazole-6-carboxamide (4i)**
59
60

1
2
3 White solid. 74 % yield. ^1H NMR (400 MHz, $\text{DMSO-}d_6$) δ 3.63 (s, 3H), 3.75 (s, 6H), 4.40 (d, $J =$
4 5.9 Hz, 2H), 6.66 (s, 2H), 7.35 (d, $J = 8.4$ Hz, 1H), 7.62 – 7.96 (m, 3H), 8.21 (d, $J = 1.8$ Hz, 1H),
5 8.87 (s, 1H). ^{13}C NMR (101 MHz, DMSO) δ 42.90, 55.80, 59.93, 104.77, 116.77, 120.34, 125.10,
6 126.84, 130.79, 135.51, 136.29, 152.70, 155.20, 165.88, 168.43. m.p. [225°C with dec.]. $k' = 6.69$.
7
8 HRMS m/z $[\text{M}+\text{H}]^+$ Calcd. for $\text{C}_{18}\text{H}_{19}\text{N}_3\text{O}_4\text{S}$: 373.1096. Found: 373.1095.
9
10
11
12
13

14 15 **2-amino-N-(2-nitrobenzyl)benzo[d]thiazole-6-carboxamide (4j)**

16
17
18 Pale yellow solid. 36 % yield. ^1H NMR (400 MHz, $\text{DMSO-}d_6$) δ 4.76 (d, $J = 5.7$ Hz, 2H), 7.38 (d, $J =$
19 8.4 Hz, 1H), 7.48 – 7.66 (m, 2H), 7.66 – 7.95 (m, 4H), 8.05 (dd, $J = 1.3, 8.1$ Hz, 1H), 8.22 (d, $J =$
20 1.8 Hz, 1H), 8.98 (t, $J = 5.8$ Hz, 1H). ^{13}C NMR (101 MHz, DMSO) δ 40.13 (overlapping with
21 DMSO signal), 116.86, 120.41, 124.45, 125.13, 126.29, 128.10, 129.23, 130.87, 133.68, 134.43,
22 148.00, 155.44, 166.29, 168.57. m.p. [240°C with dec.]. $k' = 5.60$. HRMS m/z $[\text{M}+\text{H}]^+$ Calcd. for
23 $\text{C}_{15}\text{H}_{12}\text{N}_4\text{O}_3\text{S}$: 328.0630. Found: 328.0630.
24
25
26
27
28
29
30
31

32 33 **2-amino-N-benzhydrylbenzo[d]thiazole-6-carboxamide (4l)**

34
35
36 White solid. 70 % yield. ^1H -NMR (400 MHz, $\text{DMSO-}d_6$) δ : 6.42 (d, $J = 8.8$ Hz, 2H), 7.24-7.28 (m,
37 2H), 7.33-7.39 (m, 8H), 7.75 (s, 2H), 7.83 (dd, $J = 8.4, 1.2$ Hz, 1H), 8.28 (d, $J = 1.2$ Hz, 1H), 9.09
38 (d, $J = 8.8$ Hz, 1H). ^{13}C -NMR (101 MHz, DMSO) δ : 56.32, 116.76, 120.58, 125.60, 126.70, 126.88,
39 127.60, 128.26, 130.65, 142.47, 155.31, 165.54, 168.5. m.p [258°C with dec.]. $k' = 8.00$. HRMS
40 m/z $[\text{M}+\text{H}]^+$ Calcd. for $\text{C}_{21}\text{H}_{17}\text{N}_3\text{OS}$: 359.1092. Found: 359.1090.
41
42
43
44
45
46
47

48 49 **methyl 1-(2-aminobenzo[d]thiazole-6-carbonyl)piperidine-4-carboxylate (4m)**

50
51 White solid. 81 % yield. ^1H NMR (400 MHz, $\text{DMSO-}d_6$) δ 1.51-1.58 (m, 2H), 1.85-1.88 (m, 2H),
52 2.63-2.69 (m, 1H), 2.95-3.10 (m, 2H), 3.63 (s, 3H), 4.04 (from HSQC, 2H), 7.23 (dd, $J = 1.8, 8.2$
53 Hz, 1H), 7.33 (d, $J = 8.2$ Hz, 1H), 7.65 (s, 2H), 7.73 (dd, $J = 0.5, 1.8$ Hz, 1H). ^{13}C NMR (101 MHz,
54 DMSO) δ 14.05, 27.90, 51.50, 59.71, 116.97, 120.13, 124.75, 128.20, 130.82, 153.81, 167.90,
55
56
57
58
59
60

1
2
3 169.19, 174.27. m.p. [195°C with dec.]. $k' = 5.35$. HRMS m/z $[M+H]^+$ Calcd. for $C_{15}H_{17}N_3O_3S$:
4
5 319.0991. Found: 319.0990.
6
7

8 **2-amino-N-(2-(thiophen-2-yl)ethyl)benzo[d]thiazole-6-carboxamide (4n)**
9

10
11 Pale brown solid. 35 % yield. 1H NMR (400 MHz, DMSO- d_6) δ 3.07 (t, $J = 7.2$ Hz, 2H), 3.50 (td, J
12
13 = 5.5, 7.2 Hz, 2H), 6.91 – 6.97 (m, 2H), 7.33 – 7.36 (m, 2H), 7.73 (d, $J = 8.4$ Hz, 3H), 8.15 (d, $J =$
14
15 1.8 Hz, 1H), 8.50 (t, $J = 5.6$ Hz, 1H). ^{13}C NMR (101 MHz, DMSO) δ 29.28, 40.99, 116.79, 120.17,
16
17 123.97, 124.94, 125.07, 126.86, 127.00, 130.78, 141.61, 155.15, 165.91, 168.37. m.p. [230.5 –
18
19 231.7°C]. $k' = 6.27$. HRMS m/z $[M+H]^+$ Calcd. for $C_{14}H_{13}N_3OS_2$: 303.0500. Found: 303.0500.
20
21
22

23 **N-(2-(1H-indol-3-yl)ethyl)-2-aminobenzo[d]thiazole-6-carboxamide (4o)**
24

25
26 White solid. 59 % yield. 1H NMR (400 MHz, DMSO- d_6) δ 2.94 (t, $J = 7.1$ Hz, 2H), 3.52 (t, $J = 7.0$
27
28 Hz, 2H), 6.66 (s, 2H), 7.02 (dd, $J = 1.6, 32.8$ Hz, 2H), 7.16 (s, 1H), 7.32 (dd, $J = 1.6, 7.4$ Hz, 1H),
29
30 7.53 (dd, $J = 1.5, 7.2$ Hz, 1H), 7.66 (d, $J = 1.4$ Hz, 2H), 8.13 (t, $J = 1.0$ Hz, 1H), NH of amide
31
32 exchanges, 10.79 (s, 1H). ^{13}C -NMR (101 MHz, DMSO) δ 25.33, 40.33, 111.46, 112.50, 118.63,
33
34 118.77, 119.45, 121.08, 121.28, 122.60, 123.23, 127.64, 129.54, 131.62, 136.52, 155.96, 167.42,
35
36 169.16. m.p. [259°C with dec.]. $k' = 6.26$. HRMS m/z $[M+H]^+$ Calcd. for $C_{18}H_{16}N_4OS$: 336.1045.
37
38 Found: 336.1045.
39
40
41
42

43 **2-amino-N-benzyl-N-(3,4-dichlorobenzyl)benzo[d]thiazole-6-carboxamide (4p)**
44

45
46 Pale yellow solid. 47 % yield. 1H -NMR (400 MHz, DMSO- d_6) δ : 4.71 (s, 4H), 6.66 (s, 2H), 7.08-
47
48 7.10 (m, 1H), 7.23-7.37 (m, 7H), 7.52 (d, $J=8.0$ Hz, 1H), 7.67 (d, $J=8.0$ Hz, 1H), 7.99 (s, 1H). ^{13}C
49
50 NMR (101 MHz, DMSO) δ 51.95, 52.13, 118.92, 121.36, 122.31, 127.64, 127.76, 127.96, 128.16,
51
52 128.25, 129.60, 130.11, 130.24, 131.38, 133.25, 137.07, 137.84, 156.17, 169.16, 169.43. m.p.
53
54 [205°C with dec.]. $k' = 9.14$. HRMS m/z $[M+H]^+$ Calcd for $C_{22}H_{17}(^{35}Cl)_2N_3OS$: 441.0469. Found:
55
56 441.0470. Calcd. for $C_{22}H_{17}(^{35}Cl)(^{37}Cl)N_3OS$: 443.0440. Found: 443.0440.
57
58
59
60

2-amino-N-benzyl-N-(2-hydroxyethyl)benzo[d]thiazole-6-carboxamide (4q)

1
2
3 White solid. 35 % yield. ^1H NMR (400 MHz, $\text{DMSO-}d_6$) δ 3.40-3.55 (m, 4H), 4.55-4.75 (m, 2H),
4 4.78 (t, $J = 5.4$ Hz, 1H), 7.03 – 7.47 (m, 7H), 7.64 (s, 2H), 7.80 (s, 1H). ^{13}C NMR (101 MHz,
5 DMSO) δ 30.65, 39.81 (overlapping with DMSO signals), 58.33, 116.96, 119.95, 124.60, 126.92,
6 127.12, 128.51, 128.86, 130.77, 137.77, 153.54, 167.74, 171.14. m.p. [178°C with dec.]. $k' = 5.74$.
7
8
9
10
11
12 HRMS m/z $[\text{M}+\text{H}]^+$ Calcd. for $\text{C}_{17}\text{H}_{17}\text{N}_3\text{O}_2\text{S}$: 327.1041. Found: 327.1045.
13

14
15 **2-amino-N-(3,4-dichlorobenzyl)-N-(3,4-dimethoxybenzyl)benzo[d]thiazole-6-carboxamide (4r)**
16

17
18 Pale yellow solid. 52 % yield. ^1H NMR (400 MHz, $\text{DMSO-}d_6$) δ 3.69 (s, 3H), 3.71 (s, 3H), 4.50 (s,
19 4H), 6.73 (bs, 2H), 6.90 (d, $J = 8.2$ Hz, 1H), 7.33-7.44 (m, 4H), 7.59 (d, $J = 8.2$ Hz, 1H), 7.68 (s,
20 2H), 7.85 (s, 1H). ^{13}C NMR (101 MHz, DMSO) δ 52.20 (overlapping of 2C signals), 55.31, 55.50,
21 111.86, 112.45, 117.07, 120.07, 124.31, 124.43, 127.64, 128.04, 128.92, 19.57, 130.27, 130.58,
22 131.03, 133.41, 137.75, 148.11, 148.79, 153.90, 167.98, 171.28. m.p. [155.9-157.2°C]. $k' = 9.42$.
23
24
25
26
27
28
29
30
31
32
33
34
35
36
37
38
39
40
41
42
43
44
45
46
47
48
49
50
51
52
53
54
55
56
57
58
59
60

HRMS m/z $[\text{M}+\text{H}]^+$ Calcd for $\text{C}_{24}\text{H}_{21}(\text{}^{35}\text{Cl})_2\text{N}_3\text{O}_3\text{S}$: 501.0681. Found: 501.0680. Calcd. for
 $\text{C}_{24}\text{H}_{21}(\text{}^{35}\text{Cl})(\text{}^{37}\text{Cl})\text{N}_3\text{O}_3\text{S}$: 503.0651. Found: 503.0650.

35 **General procedure for the synthesis of benzothiazoles 4s-t**

36
37
38 2-amino-4-hydroxy-6-carboxy-benzothiazole (1 eq.) was solubilized in DMF at 0 °C. EDC (1 eq.),
39 HOBT (1 eq.) and the appropriate benzyl amine (1 eq.) was added. The mixture was stirred at room
40 temperature overnight and concentrated. The residue was solubilized in AcOEt and washed
41 consecutively with K_2CO_3 saturated solution, NH_4Cl saturated solution, brine, dried over anhydrous
42 Na_2SO_4 and concentrated. The crude was purified on silica gel to afford the desired product.
43
44
45
46
47
48
49

50 **2-amino-N-benzyl-4-hydroxybenzo[d]thiazole-6-carboxamide (4s)**
51

52
53 Pink solid. 23 % yield. ^1H -NMR (400 MHz, $\text{DMSO-}d_6$) δ : 4.44 (d, 2H, $J = 6$ Hz), 7.24 (m, 2H),
54 7.32 (m, 4H), 7.51 (s, 2H), 7.68 (s, 1H), 8.80 (t, 1H, $J = 6$ Hz), 9.44 (s, 1H). ^{13}C -NMR (400 MHz,
55 DMSO- d_6) δ : 42.57, 111.00, 11.18, 126.60, 127.15, 127.97, 128.18, 131.55, 139.90, 143.85, 146.92,
56
57
58
59
60

1
2
3 166.08, 166.29. m.p. [244°C with dec.]. $k' = 6.39$. HRMS m/z $[M+H]^+$ Calcd. for $C_{15}H_{13}N_3O_2S$:
4
5 299.0728. Found: 299.0725.
6
7

8 **2-amino-N-(3,4-dichlorobenzyl)-4-hydroxybenzo[d]thiazole-6-carboxamide (4t)**

9
10
11 Yellow solid. 32 % yield. 1H -NMR (400 MHz, $DMSO-d_6$) δ : 4.43 (d, 2H, $J = 5.6$ Hz), 7.21 (s, 1H),
12
13 7.30 (dd, 1H, $J = 8.4, 2.0$ Hz), 7.53 (s, 2H), 7.55 (d, 1H, $J = 1.6$ Hz), 7.59 (d, 1H, $J = 8.4$ Hz), 7.67
14
15 (d, 1H, $J = 1.6$ Hz), 8.86 (t, 1H, $J = 6$ Hz), 9.45 (s, 1H). ^{13}C -NMR (400 MHz, $DMSO-d_6$) δ : 41.66,
16
17 111.12, 117.74, 125.57, 127.60, 129.19, 2x130.42, 130.79, 131.61, 141.22, 144.08, 146.95, 166.21,
18
19 166.37. m.p. [251°C with dec.]. $k' = 5.41$. HRMS m/z $[M+H]^+$ Calcd. for $C_{15}H_{11}(^{35}Cl)_2N_3O_2S$:
20
21 366.9949. Found: 366.9950. Calcd for $C_{15}H_{11}(^{35}Cl)(^{37}Cl)N_3O_2S$: 368.9920. Found: 368.9920.
22
23
24
25

26 **General procedure for the synthesis of the 4-amido-benzothiazoles 5a-c**

27
28
29 To a solution of **13a-c** (1 eq.) in dry DCM (20 mL) at 0 °C under an inert atmosphere a solution 1M
30
31 of BBr_3 (3 eq. *per* CH_3O) in DCM was added drop wise. The reaction was spontaneously warmed at
32
33 room temperature and stirred for 4 hours. The mixture was quenched with 10 mL of MeOH and
34
35 concentrated. The residue was suspended in water and extracted in AcOEt. The organic phase was
36
37 washed with $NaHCO_3$ saturated solution and brine, dried over anhydrous Na_2SO_4 and concentrated.
38
39 The crude was purified over silica gel to give the desired product.
40
41
42

43 **2-amino-N-benzyl-N-(3,4-dichlorobenzyl)-6,7-dihydroxybenzo[d]thiazole-4-carboxamide (5a)**

44
45
46 Purple solid. 68 % yield. 1H NMR (400 MHz, $DMSO-d_6$) δ 4.33 (s, 2H), 4.59 (s, 2H), 6.71 (s, 2H),
47
48 6.96 – 7.45 (m, 6H), 7.46 – 7.71 (m, 2H), 7.74 (d, $J = 8.3$ Hz, 1H), 9.15 (bs, 1H), 9.43 (bs, 1H). ^{13}C
49
50 NMR (101 MHz, DMSO) δ 45.82, 51.84, 112.8, 116.45, 127.33, 127.43, 127.51, 128.47, 129.12,
51
52 129.22 (overlap of 2C signals), 130.43, 130.72, 130.86, 136.90, 138.74, 139.03, 139.07, 165.24,
53
54 169.86. m.p. [215°C with dec.]. $k' = 7.80$. HRMS m/z $[M+H]^+$ Calcd. for $C_{22}H_{17}(^{35}Cl)_2N_3O_3S$:
55
56 473.0368. Found: 473.0365. Calcd. for $C_{22}H_{17}(^{35}Cl)(^{37}Cl)N_3O_3S$: 475.0338. Found: 475.0340.
57
58
59
60

2-amino-N-(3,4-dichlorobenzyl)-6,7-dihydroxybenzo[d]thiazole-4-carboxamide (5b)

1
2
3 Green solid. 62 % yield. ^1H NMR (400 MHz, $\text{DMSO-}d_6$) δ 4.57 (d, $J = 6.1$ Hz, 2H), 7.30 (dd, $J =$
4 2.1, 8.3 Hz, 1H), 7.50-7.74 (m, 6H), 9.36 (s, 1H), 10.19 (s, 1H). ^{13}C NMR (101 MHz, DMSO) δ
5 41.24, 109.16, 115.25, 118.90, 124.74, 126.76, 126.81, 127.51, 128.02, 137.34, 143.53, 144.85,
6 145.23, 161.7, 164.07. m.p. [170°C with dec.]. $k' = 5.69$. HRMS m/z $[\text{M}+\text{H}]^+$ Calcd for
7 $\text{C}_{15}\text{H}_{11}({}^{35}\text{Cl})_2\text{N}_3\text{O}_3\text{S}$: 382.9898. Found: 382.9900. Calcd. for $\text{C}_{15}\text{H}_{11}({}^{35}\text{Cl})({}^{37}\text{Cl})\text{N}_3\text{O}_3\text{S}$: 384.9869.
8 Found: 384.9870.
9

16 17 **2-amino-N-benzyl-6,7-dihydroxybenzo[d]thiazole-4-carboxamide (5c)**

18
19
20 Dark yellow solid. 70 % yield. ^1H NMR (400 MHz, $\text{DMSO-}d_6$) δ 4.60 (d, $J = 6.1$ Hz, 2H), 7.15 –
21 7.45 (m, 5H), 7.52 (s, 1H), 7.71 (s, 2H), 9.32 (s, 1H), 9.82 (s, 1H), 10.17 (t, $J = 6.2$ Hz, 1H). ^{13}C
22 NMR (101 MHz, DMSO) δ 42.11, 112.42, 114.82, 117.89, 126.64, 126.83, 128.36, 138.96, 139.09,
23 139.88, 142.41, 164.55, 166.38. m.p. [192°C with dec.]. $k' = 4.73$. HRMS m/z $[\text{M}+\text{H}]^+$ Calcd. for
24 $\text{C}_{15}\text{H}_{13}\text{N}_3\text{O}_3\text{S}$: 315.0678. Found: 315.0678.
25
26
27
28
29
30
31

32 33 **6-hydroxybenzo[d]thiazol-2-amine (6)**

34
35 To a solution of thiourea (500 mg, 6.58 mmol, 1 eq.) in ethanol (10 mL), concentrated hydrochloric
36 acid (55 μL , 0.66 mmol, 0.1 eq.) was added, followed by the drop wise addition of a hot solution of
37 benzoquinone (1448 mg, 13.66 mmol, 2 eq.) in ethanol over a period of 30 minutes. The solution
38 was refluxed for 6 hours and then concentrated. The crude was titrated with hot acetonitrile and
39 filtered. The solid was re-suspended in water and neutralized with sodium acetate. A purple solid
40 precipitated, which was collected, washed with hot acetone and filtered to give 830 mg of a brick-
41 red solid (76 % yield). ^1H -NMR (400 MHz, $\text{DMSO-}d_6$) δ 6.63 (dd, $J = 8.4, 2.4$ Hz, 1H), 7.00 (d, J
42 = 2.4, 1H), 7.06 (s, 2H), 7.11(d, $J = 8.4, 1\text{H}$), 9.060 (s, 1H). ^{13}C -NMR (101 MHz, DMSO) δ 107.36,
43 113.97, 118.55, 132.31, 146.13, 152.54, 164.40.
44
45
46
47
48
49
50
51
52
53
54
55
56

57 **General procedure for the synthesis of nitrobenzene-sulfides 7a-f**

To a solution of 4-nitro-thiophenol (1 eq.) in DMF (5 mL per mmol) K_2CO_3 (2.5 eq.) was added at room temperature. After 10 minutes, the appropriate alkyl bromide (1.2 eq., for **7b-h**) or iodomethane (1.2 eq., for **7a**) was added and the mixture stirred in the same conditions for 24 hours and then concentrated. The residue was suspended in AcOEt and washed with a saturated solution of K_2CO_3 , brine, dried over anhydrous Na_2SO_4 and concentrated to afford the desired product.

methyl(4-nitrophenyl)sulfane (7a)

Yellow liquid. 92 % yield. 1H NMR (400 MHz, Chloroform-*d*) δ 2.45 (s, 3H), 7.49 (d, $J = 7.6$ Hz, 2H), 8.15 (d, $J = 7.5$ Hz, 2H). MS m/z $[M+H]^+$: 170.2.

(4-nitrophenyl)(trifluoromethyl)sulfane (7b)

Pale yellow solid. 84 % yield. 1H NMR (400 MHz, Chloroform-*d*) δ 7.57 (d, $J = 7.4$ Hz, 2H), 8.16 (d, $J = 7.6$ Hz, 2H). MS m/z $[M+H]^+$: 224.3.

benzyl(4-nitrophenyl)sulfane (7c)

Yellow solid. 95 % yield. 1H NMR (400 MHz, Chloroform-*d*) δ 4.33 (s, 2H), 7.09 – 7.36 (m, 5H), 7.37 – 7.56 (m, 2H), 8.04 – 8.21 (m, 2H). MS m/z $[M+H]^+$: 246.4.

(3,4-dichlorobenzyl)(4-nitrophenyl)sulfane (7d)

Yellow solid. 86 % yield. 1H NMR (400 MHz, Chloroform-*d*) δ 4.33 (s, 2H), 6.67 – 7.06 (m, 1H), 7.14 – 7.44 (m, 2H), 7.44 – 7.77 (m, 2H), 8.06 – 8.29 (m, 2H). MS m/z $[M+H]^+$: 314.1, 316.2.

4-(((4-nitrophenyl)thio)methyl)benzonitrile (7e)

Yellow solid. 82 % yield. 1H NMR (400 MHz, Chloroform-*d*) δ 4.33 (s, 2H), 7.27 – 7.42 (m, 2H), 7.50-7.54 (m, 4H), 8.15 (d, $J = 7.6$ Hz, 2H). MS m/z $[M+H]^+$: 271.4.

methyl 4-(((4-nitrophenyl)thio)methyl)benzoate (7f)

1
2
3 Yellow solid. 75 % yield. ^1H NMR (400 MHz, Chloroform-*d*) δ 3.95 (s, 3H), 4.33 (s, 2H), 6.97 –
4 7.32 (m, 2H), 7.48 (d, $J = 7.5$ Hz, 2H), 7.82 (d, $J = 7.7$ Hz, 2H), 8.14 (d, $J = 7.6$ Hz, 2H). MS m/z
5
6 [M+H] $^+$: 304.4.
7
8
9

10 **General procedure for the synthesis of aminobenzene-sulfides 8a-f**

11
12
13 To a solution of the appropriate 4-nitrophenylsulfane **7a-f** (1 eq.) in methanol (10 mL *per* mmol)
14
15 NH_4Cl (2.5 eq.) and zinc (2 eq.) were added at room temperature. The suspension was refluxed for
16
17 2-6 hours and concentrated. The residue was suspended in water and AcOEt and the aqueous phase
18
19 alkalinized with 6N NaOH. The suspension was filtered over celite. The organic phase was
20
21 collected, dried over anhydrous Na_2SO_4 and concentrated. The crude was purified on silica gel to
22
23 afford the desired product.
24
25
26

27 **4-(methylthio)aniline (8a)**

28
29
30
31 Yellow liquid. 64 % yield. ^1H NMR (400 MHz, Chloroform-*d*) δ 2.45 (s, 3H), 6.53 (d, $J = 7.6$ Hz,
32
33 2H), 7.07 (d, $J = 7.6$ Hz, 2H). MS m/z [M+H] $^+$: 140.2.
34
35

36 **4-((trifluoromethyl)thio)aniline (8b)**

37
38
39 Yellow liquid. 32 % yield. ^1H NMR (400 MHz, Chloroform-*d*) δ 6.54 (d, $J = 7.6$ Hz, 2H), 7.14 (d, J
40
41 = 7.5 Hz, 2H). MS m/z [M+H] $^+$: 194.1.
42
43
44

45 **4-(benzylthio)aniline (8c)**

46
47 Yellow solid. 75 % yield. ^1H NMR (400 MHz, DMSO-*d*₆) δ 4.33 (d, $J = 1.1$ Hz, 2H), 6.55 (d, $J =$
48
49 7.4 Hz, 2H), 6.91 – 7.36 (m, 7H), 7.34 – 7.52 (m, 2H). MS m/z [M+H] $^+$: 216.2.
50
51
52

53 **4-((3,4-dichlorobenzyl)thio)aniline (8d)**

54
55
56 Yellow solid. 69 % yield. ^1H NMR (400 MHz, DMSO-*d*₆) δ 4.30 (m, 2H), 6.57 (d, $J = 7.6$ Hz, 2H),
57
58 6.92 – 7.36 (m, 5H), 7.37 – 7.56 (m, 1H), 7.62 (d, $J = 7.5$ Hz, 1H). MS m/z [M+H] $^+$: 284.1, 286.1.
59
60

4-(((4-aminophenyl)thio)methyl)benzonitrile (8e)

Yellow solid. 58 % yield. ¹H NMR (400 MHz, DMSO-*d*₆) δ 4.35 (s, 2H), 6.54 (d, *J* = 7.4 Hz, 2H), 7.04 – 7.47 (m, 6H), 7.64 (d, *J* = 7.4 Hz, 2H). MS *m/z* [M+H]⁺: 241.2.

methyl 4-(((4-aminophenyl)thio)methyl)benzoate (8f)

Yellow solid. 63 % yield. ¹H NMR (400 MHz, DMSO-*d*₆) δ 3.85 (s, 3H), 4.32 (d, *J* = 1.1 Hz, 2H), 6.55 (d, *J* = 7.6 Hz, 2H), 6.97 – 7.42 (m, 6H), 7.82 (d, *J* = 7.6 Hz, 2H). MS *m/z* [M+H]⁺: 274.4.

General procedure for the synthesis of amine 9p-r

To a solution of the amine (2 eq.) in DMF, K₂CO₃ (2.5 eq.) and the appropriate alkyl bromide were added at room temperature. The mixture was stirred in the same condition for 6 hours and concentrated. The residue was suspended in DCM and washed with brine. The organic phase was dried over anhydrous Na₂SO₄ and concentrated. The crude was chromatographed to afford the desired product.

N-benzyl-1-(3,4-dichlorophenyl)methanamine (9p)

Yellowish liquid. 35 % yield. ¹H NMR (400 MHz, Chloroform-*d*) δ 3.65 (s, 4H), 7.18 – 7.39 (m, 6H), 7.39 – 7.49 (m, 2H). MS *m/z* [M+H]⁺: 265.1; 267.1.

2-(benzylamino)ethan-1-ol (9q)

Colorless liquid. 58 % yield. ¹H NMR (400 MHz, Chloroform-*d*) δ 2.74 (t, *J* = 4.5 Hz, 2H), 3.69 (q, *J* = 4.7 Hz, 2H), 4.25 (d, *J* = 1.1 Hz, 2H), 7.19 – 7.41 (m, 3H), 7.47 – 7.61 (m, 2H). MS *m/z* [M+H]⁺: 152.2.

N-(3,4-dichlorobenzyl)-1-(3,4-dimethoxyphenyl)methanamine (9r)

1
2
3 Yellowish liquid. 48 % yield. ¹H NMR (400 MHz, Chloroform-d) δ 3.64 (s, 2H), 3.66 (s, 2H), 3.88
4 (s, 3H), 3.90 (s, 3H), 6.84 (d, *J* = 7.4 Hz, 1H), 6.90 (dd, *J* = 1.6, 7.5 Hz, 1H), 7.06 (dt, *J* = 1.1, 2.1
5 Hz, 1H), 7.22 – 7.29 (m, 1H), 7.37 – 7.47 (m, 2H). MS *m/z* [M+H]⁺: 326.1; 327.2.
6
7
8
9

10 **Synthesis of 2-amino-4-hydroxybenzo[d]thiazole-6-carboxylic acid (10)**

11
12
13 To a suspension of 2-amino-4-hydroxybenzoic acid (500 mg, 3.26 mmol, 1 eq.) in glacial acetic
14 acid (6 mL), KSCN (1.6 g, 16.32 mmol, 5 eq.) was added. The mixture was chilled and a solution
15 of elemental bromine (336 μL, 6.52 mmol, 2 eq.) in acetic acid (6 mL) was added drop wise
16 keeping the temperature below 10 °C. The mixture was spontaneously warmed at room temperature
17 and stirred for 1 hour. The reaction was quenched with water, boiled for 15 minutes and filtered still
18 hot. The filtrate was chilled down and the solid crystalized removed by filtration. The pH of the
19 water was adjusted to 4 and the solid precipitated collected by filtration, rinsed with water and dried
20 to afford 290 mg (42 % yield) of a dark orange solid. ¹H NMR (400 MHz, DMSO-*d*₆) δ 6.74 (s,
21 2H), 7.63 (d, *J* = 1.7 Hz, 1H), 8.01 (d, *J* = 1.5 Hz, 1H), 10.25 (s, 1H), 12.99 (s, 1H). MS *m/z*
22 [M+H]⁺: 211.0.
23
24
25
26
27
28
29
30
31
32
33
34
35
36

37 **Synthesis of methyl 2-amino-6,7-dimethoxybenzo[d]thiazole-4-carboxylate (11)**

38
39
40 To a suspension of methyl 2-amino-4,5-dimethoxybenzoate (1.0 g, 4.73 mmol, 1 eq.) in glacial
41 acetic acid (20 mL), KSCN (2.3 g, 23.7 mmol, 5 eq.) was added. The mixture was chilled and a
42 solution of elemental bromine (488 μL, 9.46 mmol, 2 eq.) in acetic acid (10 mL) was added drop
43 wise keeping the temperature below 10 °C. The mixture was spontaneously warmed at room
44 temperature and stirred for 2 hours. The mixture was quenched with water and filtered. The filtrate
45 was alkalized at pH 9 with 30% aqueous NH₄OH and the precipitated formed collected by
46 filtration, rinsed with water and dried to give 1.02 g (yield 81 %) of a brown solid. ¹H NMR (400
47 MHz, DMSO-*d*₆) δ 3.81 (s, 3H), 3.84 (s, 3H), 3.92 (s, 3H), 7.39 (s, 1H), 7.76 (s, 2H). MS *m/z*
48 [M+H]⁺: 269.1.
49
50
51
52
53
54
55
56
57
58
59
60

2-amino-6,7-dimethoxybenzo[d]thiazole-4-carboxylic acid (12)

To a solution of **11** (500 mg, 1.86 mmol, 1 eq.) in MeOH:THF 3:1 (12 mL) aqueous 1N NaOH (2.05 mL, 2.05 mmol, 1.1 eq.) was added. The mixture was stirred at room temperature overnight and concentrated. The residue was solubilized in water and washed with AcOEt. The pH of the aqueous phase was adjusted to 4 with 1N HCl and the precipitate formed was collected by filtration, rinsed with water and dried to give 276 mg (58 % yield) of a brown solid. ¹H NMR (400 MHz, DMSO-*d*₆) δ 3.81 (s, 3H), 3.85 (s, 3H), 7.56 (s, 1H), 8.60 (bs, 2H). MS m/z [M-H]⁻: 253.0.

General procedure for the synthesis of the 4-amido-benzothiazoles 13a-c

12 (1 eq.) was solubilized in DMF at 0 °C. EDC (1 eq.), HOBt (1 eq.) and the appropriate benzyl amine (1 eq.) were consequentially added. The mixture was stirred at room temperature overnight and concentrated. The residue was solubilized in AcOEt and washed consecutively with K₂CO₃ ss, NH₄Cl ss, brine, dried over anhydrous Na₂SO₄ and concentrated. The crude was purified on silica gel to afford the desired product.

2-amino-N-benzyl-N-(3,4-dichlorobenzyl)-6,7-dimethoxybenzo[d]thiazole-4-carboxamide (13a)

Brown solid. 61 % yield. ¹H NMR (400 MHz, Chloroform-*d*) δ 3.90 (s, 3H), 3.96 (s, 3H), 4.70-4.72 (m, 4H), 6.97 – 7.11 (m, 1H), 7.18 – 7.37 (m, 6H), 7.44 (d, *J* = 7.5 Hz, 1H), 7.66 (s, 1H). MS m/z [M+H]⁺: 502.1.

2-amino-N-(3,4-dichlorobenzyl)-6,7-dimethoxybenzo[d]thiazole-4-carboxamide (13b)

Brown solid. 39 % yield. ¹H NMR (400 MHz, Chloroform-*d*) δ 3.90 (s, 3H), 3.91 (s, 3H), 4.52 (d, *J* = 1.3 Hz, 2H), 7.33 (dd, *J* = 1.5, 7.2 Hz, 1H), 7.46 – 7.62 (m, 2H), 8.11 (s, 1H). MS m/z [M+H]⁺: 413.1.

2-amino-N-benzyl-6,7-dimethoxybenzo[d]thiazole-4-carboxamide (13d)

1
2
3 Brown solid. 48 % yield. ^1H NMR (400 MHz, Chloroform-*d*) δ 3.89 (s, 3H), 3.90 (s, 3H), 4.50 (s,
4 2H), 7.12 – 7.44 (m, 5H), 7.65 (s, 1H). MS m/z $[\text{M}+\text{H}]^+$: 345.0.
5
6
7
8
9
10

11 **Molecular modelling**

12
13
14 The crystal structure of *TbPTR1* in ternary complex with NAPD(H) and DX2 inhibitor at 1.8 Å was
15 retrieved from Protein Data Bank (PDB ID: 3JQ7).²⁸ Chain A was prepared for calculations by
16 using VMD.³⁹ Missing bonds and atoms were fixed and polar hydrogens and charges were added.
17
18 Conserved water molecules previously identified for *TbPTR1* and a set of additional waters present
19 in at least 50 % of the *TbPTR1* crystal structures reported in literature were included in the binding
20 site.¹⁷ A three-dimensional grid box was centered on the oxygen atom of hydroxyl group of Tyr174.
21
22 The center and the size of the grid maps were based on AutoGrid default values (Size (x,y,z):
23 40/50/40 grid points spacing of 0.375 Å; Center (x,y,z): 6.798/-6.705/16.560). AutoDock 4.2 was
24
25 used for the docking simulation.²⁹ Lamarckian genetic algorithm (LGA) was employed for ligand
26 conformational searching and docking parameters were set as default. The docking model was
27 validated first by redocking of the ligand DX2 into the prepared crystal structure with the resulting
28 RMSD being within 0.83 Å. Ligands were first drawn with ChemBio3D Ultra 14.0,⁴⁰ and all the
29 combinations of tautomers and protonation states at pH 7.4 of the ligands were generated with
30 Discovery Studio.⁴¹ AutoDockTools 1.5.6²⁹ package scripts were used to convert structures of
31 ligands and prepared protein to AutoDock 4.2 format. A total of 20 conformations with the best
32 scores were retained for each ligand. Finally, docking poses were ranked according to the predicted
33 scores and visually inspected with AutodockTools 1.5.6²⁹ and Discovery Studio software.⁴¹
34
35
36
37
38
39
40
41
42
43
44
45
46
47
48
49
50
51
52
53
54

55 **Protein expression and purification**

56
57 Recombinant *TbPTR1* was expressed and purified by established methods.²⁴
58
59

60 **Protein crystallization**

1
2
3 Crystals of *TbPTR1* were grown using the vapor diffusion hanging drop technique at 297 K.⁴²
4
5 Drops were prepared by mixing equal volumes (3 μL) of protein (histidine tagged *TbPTR1* 8-10 mg
6
7 mL^{-1} in 20 mM TRIS, pH 7.5) and precipitant (2 – 2.5 M sodium acetate, 0.1 M sodium citrate, pH
8
9 5) solutions. The ternary complexes *TbPTR1*-cofactor-inhibitor were obtained by the soaking
10
11 technique using preformed monoclinic protein crystals, grown after few days of equilibration at 297
12
13 K. The complexes with the compounds **3a**, **4c** and **4g** were obtained by transferring crystals to a
14
15 cryo-protectant/soaking solution prepared by adding 30 % v/v glycerol and 4 mM inhibitor
16
17 (solubilized in DMSO) to the precipitant solution (the final DMSO concentration was kept lower
18
19 than 10 % v/v), according to an established procedure.²² Crystals were flash-frozen in liquid
20
21 nitrogen after 7 – 20 hours. All the other complexes were obtained by adding 2 – 4 mM inhibitor
22
23 (solubilized in DMSO) in the crystallization drop (the DMSO concentration in the drop was kept
24
25 lower than 10 % v/v), as previously reported.¹⁷ After 1 – 2 hours crystals were transferred to the
26
27 cryo-protectant solution (obtained by adding 30 % v/v glycerol to the precipitant solution) and
28
29 flash-frozen in liquid nitrogen.
30
31
32
33
34

35 36 **Data collection, structure solution and refinement**

37
38 Diffraction data were collected using the synchrotron radiation either at the Diamond Light Source
39
40 (DLS, Didcot, United Kingdom) beam line I04 and I04-1 equipped with a Dectris Pilatus 6M-F
41
42 detector or at the European Synchrotron Radiation Facility (ESRF, Grenoble, France) beam line
43
44 ID23-1 and ID23-2 equipped with a Pilatus 6M-F and a Pilatus3 X 2M, respectively. Reflections
45
46 were integrated using either Mosflm^{43,44} or XDS⁴⁵ and scaled with Scala^{46,47} from the CCP4
47
48 suite.⁴⁸ The *TbPTR1* crystals belonged to the primitive monoclinic space group $P2_1$, with a
49
50 functional tetramer in the asymmetric unit. Data collection and processing statistics are reported in
51
52 Table SI-2-3. Structures were solved by the molecular replacement technique using the software
53
54 MOLREP⁴⁹ and a functional tetramer of *TbPTR1* (PDB ID 5JDC²⁴) as the searching model
55
56 (solvent and non-protein molecules were preventively excluded). The protein structures were
57
58
59
60

1
2
3 refined using REFMAC5⁵⁰ and a protocol involving sequential iterative manual rebuilding of the
4
5 models and maximum likelihood refinement. The molecular graphic software Coot^{51,52} was used
6
7 for visual inspection and modeling of missing atoms in the electron density. Ligand occupancy was
8
9 estimated using a criterion based on keeping the atomic displacement parameters of each molecule
10
11 comparable with those of the surrounding residues (in fully occupied sites). Water molecules were
12
13 added using the program ARP/wARP⁵³ and inspected with Coot. The final models were checked
14
15 both manually and through the programs Coot and Procheck⁵⁴ and rendered using CCP4mg⁵⁵.
16
17 Final refinement statistics are reported in Table SI-2.
18
19
20
21

22 Coordinates and structure factors were deposited in the Protein Data Bank under the codes **6GCK**
23
24 (*TbPTR1* – NADP(H)– **1e**), **6GCQ** (*TbPTR1* – NADP(H)– **2b**), **6GCP** (*TbPTR1* – NADP(H)– **2d**),
25
26 **6GDO** (*TbPTR1* – NADP(H)– **2g**), **6GEX** (*TbPTR1* – NADP(H)– **2h**), **6GCL** (*TbPTR1* –
27
28 NADP(H)– **3a**), **6GD4** (*TbPTR1* – NADP(H)– **4c**), **6GEY** (*TbPTR1* – NADP(H)– **4d**), **6GD0**
29
30 (*TbPTR1* – NADP(H)– **4g**), and **6GDP** (*TbPTR1* – NADP(H)– **4l**).
31
32
33
34
35
36

37 *In-vitro* biological assays

38
39
40 ***TbPTR1*, *LmPTR1* inhibition assays.** The *in-vitro* assays for the detection of PTR1 inhibition,
41
42 used in the current study, were based upon those reported in the literature.⁵⁶ Since PTR1 enzymes
43
44 use dihydrobiopterine (H₂B) as a substrate and also require NADPH for the reaction, the reduction
45
46 of H₂B to tetrahydrobiopterine (H₄B) by PTR1 is non-enzymatically linked with the reduction of
47
48 cytochrome c in this assay, which is detected at 550 nm. The formation of cyt c Fe²⁺ results in a
49
50 signal increase in the photometric readout.
51
52
53

54
55 **Evaluation of activity against *T. brucei*.** The anti-parasitic activity of compounds was evaluated
56
57 using a modified resazurin-based assay previously described in the literature.⁵⁷ Mid-log *T. brucei*
58
59 bloodstream forms were added to an equal volume of serial dilutions of compounds in
60

1
2
3 supplemented complete HMI-9 medium at a final cell density of 5×10^3 /mL. Following incubation
4
5 for 72 hours at 37 °C 5 % CO₂, 20 μL of a 0.5 mM resazurin solution was added and plates were
6
7 incubated for a further 4 hours under the same conditions. Fluorescence was measured at 540 nm
8
9 and 620 nm excitation and emission wavelength, respectively, using a Synergy 2 Multi-Mode
10
11 Reader (Biotek). The anti-trypanosomatid effect was evaluated by the determination of the EC₅₀
12
13 value (concentration required to inhibit growth by 50 %) and calculated by non-linear regression
14
15 analysis using GraphPad Prism, Version 5.00 for Windows, GraphPad Software, San Diego
16
17 California USA (www.graphpad.com). For potentiation experiments the synergy index was
18
19 calculated as the ratio between the activity of the combination (10 μM of compound in the presence
20
21 of 4 μM MTX) and the added activity of the components of the combination alone (activity of 10
22
23 μM of benzothiazole + activity of 4 μM MTX).

24
25
26
27
28
29 **Evaluation of activity against *L. infantum* intramacrophage amastigotes.** Anti-parasitic activity
30
31 against *L. infantum* intracellular amastigotes at 10 μM compound concentration was determined
32
33 according to a previously published procedure with some modifications.⁵⁸ Briefly, 1×10^6 THP-1-
34
35 derived macrophages were infected with luciferase-expressing *L. infantum* axenic amastigotes in a
36
37 macrophage:amastigotes ratio of 1:10 for 4 h at 37 °C, 5% CO₂. Non-internalized parasites were
38
39 washed, and compounds were added at different concentrations (20 - 0.6 μM). After 72 h of
40
41 incubation at 37 °C and 5% CO₂, media was substituted by PBS. Macrophages were lysed by
42
43 addition of 25 μL of Glo-lysis buffer (Promega). Steady-Glo reagent (Promega) was then added,
44
45 and the content of each well was transferred to white-bottom 96-well plates. Luminescence intensity
46
47 was read using a Synergy 2 multi-mode reader (Biotek). The anti-leishmanial effect was evaluated
48
49 by the determination of the IC₅₀ value (concentration required to inhibit growth in 50%) and
50
51 calculated by nonlinear regression analysis using GraphPad Prism version 5.00 for Windows,
52
53 GraphPad Software, San Diego, California (www.graphpad.com).

1
2
3 **Evaluation of activity against *T. cruzi*.** The drug assay method consisted of measuring compound
4 activity on the U2OS (osteosarcoma) cell-line infected with *T. cruzi*, as previously described.³⁴ The
5 U2OS cell-line, which presents a large cytoplasm that allow for improved quantification of *T. cruzi*
6 amastigotes in high content analysis, was plated and allowed to grow as a monolayer for 24 h prior
7 to infection with tissue-derived trypomastigote forms of *T. cruzi*. Compounds were plated at a final
8 concentration of either 50 μ M (for single concentration screening) or variable concentrations (for
9 dose-response tests) 24 h after infection. Infected cultures were exposed to compounds for 72 hours.
10 Plates were processed for high content imaging and normalized compound activity was determined
11 in relation to infected and non-infected controls.
12
13
14
15
16
17
18
19
20
21
22
23
24
25

26 ***In-vitro* early ADME-Toxicity assays**

27
28 ***h*ERG inhibition.** This assay made use of Invitrogen's Predictor™ *h*ERG Fluorescence
29 Polarisation Assay. The assay uses a membrane fraction containing *h*ERG channel (Predictor™
30 *h*ERG Membrane) and a high-affinity red fluorescent *h*ERG channel ligand, or "tracer"
31 (Predictor™ *h*ERG Tracer Red), whose displacement by test compounds can be determined in a
32 homogenous, Fluorescence Polarization based format.⁵⁹
33
34
35
36
37
38
39
40
41

42 **Cytochrome P450 1A2, 2C9, 2C19, 2D6 and 3A4 inhibition.** These assays made use of the
43 Promega P450-Glo™ assay platform. Each cytochrome P450 isoform assay made use of
44 microsomal preparations of cytochromes from baculovirus infected insect cells. Action of the
45 cytochrome P450 enzymes upon each substrate ultimately resulted in the generation of light and a
46 decrease in this was indicative of inhibition of the enzymes.⁵⁹
47
48
49
50
51
52
53
54
55

56 **Cytotoxicity assay against A549 cell-line.** The assays were performed using the Cell Titer-Glo®
57 assay from Promega. The assay detects cellular ATP content with the amount of ATP being directly
58 proportional to the number of cells present. The A549 cell-line was obtained from DSMZ (German
59
60

1
2
3 Collection of Microorganisms and Cell Cultures, Braunschweig, Germany) and was grown in
4
5 DMEM with FCS (10 % v/v), streptomycin (100 µg/ml) and penicillin G (100 U/ml).⁵⁹
6
7
8
9

10 **Cytotoxicity assessment against THP-1 macrophages and U2OS cells.** The cytotoxicity of THP-
11
12 1-derived macrophages was assessed by the colorimetric (3-(4,5-dimethylthiazol-2-yl)-2,5-diphenyl
13
14 tetrazolium bromide (MTT) assay.⁵⁹ The cytotoxicity against U2OS cells was determined from the
15
16 anti-*T. cruzi* assay, based on the reduction of cell number in treated wells in comparison with
17
18 infected, non-treated wells.³⁴
19
20
21
22
23

24
25 **Mitochondrial toxicity.** This assay made use of MitoTracker[®] Red chloromethyl-X-rosamine
26
27 (CMXRos) uptake and High Content Imaging to monitor compound mediated mitochondrial
28
29 toxicity in the 786-O (renal carcinoma) cell line. Cells were maintained using RPMI-1640 medium
30
31 containing 2 mM glutamine, FCS (10 % v/v), streptomycin (100 µg/ml) and penicillin G (100
32
33 U/ml).⁵⁹
34
35
36
37
38
39

40 **Pharmacodynamic solubility.** The pharmacodynamics solubility of **4c** in four media (Milli-Q
41
42 water, PBS, PBS + 10%DMSO and PBS + 50%DMSO) was spectrophotometrically measured by
43
44 the methodology described by Bard et al. with slight modification.³⁵ The molar extinction
45
46 coefficient (ϵ) at 340 nm was determined first. Four over-saturated solutions, with maximum
47
48 theoretical concentration of 100 µg/mL were prepared and the suspensions stirred at 1200 rpm for
49
50 24 hours at 25 °C. The suspensions were filtered (0.2 µm) and diluted 1:1 with ACN and the
51
52 concentration of the compound in the filtrate was quantified spectrophotometrically.
53
54
55
56
57

58 ***In-vivo* assays**
59
60

1
2
3 **Pharmacokinetics of compound 4c by LC-MS.** The snapshot PK studies were carried out
4 according to literature.⁶⁰ BALB/c mice were treated with compound **4c** administered alone (8%
5 DMSO) (1 mg/kg IV or 20 mg/kg *per os*), compound **4c** solubilized with hydroxypropil- β -
6 cyclodextrin (50%) (20 mg/kg *per os*) or with a mixture of cyclodextrins (25%) plus polyethylene
7 cyclodextrin (50%) (20 mg/kg *per os*) or with a mixture of cyclodextrins (25%) plus polyethylene
8 glycol 400 (Quimidroga) (50%) (20 mg/kg *per os*). Plasma samples were analyzed by LC-MS.
9
10 Chromatographic separation was carried out using a Shimadzu LC system consisting of two pumps,
11 column oven, degasser and autosampler. Attached to this system was an analytical column (C18,
12 Gemini 5 μ m 110 A Phenomenex, 150 x 2 mm). The HPLC system was connected to a
13 triplequadrupole mass spectrometer equipped with a turboionspray source operated with unit
14 resolution in the positive ion mode (ESI-QQQMS, Shimadzu LCMS-30). Under these conditions a
15 retention time of approximately 4 minutes for the molecule was obtained. Mobile phase consisted of
16 a mixture (80:20) of acetonitrile: purified water at a flow rate of 0.2 mL/min rate in isocratic mode.
17 Run time was 10 minutes and the injection volume was 5 μ L. The mass transition of m/z was:
18 Quantifier (m/z): 315.0 > 161.0 CE: - 20; Qualifier (m/z): 315.0 > 132.9 CE: -34. Plasma samples
19 of mice (NMRI and BALB/c) were obtained by serial sampling from submandibular vein and stored
20 at -20 °C until being analyzed.
21
22
23
24
25
26
27
28
29
30
31
32
33
34
35
36
37
38
39

40 ***In-vivo* evaluation of anti-*T.brucei* activity of 4c.** Five-week-old BALCB/c female mice were
41 purchased from Charles River Laboratories (Saint-Germain-Nuelles, France), and housed in the
42 animal facility of the Instituto de Investigaç o e Inovaç o em Sa de (i3S). The animals were kept in
43 individually ventilated cages with high efficiency particulate air (HEPA) filters and were fed ad
44 libitum with sterilized food and water for one week prior to experimental infections. The
45 *Trypanosoma brucei brucei*, GVR35 line, expressing the red-shifted luciferase⁶¹ was kindly
46 provided by Prof. Jeremy Mottram, York University. Mice were infected by intraperitoneal
47 injection with blood containing 1×10^5 parasites harvested at the first peak of parasitemia from a
48 donor mouse. Control animals were similarly injected with the same volume of PBS. Compound **4c**
49
50
51
52
53
54
55
56
57
58
59
60

1
2
3 was administered orally as a suspension in a 2 g/mL (2-Hydroxypropyl)- β -cyclodextrin solution at
4
5 the dose of 40 mg/kg twice a day in order to possibly circumvent their limited bioavailability.
6
7 Pentamidine, at the dose of 5 mg/kg/day via IP administration, was used as positive control.
8
9 Parasite loads were assessed by bioluminescence imaging using the IVIS Lumina LT *in vivo*
10
11 imaging system (PerkinElmer, Waltham MA, USA). *T. b. brucei* GVR35-infected mice were
12
13 anesthetized with 2.5% isoflurane (O₂ flow of 1 L/min) and D-luciferin (2.4 mg, Perkin Elmer) was
14
15 administered subcutaneously five minutes prior to image acquisition. Mice were then transferred to
16
17 the stage of an intensified charge-coupled device photon-counting video camera box where
18
19 anaesthesia was maintained with 2.5% isoflurane (O₂ flow of 0.3 L/min). Exposure to isoflurane
20
21 was standardized among groups and throughout all time points and signal acquisition was
22
23 controlled by the Living Image software (Perkin Elmer). The detection of the bioluminescence
24
25 signal by the system resulted in the generation of signal maps automatically superimposed to the
26
27 grey-scale photograph of the mice. The regions of interest (ROI) encompassing most of the ventral
28
29 view of the animal body, the head, the thorax, the liver, the spleen, the abdomen, and the lower
30
31 abdomen were manually defined. The quantifications were performed using the Living Image
32
33 software (Perkin Elmer). The total flux (photons/second) and average radiance
34
35 (photons/second/cm²/steradian) within these ROIs were automatically calculated. The percentage of
36
37 bioluminescence signal in the defined regions was calculated by dividing the total flux of the
38
39 respective ROI by the total flux of the ventral animal body ROI.
40
41
42
43
44
45
46
47
48
49

50 ANCILLARY INFORMATION

53 Supporting Information

56 The Supporting Information is available free of charge on the ACS Publications website, including
57
58 (i) active site view of *TbPTR1* in complex with the cofactor NADP(H) and **4d**; (ii) calculated rule
59
60 of 5 (RO5) properties; (iii) data collection and processing statistics; (iv) structure solution and

1
2
3 refinement; (v) correlation between the pIC₅₀ against TbPTR1 and the Autodock Score; (vi) TIP
4 criteria; (vii) ¹H and ¹³C-NMR spectra of the tested compounds (PDF); (viii) PDB files of the
5 following docked complexes: 3jq7_1c_dockedcomplex (PDB) 3jq7_2c_dockedcomplex (PDB)
6 3jq7_2e_dockedcomplex (PDB) 3jq7_2g_dockedcomplex (PDB) 3jq7_3c_dockedcomplex (PDB)
7 3jq7_4c_dockedcomplex (PDB) 3jq7_5b_dockedcomplex (PDB); and (ix) Molecular Formula
8 String.

16 PDB ID Codes

19
20 Crystal structures of the ternary complexes of five compounds have been deposited with the
21 following PDB accession codes: **6GCK** (*TbPTR1* – NADP(H)– **1e**), **6GCQ** (*TbPTR1* – NADP(H)–
22 **2b**), **6GCP** (*TbPTR1* – NADP(H)– **2d**), **6GDO** (*TbPTR1* – NADP(H)– **2g**), **6GEX** (*TbPTR1* –
23 NADP(H)– **2h**), **6GCL** (*TbPTR1* – NADP(H)– **3a**), **6GD4** (*TbPTR1* – NADP(H)– **4c**), **6GEY**
24 (*TbPTR1* – NADP(H)– **4d**), **6GD0** (*TbPTR1* – NADP(H)– **4g**), and **6GDP** (*TbPTR1* – NADP(H)–
25 **4l**). Authors will release the atomic coordinates and experimental data upon article publication.

33 Corresponding Authors

34
35 *E-mail: p.linciano@unimore.it Phone: 0039-059-205-8661 (P.L.).

36
37 *E-mail: stefano.mangani@unisi.it Phone: 0039-0577234255 (S.M.)

38
39 *E-mail: luca.costantino@unimore.it Phone: 0039-0592058572 (L.C.)

40
41 *E-mail: mariapaola.costi@unimore.it, costimp@unimore.it. Phone: 0039-059-205-8579 (M.P.C.).

46 ORCID

47
48 Pasquale Linciano: 0000-0003-0382-7479

49
50 Maria Paola Costi: 0000-0002-0443-5402

55 Acknowledgements

1
2
3 This project has received funding from the European Union's Seventh Framework Programme for
4 Research, Technological Development, and Demonstration under grant agreement no. 603240
5 (NMTrypI-New Medicines for Trypanosomatidic Infections). I.P. acknowledges the financial
6 support of the Klaus Tschira Foundation. I.P. is a member of the Heidelberg Biosciences
7 International Graduate School. The authors thank Rebecca Wade and Joanna Panecka-Hofman for
8 helpful discussions.
9
10
11
12
13
14
15
16

17 **Ethics Statement.** All experiments with mice were carried out in accordance with the IBMC.INEB
18 Animal Ethics Committees and the Portuguese National Authorities for Animal Health guidelines
19 according to the statements on the directive 2010/63/EU of the European Parliament and Council.
20
21
22
23
24

25 **Abbreviations**

26
27
28 Acetonitrile: ACN; Cytochrome P450, CYP; Dihydrobiopterin: H₂B; Dihydrofolate reductase:
29 DHFR; Ethyl acetate: AcOEt; 1-Ethyl-3-(3-dimethylaminopropyl)carbodiimide: EDC; Formic acid:
30 FA; Human African trypanosomiasis: HAT; Hydroxybenzotriazole: HOBt; hydroxypropyl-β-
31 cyclodextrin, HP-β-CD; *Leishmania infantum*, *L. infantum*; *Leishmania major*, *L. major*;
32 *Leishmania major* pteridine reductase 1: *LmPTR1*; Methanol: MeOH; Methotrexate: MTX; *p*-
33 aminobenzoic acid, *pABA*; pan-assay interference compounds, PAINS; Potentiating Index, PI;
34 Pteridine reductase 1: PTR1; Sinergy Index, SI; Short-chain dehydrogenase/reductase: SDR;
35 Thymidylate Synthase, TS; *Trypanosoma brucei* pteridine reductase 1: *TbPTR1*; *Trypanosoma*
36 *brucei*: *T. brucei* or *Tb*; *Trypanosoma cruzi*: *T. cruzi*; Target Inhibitor Profile: TIP;
37 Tetrahydrobiopterin: H₄B; van der Waals, vdW.
38
39
40
41
42
43
44
45
46
47
48
49
50
51
52
53
54
55
56
57
58
59
60

REFERENCES

- 1
2
3
4
5
6 (1) Barrett, M. P.; Burchmore, R. J.; Stich, A.; Lazzari, J. O.; Frasc, A. C.; Cazzulo, J. J.;
7
8 Krishna, S. The Trypanosomiasis. *Lancet* **2003**, *362* (9394), 1469–1480.
- 9
10 (2) Brun, R.; Blum, J.; Chappuis, F.; Burri, C. Human African Trypanosomiasis. *Lancet* **2010**,
11
12 *375* (9709), 148–159.
- 13
14 (3) Croft, S. L.; Barrett, M. P.; Urbina, J. A. Chemotherapy of Trypanosomiasis and
15
16 Leishmaniasis. *Trends Parasitol.* **2005**, *21* (11), 508–512.
- 17
18 (4) Barrett, M. P.; Vincent, I. M.; Burchmore, R. J. S.; Kazibwe, A. J. N.; Matovu, E. Drug
19
20 Resistance in Human African Trypanosomiasis. *Future Microbiol.* **2011**, *6* (9), 1037–1047.
- 21
22 (5) Maxmen, A. Pill Treats Sleeping Sickness Scientists Seek Approval from Regulators for This
23
24 Relatively Quick and Easy Therapy . *Nature* **2017**, *550*, 441.
- 25
26 (6) Torreele, E.; Trunz, B. B.; Tweats, D.; Kaiser, M.; Brun, R.; Mazué, G.; Bray, M. A.; Pécoul,
27
28 B. Fexinidazole - a New Oral Nitroimidazole Drug Candidate Entering Clinical Development
29
30 for the Treatment of Sleeping Sickness. *PLoS Negl. Trop. Dis.* **2010**, *4* (12), 1–15.
- 31
32 (7) Hawser, S.; Lociuro, S.; Islam, K. Dihydrofolate Reductase Inhibitors as Antibacterial
33
34 Agents. *Biochem. Pharmacol.* **2006**, *71* (7), 941–948.
- 35
36 (8) Mangani, S.; Cancian, L.; Leone, R.; Pozzi, C.; Lazzari, S.; Luciani, R.; Ferrari, S.; Costi, M.
37
38 P. Identification of the Binding Modes of N-Phenylphthalimides Inhibiting Bacterial
39
40 Thymidylate Synthase through X-Ray Crystallography Screening. *J. Med. Chem.* **2011**, *54*
41
42 (15), 5454–5467.
- 43
44 (9) Nare, B.; Hardy, L. W.; Beverley, S. M. The Roles of Pteridine Reductase 1 and
45
46 Dihydrofolate Reductase- Thymidylate Synthase in Pteridine Metabolism in the Protozoan
47
48 Parasite *Leishmania Major*. *J. Biol. Chem.* **1997**, *272* (21), 13883–13891.
- 49
50 (10) Gilbert, I. H. Inhibitors of Dihydrofolate Reductase in *Leishmania* and Trypanosomes.
51
52
53
54
55
56
57
58
59
60 *Biochim. Biophys. Acta - Mol. Basis Dis.* **2002**, *1587* (2–3), 249–257.

- 1
2
3 (11) Bello, a R.; Nare, B.; Freedman, D.; Hardy, L.; Beverley, S. M. PTR1: A Reductase
4
5 Mediating Salvage of Oxidized Pteridines and Methotrexate Resistance in the Protozoan
6
7 Parasite *Leishmania Major*. *Proc. Natl. Acad. Sci. U. S. A.* **1994**, *91* (24), 11442–11446.
8
9
10 (12) Ong, H. B.; Sienkiewicz, N.; Wyllie, S.; Fairlamb, A. H. Dissecting the Metabolic Roles of
11
12 Pteridine Reductase 1 in *Trypanosoma Brucei* and *Leishmania Major*. *J. Biol. Chem.* **2011**,
13
14 *286* (12), 10429–10438.
15
16
17 (13) Dawson, A.; Gibellini, F.; Sienkiewicz, N.; Tulloch, L. B.; Fyfe, P. K.; McLuskey, K.;
18
19 Fairlamb, A. H.; Hunter, W. N. Structure and Reactivity of *Trypanosoma Brucei* Pteridine
20
21 Reductase: Inhibition by the Archetypal Antifolate Methotrexate. *Mol. Microbiol.* **2006**, *61*
22
23 (6), 1457–1468.
24
25
26 (14) Spinks, D.; Ong, H. B.; Mpamhanga, C. P.; Shanks, E. J.; Robinson, D. A.; Collie, I. T.;
27
28 Read, K. D.; Frearson, J. A.; Wyatt, P. G.; Brenk, R.; Fairlamb, A. H.; Gilbert, I. H. Design,
29
30 Synthesis and Biological Evaluation of Novel Inhibitors of *Trypanosoma Brucei* Pteridine
31
32 Reductase 1. *ChemMedChem* **2011**, *6* (2), 302–308.
33
34
35 (15) Ferrari, S.; Morandi, F.; Motiejunas, D.; Nerini, E.; Henrich, S.; Luciani, R.; Venturelli, A.;
36
37 Lazzari, S.; Calò, S.; Gupta, S.; Hannaert, V.; Michels, P. A. M.; Wade, R. C.; Costi, M. P.
38
39 Virtual Screening Identification of Nonfolate Compounds, Including a CNS Drug, as
40
41 Antiparasitic Agents Inhibiting Pteridine Reductase. *J. Med. Chem.* **2011**, *54* (1), 211–221.
42
43
44 (16) Cavazzuti, A.; Paglietti, G.; Hunter, W. N.; Gamarro, F.; Piras, S.; Loriga, M.; Allecca, S.;
45
46 Corona, P.; McLuskey, K.; Tulloch, L.; Gibellini, F.; Ferrari, S.; Costi, M. P. Discovery of
47
48 Potent Pteridine Reductase Inhibitors to Guide Antiparasite Drug Development. *Proc. Natl.*
49
50 *Acad. Sci. U. S. A.* **2008**, *105*, 1448–1453.
51
52
53 (17) Linciano, P.; Dawson, A.; Pöhner, I.; Costa, D. M.; Sá, M. S.; Cordeiro-da-Silva, A.;
54
55 Luciani, R.; Gul, S.; Witt, G.; Ellinger, B.; Kuzikov, M.; Gribbon, P.; Reinshagen, J.; Wolf,
56
57 M.; Behrens, B.; Hannaert, V.; Michels, P. A. M.; Nerini, E.; Pozzi, C.; di Pisa, F.; Landi, G.;
58
59 Santarem, N.; Ferrari, S.; Saxena, P.; Lazzari, S.; Cannazza, G.; Freitas-Junior, L. H.;
60

- 1
2
3 Moraes, C. B.; Pascoalino, B. S.; Alcântara, L. M.; Bertolacini, C. P.; Fontana, V.; Wittig,
4 U.; Müller, W.; Wade, R. C.; Hunter, W. N.; Mangani, S.; Costantino, L.; Costi, M. P.
5 Exploiting the 2-Amino-1,3,4-Thiadiazole Scaffold To Inhibit *Trypanosoma Brucei* Pteridine
6 Reductase in Support of Early-Stage Drug Discovery. *ACS Omega* **2017**, *2* (9), 5666–5683.
7
8
9
10
11
12 (18) Gilbert, I. H. Drug Discovery for Neglected Diseases: Molecular Target- Based and
13 Phenotypic Approaches. *J. Med. Chem.* **2013**, *56*, 7719–7726.
14
15
16 (19) Mpamhanga, C. P.; Spinks, D.; Tulloch, L. B.; Shanks, E. J.; Robinson, D. A.; Collie, I. T.;
17 Fairlamb, A. H.; Wyatt, P. G.; Frearson, J. A.; Hunter, W. N.; Gilbert, I. H.; Brenk, R. One
18 Scaffold, Three Binding Modes: Novel and Selective Pteridine Reductase 1 Inhibitors
19 Derived from Fragment Hits Discovered by Virtual Screening. *J. Med. Chem.* **2009**, *52* (14),
20 4454–4465.
21
22
23
24
25
26
27
28 (20) Corona, P.; Gibellini, F.; Cavalli, A.; Saxena, P.; Carta, A.; Loriga, M.; Luciani, R.; Paglietti,
29 G.; Guerrieri, D.; Nerini, E.; Gupta, S.; Hannaert, V.; Michels, P. A. M.; Ferrari, S.; Costi, P.
30 M. Structure-Based Selectivity Optimization of Piperidine-Pteridine Derivatives as Potent
31 Leishmania Pteridine Reductase Inhibitors. *J. Med. Chem.* **2012**, *55* (19), 8318–8329.
32
33
34
35
36
37 (21) Dawson, A.; Tulloch, L. B.; Barrack, K. L.; Hunter, W. N. High-Resolution Structures of
38 *Trypanosoma Brucei* Pteridine Reductase Ligand Complexes Inform on the Placement of
39 New Molecular Entities in the Active Site of a Potential Drug Target. *Acta Crystallogr. Sect.*
40 *D Biol. Crystallogr.* **2010**, *66* (12), 1334–1340.
41
42
43
44
45
46 (22) Di Pisa, F.; Landi, G.; Dello Iacono, L.; Pozzi, C.; Borsari, C.; Ferrari, S.; Santucci, M.;
47 Santarem, N.; Cordeiro-da-Silva, A.; Moraes, C. B.; Alcantara, L. M.; Fontana, V.; Freitas-
48 Junior, L. H.; Gul, S.; Kuzikov, M.; Behrens, B.; Pöhner, I.; Wade, R. C.; Costi, M. P.;
49 Mangani, S. Chroman-4-One Derivatives Targeting Pteridine Reductase 1 and Showing Anti-
50 Parasitic Activity. *Molecules* **2017**, *22* (3), 426.
51
52
53
54
55
56
57 (23) Tulloch, L. B.; Martini, V. P.; Iulek, J.; Huggan, J. K.; Lee, J. H.; Gibson, C. L.; Smith, T.
58 K.; Suckling, C. J.; Hunter, W. N. Structure-Based Design of Pteridine Reductase Inhibitors
59
60

- 1
2
3 Targeting African Sleeping Sickness and the Leishmaniases. *J. Med. Chem.* **2010**, *53* (1),
4
5 221–229.
6
- 7 (24) Borsari, C.; Lucian, R.; Pozz, C.; Poehner, I.; Henrich, S.; Trande, M.; Cordeiro-Da-silva, A.;
8
9 Santarem, N.; Baptista, C.; Tait, A.; Di Pisa, F.; Iacono, L. Dello; Landi, G.; Gul, S.; Wolf,
10
11 M.; Kuzikov, M.; Ellinger, B.; Reinshagen, J.; Witt, G.; Gribbon, P.; Kohler, M.; Keminer,
12
13 O.; Behrens, B.; Costantino, L.; Nevado, P. T.; Bifeld, E.; Eick, J.; Clos, J.; Torrado, J.;
14
15 Corral, M. J.; Alunda, J.; Pellati, F.; Wade, R. C.; Ferrari, S.; Mangani, S.; Costi, M. P.
16
17 Profiling of Flavonol Derivatives for the Development of Antitrypanosomatidic Drugs. *J.*
18
19 *Med. Chem.* **2016**, *59* (16), 7598–7616.
20
21
- 22 (25) Katsuno, K.; Burrows, J. N.; Duncan, K.; van Huijsduijnen, R. H.; Kaneko, T.; Kita, K.;
23
24 Mowbray, C. E.; Schmatz, D.; Warner, P.; Slingsby, B. T. Hit and Lead Criteria in Drug
25
26 Discovery for Infectious Diseases of the Developing World. *Nat. Rev. Drug Discov.* **2015**, *14*
27
28 (11), 751–758.
29
30
- 31 (26) Wyatt, P. G.; Gilbert, I. H.; Read, K. D.; Fairlamb, A. H. Target Validation: Linking Target
32
33 and Chemical Properties to Desired Product Profile. *Curr. Top. Med. Chem.* **2011**, *11* (10),
34
35 1275–1283.
36
37
- 38 (27) Dawson, A.; Gibellini, F.; Sienkiewicz, N.; Tulloch, L. B.; Fyfe, P. K.; McLuskey, K.;
39
40 Fairlamb, A. H.; Hunter, W. N. Structure and Reactivity of Trypanosoma Brucei Pteridine
41
42 Reductase: Inhibition by the Archetypal Antifolate Methotrexate. *Mol. Microbiol.* **2006**, *61*
43
44 (6), 1457–1468.
45
46
- 47 (28) Tulloch, L. B.; Martini, V. P.; Iulek, J.; Huggan, J. K.; Lee, J. H.; Gibson, C. L.; Smith, T.
48
49 K.; Suckling, C. J.; Hunter, W. N. Structure-Based Design of Pteridine Reductase Inhibitors
50
51 Targeting African Sleeping Sickness and the Leishmaniases. *J. Med. Chem.* **2010**, *53* (1),
52
53 221–229.
54
55
- 56 (29) Morris, G. M.; Huey, R.; Lindstrom, W.; Sanner, M. F.; Belew, R. K.; Goodsell, D. S.;
57
58 Olson, A. J. AutoDock4 and AutoDockTools4: Automated Docking with Selective Receptor
59
60

- Flexibility. *J. Comput. Chem.* **2009**, *30* (16), 2785–2791.
- (30) Kenny, P. W. Comment on the Ecstasy and Agony of Assay Interference Compounds. *J. Chem. Inf. Model.* **2017**, *57* (11), 2640–2645.
- (31) Lagorce, D.; Sperandio, O.; Baell, J.; Miteva, M.; Villoutreix, B. FAFDrugs4 <http://fafdrugs4.mti.univ-paris-diderot.fr> (accessed Sep 10, 2017).
- (32) Faria, J.; Moraes, C. B.; Song, R.; Pascoalino, B. S.; Lee, N.; Siqueira-Neto, J. L.; Cruz, D. J. M.; Parkinson, T.; Ioset, J.-R.; Cordeiro-da-Silva, A.; Freitas-Junior, L. H. Drug Discovery for Human African Trypanosomiasis: Identification of Novel Scaffolds by the Newly Developed HTS SYBR Green Assay for Trypanosoma Brucei. *J. Biomol. Screen.* **2015**, *20* (1), 70–81.
- (33) Baker, N.; Glover, L.; Munday, J. C. J. C.; Aguinaga Andrés, D.; Barrett, M. P. M. P.; de Koning, H. P. H. P.; Horn, D.; Aguinaga Andres, D.; Barrett, M. P. M. P.; de Koning, H. P. H. P.; Horn, D. Aquaglyceroporin 2 Controls Susceptibility to Melarsoprol and Pentamidine in African Trypanosomes. *Proc. Natl. Acad. Sci. U. S. A.* **2012**, *109* (27), 10996–11001.
- (34) Moraes, C. B.; Giardini, M. a; Kim, H.; Franco, C. H.; Araujo-Junior, A. M.; Schenkman, S.; Chatelain, E.; Freitas-Junior, L. H. Nitroheterocyclic Compounds Are More Efficacious than CYP51 Inhibitors against Trypanosoma Cruzi: Implications for Chagas Disease Drug Discovery and Development. *Sci. Rep.* **2014**, *4*, 4703.
- (35) Bard, B.; Martel, S.; Carrupt, P. A. High Throughput UV Method for the Estimation of Thermodynamic Solubility and the Determination of the Solubility in Biorelevant Media. *Eur. J. Pharm. Sci.* **2008**, *33* (3), 230–240.
- (36) Lipinski, C. A. Drug-like Properties and the Causes of Poor Solubility and Poor Permeability. *J. Pharmacol. Toxicol. Methods* **2000**, *44* (1), 235–249.
- (37) Bandyopadhyay, A. Target Product Profile : A Planning Tool for the Drug Development. **2017**, *3* (4), 3–4.
- (38) Linciano, P.; Moraes, C. B.; Alcantara, L. M.; Franco, C. H.; Pascoalino, B.; Freitas-Junior,

1
2
3
4
5
6
7
8
9
10
11
12
13
14
15
16
17
18
19
20
21
22
23
24
25
26
27
28
29
30
31
32
33
34
35
36
37
38
39
40
41
42
43
44
45
46
47
48
49
50
51
52
53
54
55
56
57
58
59
60

L. H.; Macedo, S.; Santarem, N.; Cordeiro-da-Silva, A.; Gul, S.; Witt, G.; Kuzikov, M.; Ellinger, B.; Ferrari, S.; Luciani, R.; Quotadamo, A.; Costantino, L.; Costi, M. P. Aryl Thiosemicarbazones for the Treatment of Trypanosomatidic Infections. *Eur. J. Med. Chem.* **2018**, *146*, 423–434.

- (39) Humphrey, W.; Dalke, A.; Schulten, K. VMD: Visual Molecular Dynamics. *J. Mol. Graph.* **1996**, *14* (1), 33–38.
- (40) ChemBio3D Ultra. PerkinElmer 2014.
- (41) BIOVIA, D. S. Discovery Studio. 2014.
- (42) Benvenuti, M.; Mangani, S. Crystallization of Soluble Proteins in Vapor Diffusion for X-Ray Crystallography. *Nat. Protoc.* **2007**, *2* (7), 1633–1651.
- (43) Batty, T. G. G.; Kontogiannis, L.; Johnson, O.; Powell, H. R.; Leslie, A. G. W. IMOSFLM: A New Graphical Interface for Diffraction-Image Processing with MOSFLM. *Acta Crystallogr. Sect. D Biol. Crystallogr.* **2011**, *67* (4), 271–281.
- (44) Powell, H. R.; Johnson, O.; Leslie, A. G. W. Autoindexing Diffraction Images with IMosflm. *Acta Crystallogr. Sect. D Biol. Crystallogr.* **2013**, *69* (7), 1195–1203.
- (45) Kabsch, W. XDS. *Acta Crystallogr. D. Biol. Crystallogr.* **2010**, *66* (Pt 2), 125–132.
- (46) Evans, P. Scaling and Assessment of Data Quality. *Acta Crystallogr. Sect. D Biol. Crystallogr.* **2006**, *62* (1), 72–82.
- (47) Evans, P. R. An Introduction to Data Reduction: Space-Group Determination, Scaling and Intensity Statistics. *Acta Crystallogr. Sect. D Biol. Crystallogr.* **2011**, *67* (4), 282–292.
- (48) The CCP4 Suite: Programs for Protein Crystallography. *Acta Crystallogr. D. Biol. Crystallogr.* **1994**, *50* (Pt 5), 760–763.
- (49) Vagin, A.; Teplyakov, A. Molecular Replacement with MOLREP. *Acta Crystallogr. D. Biol. Crystallogr.* **2010**, *66* (Pt 1), 22–25.
- (50) Murshudov, G. N.; Skubák, P.; Lebedev, A. A.; Pannu, N. S.; Steiner, R. A.; Nicholls, R. A.; Winn, M. D.; Long, F.; Vagin, A. A. REFMAC5 for the Refinement of Macromolecular

- 1
2
3 Crystal Structures. *Acta Crystallogr. D. Biol. Crystallogr.* **2011**, 67 (Pt 4), 355–367.
- 4
5 (51) Emsley, P.; Cowtan, K. Coot: Model-Building Tools for Molecular Graphics. *Acta*
6
7 *Crystallogr. Sect. D Biol. Crystallogr.* **2004**, 60 (12 I), 2126–2132.
- 8
9
10 (52) Emsley, P.; Lohkamp, B.; Scott, W. G.; Cowtan, K. Features and Development of Coot. *Acta*
11
12 *Crystallogr. D. Biol. Crystallogr.* **2010**, 66 (Pt 4), 486–501.
- 13
14 (53) Langer, G.; Cohen, S. X.; Lamzin, V. S.; Perrakis, A. Automated Macromolecular Model
15
16 Building for X-Ray Crystallography Using ARP/WARP Version 7. *Nat. Protoc.* **2008**, 3 (7),
17
18 1171–1179.
- 19
20
21 (54) Laskowski, R. A.; MacArthur, M. W.; Thornton, J. M. Validation of Protein Models Derived
22
23 from Experiment. *Curr. Opin. Struct. Biol.* **1998**, 8 (5), 631–639.
- 24
25
26 (55) Potterton, L.; McNicholas, S.; Krissinel, E.; Gruber, J.; Cowtan, K.; Emsley, P.; Murshudov,
27
28 G. N.; Cohen, S.; Perrakis, A.; Noble, M. Developments in the CCP4 Molecular-Graphics
29
30 Project. *Acta Crystallogr. D. Biol. Crystallogr.* **2004**, 60 (Pt 12 Pt 1), 2288–2294.
- 31
32
33 (56) Shanks, E. J.; Ong, H. B.; Robinson, D. A.; Thompson, S.; Sienkiewicz, N.; Fairlamb, A. H.;
34
35 Frearson, J. A. Development and Validation of a Cytochrome C-Coupled Assay for Pteridine
36
37 Reductase 1 and Dihydrofolate Reductase. *Anal. Biochem.* **2010**, 396 (2), 194–203.
- 38
39
40 (57) Bowling, T.; Mercer, L.; Don, R.; Jacobs, R.; Nare, B. Application of a Resazurin-Based
41
42 High-Throughput Screening Assay for the Identification and Progression of New Treatments
43
44 for Human African Trypanosomiasis. *Int. J. Parasitol. Drugs Drug Resist.* **2012**, 2, 262–270.
- 45
46
47 (58) Borsari, C.; Santarem, N.; Torrado, J.; Isabel, A.; Jesús, M.; Baptista, C.; Gul, S.; Wolf, M.;
48
49 Kuzikov, M.; Ellinger, B.; Witt, G.; Gribbon, P.; Reinshagen, J.; Linciano, P.; Tait, A.;
50
51 Costantino, L.; Freitas-junior, L. H.; Moraes, C. B.; Bruno, P.; Maria, L.; Franco, C. H.;
52
53 Bertolacini, C. D.; Fontana, V.; Tejera, P.; Clos, J.; Cordeiro-da-silva, A.; Ferrari, S.; Paola,
54
55 M. Methoxylated 2'-Hydroxychalcones as Antiparasitic Hit Compounds. *Eur. J. Med.*
56
57 *Chem.* **2017**, 126, 1129–1135.
- 58
59
60 (59) Borsari, C.; Lucian, R.; Pozz, C.; Poehner, I.; Henrich, S.; Trande, M.; Cordeiro-Da-silva, A.;

1
2
3
4
5
6
7
8
9
10
11
12
13
14
15
16
17
18
19
20
21
22
23
24
25
26
27
28
29
30
31
32
33
34
35
36
37
38
39
40
41
42
43
44
45
46
47
48
49
50
51
52
53
54
55
56
57
58
59
60

Santarem, N.; Baptista, C.; Tait, A.; Di Pisa, F.; Iacono, L. Dello; Landi, G.; Gul, S.; Wolf, M.; Kuzikov, M.; Ellinger, B.; Reinshagen, J.; Witt, G.; Gribbon, P.; Kohler, M.; Keminer, O.; Behrens, B.; Costantino, L.; Nevado, P. T.; Bifeld, E.; Eick, J.; Clos, J.; Torrado, J.; Jimenez-Antón, M. D.; Corral, M. J.; Alunda, J. M.; Pellati, F.; Wade, R. C.; Ferrari, S.; Mangani, S.; Costi, M. P. Profiling of Flavonol Derivatives for the Development of Antitrypanosomatidic Drugs. *J. Med. Chem.* **2016**, *59* (16), 7598–7616.

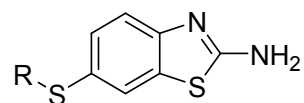
(60) Liu, B.; Chang, J.; Gordon, W. P.; Isbell, J.; Zhou, Y.; Tuntland, T. Snapshot PK: A Rapid Rodent in Vivo Preclinical Screening Approach. *Drug Discov. Today* **2008**, *13* (7–8), 360–367.

(61) McLatchie, A. P.; Burrell-Saward, H.; Myburgh, E.; Lewis, M. D.; Ward, T. H.; Mottram, J. C.; Croft, S. L.; Kelly, J. M.; Taylor, M. C. Highly Sensitive In Vivo Imaging of Trypanosoma Brucei Expressing “Red-Shifted” Luciferase. *PLoS Negl. Trop. Dis.* **2013**, *7* (11), 1–12.

Table 1. Chemical structures, enzymatic evaluation and anti-parasitic activity of etheric benzothiazoles **1a-g**.

Compound	R	IC ₅₀ in μM ^a (%inhibition at 50μM)		% cell growth inhibition [EC ₅₀ in μM]		
		<i>Tb</i> PTR1	<i>Lm</i> PTR1	<i>T. brucei</i> ^b	Amastigote <i>L. infantum</i> ^b	Amastigote <i>T. cruzi</i> ^{a,c}
1a	-CH ₃	(29.9 %)	(15.2 %)	6±0	NI	32.9
1b	-CF ₃	15.1	94.1	NI	NI	NI
1c		13.4	NI	28±15	NI	NI
1d		3.4	NI	42±11	NI	7.24
1e		0.67	86.5	27±0	NI	15.4
1f		1.7	66.6	22±0	NI	8.79
1g		3.3	31.9	52±0	NI	27.0

- a. Standard deviation is within ±10% of the value.
 b. Compounds tested at 10 μM. NI: no inhibition.
 c. Compounds tested at 50 μM . NI: no inhibition.

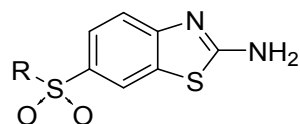
Table 2. Chemical structures, enzymatic evaluation and anti-parasitic activity of sulfide benzothiazoles **2a-h**.

Compound	R	IC ₅₀ in μM ^a (%inhibition at 50μM)		% cell growth inhibition [EC ₅₀ in μM]		
		<i>Tb</i> PTR1	<i>Lm</i> PTR1	<i>T. brucei</i> ^b	Amastigote <i>L. infantum</i> ^b	Amastigote <i>T. cruzi</i> ^{a,c}
2a	-CH ₃	(16.7 %)	(26.9 %)	12±1	NI	22.5
2b	-CF ₃	0.50	1.9	11±0	NI	37.4
2c		1.9	81	14±17	NI	NI
2d		0.90	10	46±1	NI	21.4
2e		0.35	12.4	35±0	NI	27.3
2f		0.92	47.6	17±0	NI	23.0
2g		0.93	15.1	42±5	NI	16.3
2h		0.50	30	26±2	NI	19.2

d. Standard deviation is within ±10% of the value.

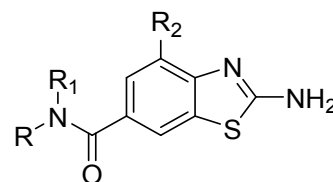
e. Compounds tested at 10 μM . NI: no inhibition.

f. Compounds tested at 50 μM . NI: no inhibition.

Table 3. Chemical structures, enzymatic evaluation and anti-parasitic activity of sulfone benzothiazoles **3a,c-g**.

Compound	R	IC ₅₀ in μM ^a (%inhibition at 50μM)		% cell growth inhibition [EC ₅₀ in μM]		
		<i>Tb</i> PTR1	<i>Lm</i> PTR1	<i>T. brucei</i> ^b	Amastigote <i>L. infantum</i> ^b	Amastigote <i>T. cruzi</i> ^{a,c}
3a	-CH ₃	34.2	32.9	17±9	NI	17.4
3c		57.6	(27.1 %)	5±17	NI	NI
3d		(16.7 %)	(26.9 %)	37±11	21±5	32.8
3e		3.00	(55.5 %)	9±0	NI	NI
3f		15.1	65.9	14±1	12±17	NI
3g		24.3	50	NI	NI	NI

- a. Standard deviation is within ±10% of the value.
 b. Compounds tested at 10 μM . NI: no inhibition.
 c. Compounds tested at 50 μM . NI: no inhibition.

Table 4. Chemical structures, enzymatic evaluation and anti-parasitic activity of 6-amide benzothiazoles **4c-t**.

Compound	R	R ₁	R ₂	IC ₅₀ in μM ^a (%inhibition at 50μM)		% cell growth inhibition [EC ₅₀ in μM]		
				<i>Tb</i> PTR1	<i>Lm</i> PTR1	<i>T. brucei</i> ^b	Amastigote <i>L. infantum</i> ^b	Amastigote <i>T. cruzi</i> ^{a,c}
4c		H-	H-	10.0	61.3	[7.0±0.5]	NI	51.3
4d		H-	H-	5.4	15.3	5±8	5±5	NI
4e		H-	H-	42.9	73.3	8±4	NI	NI
4f		H-	H-	16.5	36.0	16±2	NI	NI
4g		H-	H-	21.8	(1.97 %)	24±11	NI	NI
4h		H-	H-	6.85	18.9	53±0	NI	NI
4i		H-	H-	(30.8 %)	(67.1 %)	9±17	NI	19.8
4j		H-	H-	6.46	3.51	18±0	NI	19.0

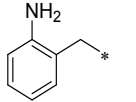
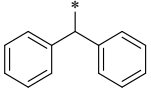
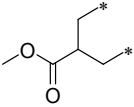
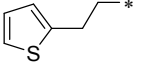
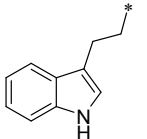
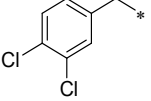
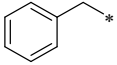
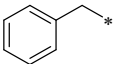
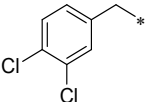
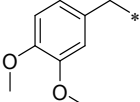
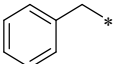
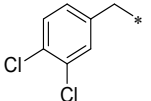
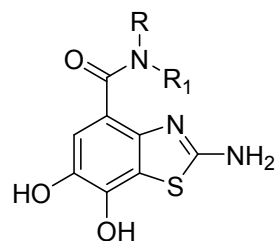
1									
2									
3	4k		H-	H-	13.9	64.7	8±0	NI	6.10
4									
5									
6	4l		H-	H-	18.5	88.5	10±11	15±21	37.8
7									
8									
9	4m		H-	H-	(36.4 %)	(23.3 %)	19±8	8±12	64.2
10									
11									
12	4n		H-	H-	7.5	(18.3 %)	17±4	NI	29.8
13									
14									
15	4o		H-	H-	23.3	NI	27±6	NI	1.64
16									
17									
18	4p			H-	12.0	NI	26±2	NI	62.1
19									
20	4q		CH ₂ CH ₂ OH	H-	58.1	(24.1 %)	8±17	20±7	NI
21									
22	4r			H-	15.9	NI	[9.7±2.5]	9±8	47.9
23									
24	4s		H-	-OH	(47.8 %)	2.48	15±6	11±15	28.8
25									
26	4t		H-	-OH	(11.8 %)	(8.7 %)	[5.9±0.2]	24±15	42.0
27									
28									
29									
30									
31									
32									
33									
34									
35	a.	Standard deviation is within ±10% of the value.							
36	b.	Compounds tested at 10 μM. NI: no inhibition.							
37	c.	Compounds tested at 50 μM. NI: no inhibition.							
38									
39									
40									
41									
42									
43									
44									
45									
46									

Table 5. Chemical structures, enzymatic evaluation and antiparasitic activity of 4-amide cathecolic benzothiazoles **5a-c**.

Compound	R	R ₁	IC ₅₀ in μM ^a (%inhibition at 50μM)		% cell growth inhibition [EC ₅₀ in μM]		
			<i>Tb</i> PTR1	<i>Lm</i> PTR1	<i>T. brucei</i> ^b	Amastigote <i>L. infantum</i> ^b	Amastigote <i>T. cruzi</i> ^{a,c}
5a			11.4	15.2	25±20	NI	NI
5b		H-	32.3	36.8	16±0	NI	18.3
5c		H-	30.9	30.1	15±0	NI	5.85

- a. Standard deviation is within ±10% of the value.
 b. Compounds tested at 10 μM . NI: no inhibition.
 c. Compounds tested at 50 μM . NI: no inhibition.

TOC Graphic

